Influence of H_2O, HCl and H_2S on the Release and Condensation of Trace Metals in Gasification

María Benito Abascal

Energie & Umwelt / Energy & Environment
Band / Volume 310
ISBN 978-3-95806-125-5

JÜLICH
FORSCHUNGSZENTRUM

Schriften des Forschungszentrums Jülich
Reihe Energie & Umwelt / Energy & Environment Band / Volume 310

Forschungszentrum Jülich GmbH
Institute of Energy and Climate Research (IEK)
Microstructure and Properties of Materials (IEK-2)

Influence of H_2O, HCl and H_2S on the Release and Condensation of Trace Metals in Gasification

María Benito Abascal

Schriften des Forschungszentrums Jülich
Reihe Energie & Umwelt / Energy & Environment Band / Volume 310

ISSN 1866-1793 ISBN 978-3-95806-125-5

Bibliographic information published by the Deutsche Nationalbibliothek.
The Deutsche Nationalbibliothek lists this publication in the Deutsche Nationalbibliografie; detailed bibliographic data are available in the Internet at http://dnb.d-nb.de.

Publisher and Distributor: Forschungszentrum Jülich GmbH
Zentralbibliothek
52425 Jülich
Tel: +49 2461 61-5368
Fax: +49 2461 61-6103
Email: zb-publikation@fz-juelich.de
www.fz-juelich.de/zb

Cover Design: Grafische Medien, Forschungszentrum Jülich GmbH

Printer: Grafische Medien, Forschungszentrum Jülich GmbH

Schriften des Forschungszentrums Jülich
Reihe Energie & Umwelt / Energy & Environment, Band / Volume 310

D 82 (Diss. RWTH Aachen University, 2015)

ISSN 1866-1793
ISBN 978-3-95806-125-5

The complete volume is freely available on the Internet on the Jülicher Open Access Server (JuSER) at www.fz-juelich.de/zb/openaccess.

Abstract

High temperature coal utilization processes such as gasification emit hazardous traces of heavy metals into the atmosphere, impacting the environment, human health and causing technological problems in gasification plants. These trace metals present in parts per million levels in coal give rise to several tons of these pollutants in the environment per year. Therefore, the development of cleaner and more efficient techniques in next generation coal power plants is essential. A promising coal utilization process is the Integrated Gasification Combined Cycle (IGCC) with integrated hot gas purification and CO_2 separation. An increased efficiency and a decreased amount of heavy metal species can be accomplished through hot fuel gas cleaning. However, in order to develop clean up techniques that reduce or remove heavy metal traces, it is necessary to understand their behaviour during the gasification process. Some studies have already determined that the chlorine, sulphur and moisture content of fuels have a significant influence on the behaviour of some trace metals. Hereby, the influence of steam, HCl and H_2S on the release and condensation of Zn, Cd, Pb, As, Sn and V was experimentally investigated. The condensation behaviour (temperature and speciation) of the heavy metal vapours was investigated in a heated flow channel reactor housed in a furnace with a gas cooling zone. Experiments on the release of the inorganic vapours were carried out in a heated flow channel reactor coupled to a molecular beam mass spectrometer (MBMS) in order to analyse the gas in-situ. The results of the experimental investigation were compared with “Scheil-Gulliver Cooling” calculations performed by FactSage 6.3. Furthermore, thermodynamic pseudo-equilibrium calculations were carried out to predict the condensation behaviour of the heavy metals under the influence of super-cooling and chemical reaction control. A better understanding of the gasification process and a new insight into the optimization of the process to reduce the trace metal emissions was achieved.

Zusammenfassung

Der Ausstoß gefährlicher Schwermetalle in die Atmosphäre sorgt bei kohleverwertenden Hochtemperaturprozessen wie der Kohlevergasung nicht nur für technologische Probleme, sondern macht diese auch zu einer Belastung für Mensch und Natur. Auch wenn der Anteil der an die Umgebung abgegebenen Spurenmetalle im Verhältnis zum restlichen Ausstoß auf einem nur in ppm darstellbaren Niveau liegt, so beläuft sich der übers Jahr gesehene weltweite Ausstoß auf mehrere Tonnen. Aus diesem Grund ist die Entwicklung entsprechender Reinigungsverfahren und effizienterer Prozesse für die kommenden Kohlekraftwerksgenerationen essentiell. Ein mit Bezug darauf vielversprechender kohleverwertender Prozess ist der *Integrated Gasification Combined Cycle* (IGCC) mit integrierter Heißgasreinigung und CO_2-Abscheidung. Durch Brenngasreinigung kann schon heute eine erhöhte Effizienz bei verringertem Schwermetallausstoß erzielt werden. Um aber Reinigungstechniken zu entwickeln, welche den Anteil an Schwermetallen weiter reduzieren oder gar eliminieren, ist es unbedingt erforderlich, deren Verhalten während des Vergasungsprozesses genau zu verstehen. Einige Studien zu diesem Thema haben bereits aufgedeckt, dass Chlor-, Schwefel- und Feuchtigkeitsgehalt von Brennstoffen einen signifikanten Einfluss auf das Verhalten einiger Schwermetalle haben. Im selben Zusammenhang war es auch möglich, Wasserdampf, HCl und H_2S einen Einfluss auf die Freisetzung und Kondensation von Zn, Cd, Pb, Sn und V experimentell nachzuweisen. Darauf aufbauend wurde im Rahmen der vorliegenden Arbeit das Kondensationsverhalten von Schwermetalldämpfen im Hinblick auf Temperatur und Artbildung in einem beheizten Strömungskanalreaktor untersucht, welcher in einem Ofen mit Gaskühlzone untergebracht war. Experimente zur Freisetzung anorganischer Dämpfe wurden ebenfalls unter Nutzung eines beheizten Strömungskanalreaktors durchgeführt. Allerdings wurde der Reaktor hierbei an ein Molekularstrahlmassenspektrometer gekoppelt, um in situ Analysen des zu untersuchenden Gases durchzuführen. Im Anschluss wurden die Versuchsergebnisse mit Simulationsergebnissen verglichen, welche auf Basis des Scheil-Gulliver-Cooling-Models mit der Simulationssoftware FactSage 6.3 ermittelt wurden. Außerdem wurden Berechnungen zum thermodynamischen Pseudo-Gleichgewicht mit dem Ziel durchgeführt, das Kondensationsverhalten der Schwermetalle bei Unterkühlung und unter Einfluss chemischer Reaktionskontrolle vorherzusagen. Durch die vorliegende Arbeit konnte ein besseres Verständnis über den Vergasungsprozess und neue Erkenntnisse für die Optimierung des Prozesses zur Reduzierung von Emissionen von Spurenmetallen gewonnen werden.

Contents

List of tables

List of figures

List of symbols and abbreviations

Symbols

α	Proportion of a vapour that does not condense in a cooling stage (Thermodynamic pseudo-equilibrium model)
p	Pressure (atm)
T	Temperature (°C)

Abbreviations

AGR	Acid gas removal
CCS	Carbon capture and storage
FZJ	Forschungszentrum Jülich
IC	Ion chromatography
ICP-OES	Inductively coupled plasma with optical emission spectroscopy
IGCC	Integrated gasification combined cycle
m/z	Mass-to-charge ratio
MBMS	Molecular beam mass spectrometer
ppb	Parts-per-billion
ppm	Parts-per-million
TE	Trace element
WGS	Water-gas shift
ZEA-3	Zentralinstitut für Engineering, Elektronik und Analytik (Central Institute for Engineering, Electronics and Analytics)

1. Introduction

1.1. Background

The International Energy Agency predicted a 76 % increase in the global energy demand from the year 2007 to 2030 with fossil fuels continuing to dominate the fuel mix [1]. Coal is the world´s most abundant fossil fuel reserve and it is responsible for about 40 % of electricity in the world, with a significant increase being expected in the next years [1, 2]. Coal is projected to account at least one-quarter of all energy needs by 2030 [3]. Furthermore, coal reserves are widely distributed throughout the world and the total recoverable reserves of coal are estimated to be more than 930 billion short tons. This is enough coal to last approximately 150 years at current consumption levels [4].

In general, but in terms of the measurable reserves, coal constitutes ca. 33 % of the fossil fuel supplies of the world as is shown in Figure 1. In terms of the energy content, coal (68 %) and natural gas (13 %) are the major energy-containing fossil fuels, petroleum (19 %) making up the remainder.

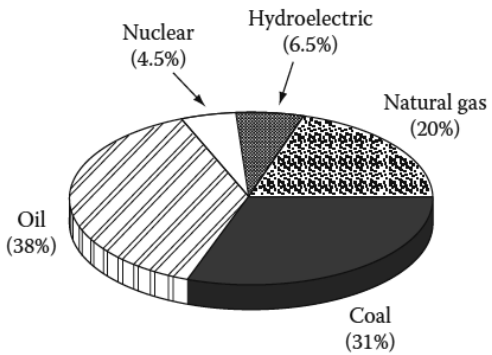

Figure 1. Distribution of world energy supplies [21].

However, coal utilisation leads to high emissions of CO_2 in comparison with other fossil fuels like natural gas or crude oil [6, 7]. For that reason, along with the increase of coal use, the concern about the environment and climate change grows [5]. Clean and more efficient technologies in the energy production are indispensable for addressing the rising energy demand and environmental issues [8].

Despite the efforts to replace fossil fuels with regenerative energies, it is predictable that coal will be the primary source of energy for the next several decades well into the next century. In Germany, the low mining costs and the abundance of low-rank coal makes this fossil fuel to play an important role in the electricity generation. Therefore, until other energy sources supplant coal, the challenge is to develop technological concepts that provide the maximum, and environmentally efficient, recovery of energy from coal [9].

There are a number of processes that are being used in coal-fired power stations that improve the efficiency and environmental acceptability of coal extraction, preparation and use, and many more are under development [10]. These processes are collectively known as *clean coal technologies*. The term clean coal technology refers to a new generation of advanced coal utilization technologies that are environmentally cleaner and in many cases more efficient and less costly than the older, and more *conventional* coal-using processes [5]. An important repowering approach attracting great interest is the IGCC system with integrated hot gas purification and CO_2 separation [11]. The IGCC is able to use a wide variety of solid, carbogeneous fuels with high efficiency [12]. Besides, this technique facilitates the CO_2 capture, making the technique environmentally friendly [13, 14]. The characteristics of the IGCC technology make it attractive for CO_2 capture because syngas is generated at elevated pressures in the gasifier and then chemically converted to enrich the CO_2 concentration. Generally, IGCC offers high efficiencies. In addition, IGCC has the advantage of using less water, about 33 %, than a similar-size pulverized coal fired plant [15].

Nevertheless, coal contains trace metals of particular environmental concern that are released in particles or in vapour form during gasification. These hazardous traces of heavy metals impact the atmosphere, human health and cause technological problems in gasification plants like corrosion and fouling of downstream components [16]. Due to the large quantities of coal consumed, large amounts of potentially hazardous trace elements are released into the environment every year [17]. An increased efficiency and a decreased amount of heavy metal species can be accomplished through hot fuel gas cleaning. However, in order to develop clean up techniques that eliminate the heavy metals, it is necessary to understand their behaviour during the gasification process. Trace element behaviour in conventional coal combustion systems is reasonably well known. However, there is a lack of similar knowledge in coal gasification, especially in the case of IGCC. Studies on the impact of flue gas impurities on the condensation of heavy metal vapours are still scarce. Therefore, there are a lot of open questions regarding the release and condensation mechanisms of heavy metals. Only a comprehensive knowledge of the release and condensation of heavy metal makes possible a better understanding of the gasification process and the development of cleaning systems capable of reducing or removing the trace metals in the process. For this purpose, it is of great interest to carry out investigations in

order to elucidate the release and condensation behaviour of heavy metals under gasification conditions.

1.2. Aim of the thesis

The aim of this thesis was to determine the condensation and release behaviour of some heavy metals under gasification conditions. The metals considered in this study were Zn, Cd, Pb, As, Sn and V. Some investigations established that the moisture, chlorine and sulphur content of coal might have a significant influence on the behaviour of some trace metals. Thereby, the main goal was to assess the influence of H_2O, HCl and H_2S on the condensation and release of the metals mentioned above. However, for a better understanding of the behaviour of the trace metals, measurements under different atmospheric conditions were needed. Qualitative and quantitative data of the species, as well as a comprehensive knowledge of the release and condensation of the trace metals are essential to develop adequate hot gas cleaning systems. Therefore, the condensation behaviour (temperature and speciation) of the heavy metal vapours was investigated in a heated flow channel reactor housed in a furnace with a gas cooling zone. Glass filters were placed on different stages along the cooling zone for the deposition of the metal compounds. The metal species deposited in the filters were firstly dissolved and afterwards determined by means of ion chromatography (IC) and inductively coupled plasma optical emission spectroscopy (ICP-OES). The release of the inorganic vapours was accomplished in a heated flow channel reactor coupled to a molecular beam mass spectrometer (MBMS) in order to analyse the gas in-situ. The experiments were carried out under typical gasification conditions. Different concentrations of H_2O, HCl and H_2S were considered in the experiments. Additionally, Scheil-Gulliver cooling calculations were performed by FactSage 6.3 in order to predict the behaviour of the trace metals under the influence of H_2O, HCl and H_2S. A thermodynamic pseudo-equilibrium model was utilized to help understanding the condensation mechanisms of the trace metals. Thus, the results of the simulations were compared with the experimental results in order to estimate the reliability of the predictions. An enhanced knowledge about the behaviour of Zn, Cd, Pb, As, Sn and V is of vital importance for the development of hot gas cleaning systems in the next generation coal power plants.

2. Fundamentals

2.1. Coal

2.1.1. Origin and nature of coal

Coal is fossilized peat. The peat that became today´s coal was laid down millions of years ago. Buried peat is converted to coal when high pressure and elevated temperature is applied to the buried layer. This process is known as coalification. The physical and chemical structure of the coal changes over time. As shown in Figure 2, the youngest (least converted) coal is known as lignite, which can be further converted to sub-bituminous coal, bituminous coal, and finally anthracite. These coal types strongly influence the properties and use of coal [18].

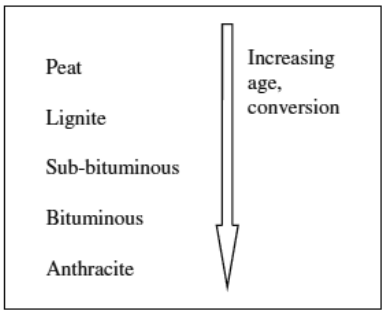

Figure 2. Coalification [18].

2.1.2. Occurrence of trace elements in coal

Coal contains most elements in the periodic table and these are released, on particles and in vapour form, by coal combustion and gasification [19]. Some of these are essential for healthy plant and animal life, whilst some others are toxic in low quantities. Due to the large quantities of coal consumed, especially for electric power generation, large amounts of potentially hazardous trace elements are released into the environment every year [17].

The trace elements are elements present in low concentrations, usually < 1000 ppm. The trace elements of particular environmental concern with respect to coal utilization are indicated in Table 1. The approach classifies the elements as those of greatest concern, moderate concern, and minor concern. The term trace element includes those elements otherwise termed *trace metals, heavy metals, micro-elements*, and *trace inorganics* [17].

Table 1. Trace and minor elements of environmental concern with respect to coal utilization [17].

Elements of greatest concern
As, B, Cd, Hg, Mo, Pb, Se
Elements of moderate concern
Cr, Cu, Ni, V, Zn
Elements of minor concern
Ba, Co, Ge, Li, Mn, Sb, Sr
Radioactive elements
Rn, Th, U
Elements of concern, but present only in very low concentrations
Be, Sn, Te, Tl

However, the concentrations of trace elements vary depending on the rank of the coal and its geological location. Therefore, the knowledge of the modes of occurrence of trace elements is essential in order to assess their behaviour during coal utilization, and its potential environmental impact [17].

A variety of other elements occur also in coal but their presence and amounts are strictly dependent upon the coal source [20].

Coal, compared to other fossil fuels, has relatively high levels of sulphur. Therefore, sulphur is an important consideration in coal utilization. Sulphur exists in coal as organic sulphur compounds and as inorganic pyrites. When coal is gasified, the reaction environment is reducing, as opposed to the oxidizing environment in coal combustion. Consequently, sulphur in coal is converted primarily to hydrogen sulphide (H_2S) gas, with lesser quantities of carbonyl sulphide (COS). Solid catalysts are used to adjust the syngas composition or convert the syngas to chemicals and hydrocarbon fuels. Besides, sulphur compounds are poisons for many of these catalysts and they need to be removed from the syngas. If the syngas is to be burned as a fuel, removal of the sulphur compounds from the syngas will avoid SO_2 emissions [18]. The amount of organic sulphur is usually 3 % w/w of the coal, but exceptional amounts of sulphur (up to 11 %) have been recorded [21].

The fate of sulphur during thermal coal utilisation was the object of comprehensive research. It was identified as a highly volatile species [22]. Most of the sulphur is converted to gaseous forms like H_2S, COS, SO_2, and CS_2, and only minor amounts can be found in the ash [23].

Chlorine occurs in coal [24] and is believed to be a factor not only in fouling problems but also in corrosion problems [25]. The chlorine content of coal is normally low, usually only a few

tenths of a percent or less. It occurs predominantly as sodium, potassium, and calcium chlorides, with magnesium and iron chlorides present in some coals. There is evidence that chlorine may also be combined with the organic matter in coal. In terms of corrosion the occurrence of chlorine in coal leads to the formation of hydrogen chloride and the condensation of water containing hydrogen chloride (hydrochloric acid) on the cooler parts of combustion equipment can lead to severe corrosion of the metal surfaces [21].

Origins of trace elements in coal

The trace elements present in coal were concentrated by processes which took place before, during, and after the formation of the coal. A variety of factors influence the trace element content of coals, including [17]:

- concentration of trace elements during growth of vegetation;
- enrichment of trace elements during the decay of plant material;
- sedimentation and *diagenesis*;
- burial and coalification;
- subsequent mineralization.

Elements are often described as being *chalcophile* or *lithophile.* Chalcophile elements have a strong affinity for sulphur, typically associated with sulphide or minerals. Lithophile elements possess a strong affinity for oxygen, and are typically associated with aluminosilicate minerals. Moreover, trace elements tend to associate with either the inorganic or organic components of coal (see Figure 3).

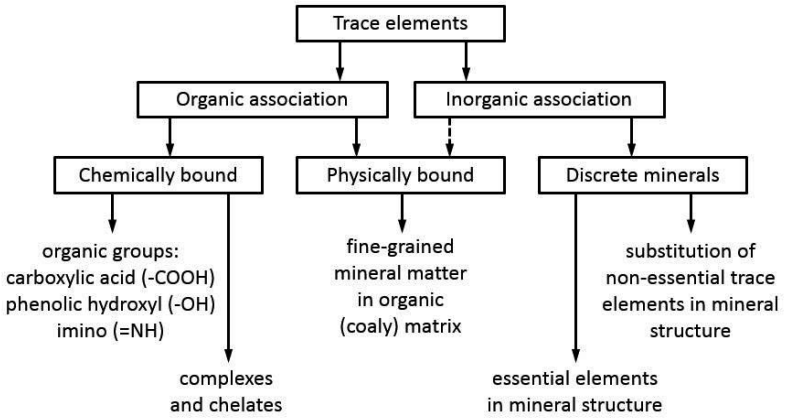

Figure 3. Modes of occurrence of trace elements in coal (adapted from [17]).

Trace elements intimately associated with the organic material may be either *chemically* bound or *physically* bound. A literature review of this topic was made by Swaine [26]. Most trace elements are associated primarily with the mineral portion of the coal, although the predominant mineral species containing a particular element can vary considerably. The major mineral phases found in coals are aluminosilicates and silicates, carbonates and sulphides [17]. Coals may also contain a wide range of accessory minerals, which may be important sources of some trace elements. Many elements of environmental concern (such as As, Cd, Hg, Pb, and Se) are typically associated with pyrite and other sulphide minerals.

However, it is probable that most elements show some degree of mixed association between organic and inorganic material [17].

Definitely, a detailed understanding of the occurrence of each element is crucial for assessing its behaviour during combustion or gasification, and its environmental impact.

Concentration of trace elements in coal

Trace element concentrations vary enormously between coals from different sources, and even between coals from the same seams. Coals from different parts of the same seam can contain quite different trace element compositions. This is the result of the complex and generally random way they entered the coal originally. The physical and chemical properties of a feed coal may be greatly altered by the mining, handling, and cleaning processes prior to combustion and gasification. Nevertheless, the usual range of trace metal concentrations in coal is known [17]. Table 2 lists typical concentrations for trace elements in world coals, soils, shale, and the crust.

Table 2. Typical concentrations (ppm) of trace elements relevant for this work in coal, soil, shale and crust (adapted from [17, 26-31]).

Element	Coal	(range)	Soil	Shale	Crust
Zinc, Zn	50	5 - 300	70	120	70
Cadmium, Cd	0.5	0.1 - 3	0.6	0.3	0.2
Lead, Pb	40	2 - 80	20	25	13
Arsenic, As	10	0.5 - 80	7	13	1
Tin, Sn	2	1 - 10	2	6	2
Vanadium, V	40	2 - 100	80	130	135

The origins and forms of trace elements in coal were reviewed in depth by Valkovic [32].

2.1.3. Coal use in the power generation industry

Coal is a combustible rock, and along with petroleum and natural gas it is one of the three most important fossil fuels, such as for the generation of electricity [21]. Coal fuels almost 40 % of

electricity worldwide. Coal has been the world´s fastest growing energy source in recent years-faster than gas, oil, nuclear, hydro, and renewables. The world currently consumes over 5 billion tons of coal per year and the majority is utilized in power generation industry (steam coal or lignite) [21].

In terms of energy reserves the world has much more coal than any other energy source [18]. A recent Coal Industry Advisory Board report [33] has highlighted that the world will remain dependent on the continued use of coal for many decades. In 2006, coal accounted for 27 % of world energy consumption, as shown in Figure 4 [5]. Coal use is projected to grow by over 60 % from 2006 to 2030, such that the developing countries will use 97 % of the projected increase [34]. However, coal is the most CO_2 intensive fossil fuel and is responsible for over 40 % of all energy related CO_2 emissions. The same report highlighted the measures needed to enable coal use to successfully meet CO_2 reduction targets [34].

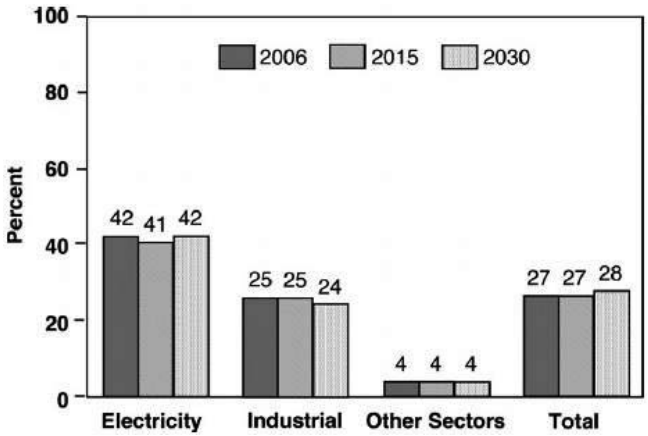

Figure 4. Coal share of world energy consumption by sector, 2005, 2015, and 2030 [5].

2.2. Gasification

Coal gasification offers one of the most versatile methods to convert coal into electricity, hydrogen, and other valuable energy-related products. In the gasifier, coal is typically exposed to steam and carefully controlled amounts of air or oxygen under high temperatures and pressures. Under these conditions, chemical reactions are initiated and typically produce a mixture of carbon monoxide, hydrogen, and other gaseous compounds.

The gasification of coal is the transformation of solid matter into gaseous fuels using O_2, H_2O, H_2 or CO_2, and heat. The product, known as synthesis gas, is a mixture consisting mainly of CO, H_2,

CO_2, H_2O, CH_4, and a small amount of minor compounds, e.g. H_2S and COS [8]. Coal gasification is carried out at temperatures between 700 – 1600 °C and at pressures up to 70 bar [35].

Gasification is an incomplete combustion of coal or another solid feedstock. The primary goals of gasification are:

1) Convert the entire non-ash fraction of the feed to gas;
2) Produce gasses that preserve, as much as possible, the heat of combustion value of the feedstock.

Combustion converts the feed to gas, but these gases cannot be further burned to generate energy. Gases from a gasifier can be burned to generate energy or chemically converted to other products [18].

Syngas leaving the gasifier contains numerous impurities such as ash, char, alkali metals, nitrogen compounds, tar, sulphur-containing compounds (including hydrogen sulphide), and (on occasion) chlorine-containing compounds. It also contains sulphur in the form of H_2S. Sulphur must be removed from syngas either to prevent emission of SO_2 when syngas is burned, or prevent catalyst poisoning in downstream reactors [18].

These elements present in coal may be low when compared to the carbon and hydrogen content but they have important environmental consequences when coal is used as fuel or as source of gaseous or liquids fuels [21].

2.2.1. The thermodynamics of gasification

During the process of gasification of solid carbon, whether in the form of coal, coke or char, the principle chemical reactions are those involving carbon, carbon monoxide, carbon dioxide, hydrogen, water (or steam) and methane. These are [36]:

Combustion reactions,

$$C + \frac{1}{2}O_2 = CO \qquad -111\frac{kJ}{mol} \qquad (2.1)$$

$$CO + \frac{1}{2}O_2 = CO_2 \qquad -283\frac{kJ}{mol} \qquad (2.2)$$

$$H_2 + \frac{1}{2}O_2 = H_2O \qquad -242\frac{kJ}{mol} \qquad (2.3)$$

the BOUDOUARD reaction,

$$C + CO_2 \rightleftarrows 2CO \qquad +172\frac{kJ}{mol} \qquad (2.4)$$

the water gas reaction

$$C + H_2O \rightleftarrows CO + H_2 \qquad +131\frac{kJ}{mol} \qquad (2.5)$$

and the methanation reaction.

$$C + 2H_2 \rightleftarrows CH_4 \qquad -75\frac{kJ}{mol} \qquad (2.6)$$

As reactions with free oxygen are all essentially complete under gasification conditions, reactions (2.1), (2.2) and (2.3) do not need to be considered in determining an equilibrium syngas composition. The three heterogeneous (i.e. gas and solid phase) reactions (2.4), (2.5) and (2.6) are sufficient.

In general, we are concerned with situations where the carbon conversion is also essentially complete. Under these circumstances, it is possible to reduce the equations (2.4) – (2.6) to the following two homogeneous gas reactions:

The CO shift reaction

$$CO + H_2O \rightleftarrows CO_2 + H_2 \qquad -41\frac{kJ}{mol} \qquad (2.7)$$

and the steam methane reforming reaction.

$$CH_4 + H_2O \rightleftarrows CO + 3H_2 \qquad +206\frac{kJ}{mol} \qquad (2.8)$$

Reactions (2.1), (2.4), (2.5) and (2.6) describe the four ways in which a carbonaceous or hydrocarbon fuel can be gasified. Reaction (2.4) is important for the production of pure CO when gasifying pure carbon with an oxygen-CO_2 mixture. Reaction (2.5) plays a predominant role in the water gas process. Reaction (2.6) is the basis of all hydrogenating gasification processes. But most gasification processes rely on a balance between reactions (2.1) (partial oxidation) and (2.5) (water gas reaction).

For real fuels (including coal, which also contains hydrogen), the overall reaction can be written as follows:

$$C_nH_m + {}^{n}/_{2}\, O_2 = nCO + {}^{m}/_{2}\, H_2 \qquad (2.9)$$

where

- for gas, as pure methane, $m = 4$ and $n = 1$, hence, $m/n = 4$
- for oil, $m/n \approx 2$, hence, $m = 2$ and $n = 1$
- for coal, $m/n \approx 1$, hence, $m = 1$ and $n = 1$

Gasification temperatures are in all cases so high that, thermodynamically as well as in practice, no hydrocarbons other than methane can be present in any appreciable quantity.

Indeed, gasification systems, when using appropriate gas cleaning methods, can meet the strictest environmental regulations pertaining to emissions of sulphur dioxide (SO_2), particulate matter, and other toxic compounds that contaminate coal such as mercury, arsenic, selenium, and cadmium. However, emissions are highly variable and depend on gasifier type, feedstock, process conditions (temperature and pressure), and gas conditioning systems [21].

2.2.2. Integrated gasification combined cycle

Gasification is one of the most versatile techniques of the thermal coal conversion. Several coal gasification technologies have been invented to handle different coals effectively and to satisfy every sector of energy demand [8, 37]. The goal of advanced coal conversion technology is to provide power generation that is highly efficient, reliable, cost-competitive, and environmentally friendly in comparison to conventional coal-fuelled power technology [38].

Integrated gasification combined cycle (IGCC) is a promising gasification process that has made significant efficiency improvements during the last decades [39]. IGCC is the integration of two different technologies: coal gasification from the chemical industry and combined-cycle power generation from the power industry [5]. In the IGCC systems, steam and hot pressurized air or oxygen combines with coal. The resulting *synthesis gas* (syngas), a mixture of carbon monoxide and hydrogen, is then cleaned and burned in a gas turbine to generate electricity. The heat energy from the gas turbine also powers a steam turbine. Since IGCC power plants convert two forms of energy, they have the potential to reach a fuel efficiency of 50 %. Sulphur species, nitrogen species, and particulate matter are removed before the fuel is burned in the gas turbine. Thus, there is a much lower volume of gas to be treated than in a post combustion scrubber. In IGCC the entrained-flow reactor works in the temperature range of 1400 to 1600 °C and at pressures up to 70 bar [8, 36, 37].

IGCC technology has proved to be commercially viable against conventional coal fired power plants. Many coal gasification plants for production of chemicals are in operation worldwide. Demonstration plants of IGCC in Spain and the Netherlands provide the reliability of this technique in commercial-scale applications [40]. The IGCC coal based power plants have high thermal efficiency (higher than 40 %), low environmental impact and can produce power as well as synthetic fuels, chemicals and marketable by-products making IGCC an attractive technology for the next century [12, 41].

One of the disadvantages of coal utilization is the release of CO_2, which is believed to contribute significantly to global warming. A challenge for clean coal technology is to produce power and to sequester carbon dioxide at a price that is competitive with alternative power sources. Inte-

grated gasification combined cycle (IGCC) coal plants with carbon capture and sequestration (CCS) have attracted a great deal of interest because the cost of electric power from these plants is only 60 % higher than conventional pulverized coal generated electricity [18]. The basic approach to minimise greenhouse emissions is to convert most of the syngas to H_2 and CO_2 using an acid gas removal (AGR). The CO_2 is sequestered [18]. To effectively reduce the CO_2 emissions from coal fired power plants, their efficiency needs to be increased. Various studies have shown that the efficiency of conventional and advanced IGCC plants with CO_2 capture is in the range of 32 – 43 % [43]. However, efficiencies of 50 % are needed to produce electricity at a competitive price [45]. It is important that the CO_2 sequestration is economically viable.

Since the increase in efficiency is not sufficient to meet national and international targets for CO_2 reduction, CO_2 shall be separated from the flue or fuel gas within the power generation process and stored [42].

To protect the combustion turbines and environment from emissions generated during coal conversion, a gas clean-up system must be employed [38]. The raw gas from any coal gasification process must be cleaned of particulate matter and sulphur gases in order to prevent erosion, fouling or corrosion of the gas turbine blades [44].

In IGCC plants the hot fuel gas is quenched and cleaned at relatively low temperatures. The gas clean-up consists of particle separation, wet scrubbing, COS hydrolysis, and wet desulfurization in order to provide a gas suitable for the gas turbine. If CO_2 needs to be separated, the gas is heated up again and the CO is shifted with high amounts of water to CO_2 and H_2. The CO_2 produced by the CO-shift is subsequently removed by a chemical or physical wash in which the gas is cooled down by a refrigeration process. This leads to a decrease of net power of approximately 2 – 3 %. Therefore, in the IGCC case with CO_2 separation the gas is cooled down twice to temperatures below 100 °C and 0 °C, respectively, and heated up again for the next step. This results in a significant efficiency loss. Hence, the overall efficiency of a state of the art IGCC with CCS technology is below 40 % depending on CO_2 removal rate. To avoid the efficiency loss in state of the art gas cleaning and CO_2 separation processes, it is necessary to develop gas cleaning and CO_2/H_2 separation processes working at a higher temperature [42, 43]. The development of H_2 and CO_2 membranes would contribute to obtain higher efficiencies.

Hot gas cleaning under gasification conditions is currently under development and it will allow the clean-up of the raw gas without cooling it to temperatures below the temperature of the next step [44].

A flow chart of an advanced IGCC power plant with integrated hot gas cleaning and CO_2 removal is presented in Figure 5.The IGCC concept with integrated hot gas cleaning and CO_2 removal consists of the following units: air separation, liquid slag separator, alkali removal, heat recov-

ery, hot gas cleaning, catalytic membrane, combustion chamber, gas turbine, heat recovery steam generator, steam turbine and generator [42].

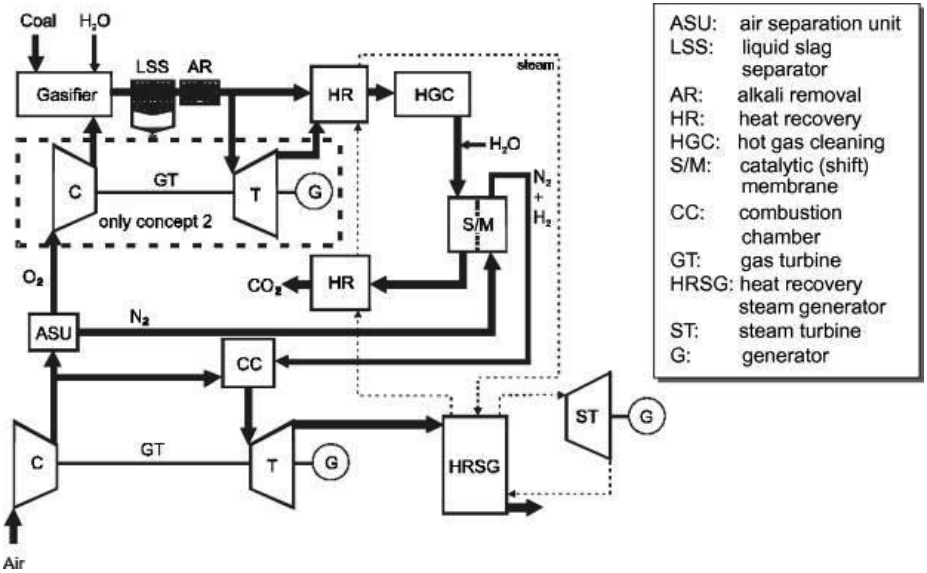

Figure 5. Flow chart of an IGCC power plant with integrated hot gas cleaning and CO_2 removal [42].

One of the challenges of designing IGCC plants is the management of slag, the semi-liquid by-product that forms from inorganic/ash forming elements in coal that do not gasify such as silicon, aluminium, and other metals. Furthermore, the most obvious disadvantages of generating power this way is the far higher capital cost of building an IGCC plant compared to conventional generation facilities [21].

2.2.3. Trace elements in gasification

Trace elements are introduced into the system in the feed coal as either inclusions in coal particles or discrete minerals and rock fragments. During combustion or gasification the particles undergo complex changes including the formation of char, agglomeration of melted inclusions, and vaporization of volatile elements. Physical processes related to plant design, turbulence, pollution control devices, temperature profiles, and other parameters affect the distribution of trace elements. Most elements are removed in the solid residues. However, varying amounts of certain trace elements are present in the flue gases in solid state and in the gas phase. These trace elements may be released into the atmosphere with the flue gases. The amount of each element emitted depends on [17]:

- the concentration in the coal;
- the size and type of boiler or gasifier;
- operating conditions;
- the efficiency of the pollution control devices;
- the distribution between various phases.

Partitioning of trace elements

Studies have shown that trace elements can be classified into three groups according to their partitioning during coal combustion [46, 47]. Trace elements show similar partitioning behaviour between different residue streams in gasification processes [48].

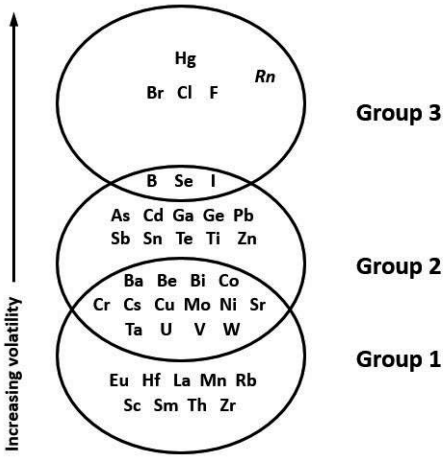

Figure 6. Classification of trace elements by their behaviour during combustion and gasification (after [17, 47-49]).

Considering this classification, the groups are as follows [17]:

Group 1 Elements which are concentrated in the coarse residues (combustor bottom ash or gasifier slag/ash), or partitioned equally between coarse residues and finer particulates (combustor fly ash or gasifier particulates) which are generally trapped by particulate control systems.

Group 2 Elements concentrated more in the particulates compared with coarse slag/ash. Elements which volatilise in the gasifier and condense downstream. They are enriched on the fine-grained particles which may escape particulate control systems.

Group 3 Elements which volatilize most readily. They are concentrated in the vapour or gas phase and are depleted in all solid phases.

Most trace elements are associated with the particulates. Volatile elements preferentially condense onto the surface of smaller particles in the flue gas stream because of the greater surface area to volume ratio. Thus the finest particles are enriched with certain Group 2 elements [17].

Figure 6 shows the overlapping classification of trace elements. This may be attributed to wide variation in operating conditions, and especially temperature, which control element volatility. Different authors use somewhat different definitions for each group. Some schemes are based on measured data such as enrichment factors.

Most elements are present in the residues remaining after combustion or gasification in the same relative proportions as in the feed coal, but are enriched in the ash by a factor equivalent to material emitted in the flue gases when the coal is burned [17].

Thus, the enrichment factor (EF) normalizes the concentration of a trace element in the input and output streams to the concentration of an element which is considered non-volatile during combustion.

$$EF = \left[(C_{te})_{output}/(C_{ne})_{output}\right] \times \left[(C_{ne})_{coal}/(C_{te})_{coal}\right] \quad (2.10)$$

C_{te} is the concentration of the trace element considered and C_{ne} is the concentration of the normalizing element in the output streams and the coal input streams.

Behaviour of trace elements during gasification

Coal is the main source of trace elements in gasification systems, although some elements are introduced in sorbents, additives, or fluxes. The distribution and behaviour of trace elements vary between individual gasification processes. However, both are very similar to the trace el-

ement behaviour within conventional power stations. The trace elements are partitioned into several output streams [17]:

- they may be retained in the gasifier slag/ash;
- they may leave with discharged particulates;
- volatilised substances may exit with flue gases.

The fate of volatiles and other chemicals species within the gasification process has been discussed by Clarke et al. [50], and is shown in Figure 7.

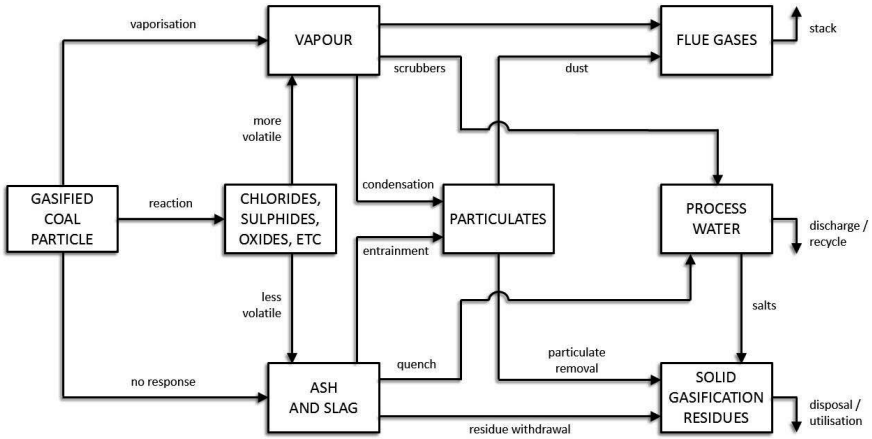

Figure 7. Fate of volatile species during the gasification process (adapted from [48]).

The partitioning is related to the trace element boiling point and chemical behaviour. The behaviour of the elements included in Group 2 in gasification is similar to that in combustion systems. In general, the concentration of trace elements tends to increase as the particle size in the exit streams decreases. For slag and particulates from slagging gasifier systems, the chalcophile trace elements (such as As, Se and Zn) are enriched in the particulates, whilst lithophile trace elements (like U and Th) are evenly distributed between the two fractions. Volatile elements, such as As and Se, may become greatly enriched as the particle size decreases. The most volatile elements (Group 3) do not condense out easily and are the most likely elements to leave the gasifier in the gaseous phase [17].

Behaviour of trace metals in gasification: The State of the Art

Investigations of the behaviour of trace metals during thermal treatment of coal, covering reducing and oxidizing conditions have been performed by several groups using several different experimental approaches, as well as by thermodynamic modelling. Experiments have been performed from lab scale and pilot-plant scale to commercial-scale IGCC plants. Although trace

element behaviour in conventional coal combustion systems is reasonably well known, there is a lack of similar knowledge in coal gasification, especially in the case of IGCC. The behaviour of volatile species in the reducing conditions of coal gasification may be different to that which occurs during combustion.

A study of the volatility and speciation of mercury during pyrolysis and gasification of five typical Chinese coals commonly used in gasification stations was presented by Li et al [51]. Laboratory-scale experiments were conducted to investigate the mercury volatility, speciation, and the following impacting factors: reaction temperature, holding time, atmosphere and compositions of coal such as halogen, sulphur and ash compositions. Temperature was the dominant factor on mercury volatility in both coal pyrolysis and gasification. The mercury volatility increased monotonically when the temperature increased. The release of mercury was slower under an inert atmosphere than under a reducing atmosphere. Hg^0 was the dominant species at most of the temperatures examined. The increases in minor halogen concentrations enhanced the volatility of Hg. It was hypothesized that Hg was oxidized mainly by chlorine species and the effects of sulphur content and iron content were negligible.

Šyc et al [52] investigated the behaviour and distribution of heavy metals in steam fluidized bed gasification of contaminated biomass. The blended fuel consisting of flax and hardwood (w/w = 40/60) was gasified by steam in a fluidized bed gasifier at about 850 °C and steam to biomass ratio of 1.01 kg kg^{-1}. Concentrations of selected heavy metals (Cd, Cu, Ni, Pb, and Zn) were determined in bed ash, cyclone ash, and in downstream producer gas. The subsequent order of heavy metals volatility was found: Cd (mostly in producer gas) > Pb > Zn > Cu > Ni.

The fate of trace elements in UK coals when gasified in a laboratory gasifier operating at 950 °C, and a pilot scale air-blown pressurized fluidized bed gasifier operated by British Coal was reported by Bushell et al [53]. The trace elements partitioned relatively uniformly between the bed ash and the primary fines, with elements such as Be, Co, Cr, Cu, Mo, Pb and V showing a slight preference for the primary fines, while Ba, La and Sr showed a marginal preference with the bed ash. They suggested that the physical association of the trace elements with the decomposed mineral matter is perhaps as much, if not more important than the relative volatility of each element.

Sekine et al [54] carried out coal combustion and gasification experiments using several kinds of coal at various temperatures and atmospheric conditions to examine the release behaviour of trace elements. The results showed that the temperature, atmosphere, and chlorine contents in coal affected the release of trace metals. Metals such as Hg, Zn, Se and Sb were partly released from coal during combustion, gasification and pyrolysis, while metals such as V, Cr, Mn, Co and Ni were not emitted at these temperatures. Oxygen or steam in the operating atmosphere affected the behaviour of Hg, Se, Sb, and Zn release from coal. Moreover, the release of

Se and Sb was promoted when steam existed in atmosphere. In that situation, the release of Hg was suppressed. The main result: the greater the chlorine contents of coal, the greater the amount of released Zn. It was considered that Se and Sb in coal were not chlorized by chlorine emitted from coal.

According to Mojtahedi [55] much greater proportions of Hg, Cd, Pb and Zn are volatilized by fluidized-bed gasification than by fluidized-bed combustion of coal, and thus, much higher concentrations of the metals could exit from the reactor in the vapour-phase. Hence, removal of the volatilized metals, should it be required, is more acute in gasification than in combustion. The calculations also reveal a greater proportion of the fuel-bound metal, to be present in the elemental form in gasification than in combustion. This could be due to the fact, that at elevated temperatures and in a reducing environment, some compounds of these metals are thermodynamically unstable and will decompose to reduced forms of the inorganic species and elemental metal. Chlorides of all four metals form in both combustion and gasification but at much lower concentrations in gasification. Oxides are found only in the combustor effluent streams.

In another study carried out by Helble et al [56], the fate of trace element pollutants in an IGCC bench-scale program, measuring the partitioning behaviour of selected trace elements during atmospheric pressure entrained flow gasification of Illinois No.6 bituminous coal was examined. It was shown that a significant mass fraction of As, Se, Sb, Hg, and Pb vaporized during gasification of this coal, whereas Cd, Cr, Co, Mn, Ni, U and Th were relatively non-volatile. Under the reducing conditions associated with the gasifier product gas, As, Sb, Pb, Hg and Se remained in the vapour phase at temperatures of 773 – 873 K. In this study the experimental data were used in conjunction with thermodynamic equilibrium calculations to investigate the downstream behaviour of the volatile elements.

The occurrence and distribution of trace elements (Pb, Zn, As, Ge, Cd, Ti, Bi, Sn, Ni, Fe and V) in condensates arising from coal gasification was investigated through the study of samples physically deposited on the gas cooling system from the Puertollano IGCC 335 MW power plant by Font et al [57]. This study provides important information on the behaviour of trace elements during coal gasification and also on the mode of occurrence of these elements in IGCC fly ash. Pb, Zn, Ge and Fe sulphides, Ni-Fe arsenides, Ge and V oxides as well as traces of K chloride and Pb, Zn and Fe sulphates were determined as the major bearing phases for these elements. Three condensation zones were differentiated as function of the condensation temperatures and metal content: 1. Pb zone (520 – 750 °C), characterized by the dominance of galena (PbS), and by the condensation of pyrrhotite ($Fe_{(1-x)}S$) and nickeline (NiAs); 2. Ge-Zn-Pb zone (520 – 470 °C), with sphalerite ((Zn,Fe)S) and wurtzite being the dominant crystalline phases and GeS_2 and GeO_2 reaching 30 % of the bulk condensates. 3. Zn zone (300 – 400 °C), characterized by

the dominance of Zn sulphides. The results obtained from these highly metalliferous condensates showed similar forms of occurrence for the studied elements to those obtained in the bulk Puertollano IGCC fly ash, where the contents of these elements are much lower.

Studies on partitioning of elements in fixed bed gasifier [58-60] revealed a similar behaviour of a number of elements in coal combustion. These studies reported Hg as a highly volatile element and Se, Cd, Pb, As (in decreasing order) as volatile elements during gasification with subsequent condensation on ash particles. Cu, Mo, Ni, and Zn showed a relatively low volatilization and condensation while Ba, Co, Cr, Mn and V were found as non-volatile elements. A good agreement between FactSage equilibrium model and measurements was attained in this study.

Reed et al. [61] used a thermodynamic equilibrium model to make predictions of the speciation of trace elements in the fuel gas from a 2 MW_t air-blown fluidized bed gasifier. In contrast to previous studies of this nature, experimental data was available to enable the validation of these predictions to be tested. Thermodynamic predictions were generated for the speciation of As, Be, B, Cd, Co, Cu, Pb, Sb, Sn, V and Zn. Calculated results were compared with data from tests covering a range of feedstock combinations (coal, sewage sludge pellets, etc.) and a range of hot gas filter temperatures. The nonvolatility of Be, Co, Cu, V and Zn under these conditions was predicted by the equilibrium modelling calculations and confirmed by the experimental data. The elements As, B, Cd, Sb, and Sn were all predicted to form a larger amount of gaseous species than measured experimentally. They attribute these differences to the current unavailability of thermodynamic data for the more complex minerals and adsorbed species that may be formed.

Thermodynamic equilibrium calculations using the HSC-Chemistry Program were performed by Díaz-Somoano et al. [62] to determine the distribution and mode of occurrence of potentially toxic and corrosive trace elements in gases from coal gasification processes. The influence of temperature, pressure and gas atmospheres on equilibrium composition was evaluated. The calculations were performed in typical coal gasification atmospheres, at a range of pressure between 0.1 and 4 MPa, and a temperature interval between 0 and 1600 °C. These temperatures include gasifier operation temperatures (1600 – 800 °C), hot (800 – 600 °C) and low (500 – 200 °C) temperatures in gas cleaning systems and flue gas emission temperatures (< 200 °C). The coal gasification atmospheres used here, differed in their H_2S and HCl content. In the reducing conditions, the behaviour of trace elements is complex, but some form of organization can be attempted. Elements were classified into three groups. The trace elements in the first group (Group A) would include those that may be totally condensed in gasification gas cleaning and emission conditions. This is the case for Mn. The elements mainly present in gas phase in most conditions (Se, Hg, and B) including flue gas emissions would be classified in Group C. The rest of the elements would form an intermediate group (Group B), which contains those ele-

ments that could be totally or partially in gas phase in gas cleaning conditions, and can be divided into two groups, depending on whether the cleaning conditions are hot or cold. Group B1 would include those elements that are totally or partially in gas phase at the temperature of hot gas cleaning systems (500 – 800 °C), as in the case of Co and Be, and subgroup B2 would contain the elements totally or partially in gas phase at low temperature gas cleaning conditions (< 500 °C), i.e. Sb, As, Cd, Pb, Zn, Ni, Cr and V.

The combustion studies have already revealed some interesting synergies and it is suspected that the chlorine and/or sulphur content of the fuels has a significant influence on the behaviour of some trace elements during combustion. These suspicions have been reinforced by the modelling studies of Frandsen et al. [63], who compared thermodynamic equilibrium predictions for trace element species during combustion with and without the presence of sulphur and chlorine. Specifically, enhanced volatilization of some elements was predicted due to the formation of gaseous chlorides, whereas volatilization of other elements may be inhibited by the formation of solid sulphates.

This dependency was also investigated experimentally by Miller et al. [64] by injecting first hydrogen chloride and then sulphur dioxide into a suspension-firing reactor burning wood-bark under simulated fluidized bed combustion conditions. Data interpretation was aided by parallel theoretical studies, using a thermodynamic equilibrium model. The influence of chlorine and sulphur was confirmed for some, but not all, of the 10 trace elements studied. Injection of HCl served to increase the emission of Cd, Cu, Mn, Zn, and possibly Cr and Ni. Injection of SO_2 served to increase emissions of Cd, but reduced emissions of As and Hg. The thermodynamic model proved valuable for interpreting the experimental data. HCl was generally more influential for trace element release than SO_2.

The partitioning of trace elements and the influence of the feed conditions (50:50 coal/petcoke feed blend and limestone addition) was investigated by Font et al. [65]. To this end, feed fuel, fly ash and slag samples were collected under different operational conditions at the 335 MW Puertollano IGCC power plant (Spain) and subsequently analysed. The partitioning in the Puertollano IGCC plant may be summarized as follows: (a) high volatile elements (70 – 99 % in gas phase): Hg, Br, I, Cl and S; (b) moderately volatile elements (up to 40 % in gas phase and > 60 % in fly ash): As, Sb, B, F, Cd, Tl, Se, Zn, and Sn; (c) elements with high condensation potential: (> 90 % in fly ash): Pb, Ge, Ga, and Bi; (d) elements enriched similarly in fly ash and slag elements (> 70 % in the slag): Cs, Rb, Co, S ,K, Cr, V, Nb, Be, Hf, Ta, Fe, U, Ti, Al, Si, Y, Sr, Th, Zr, Mg, Ba, Mn, Ca, and Li. The volatility of As, Sb, and Tl and the slagging of S, B, Cl, Cd, and low volatile elements are highly influenced by the fuel geochemistry and limestone dosages, respectively.

Jiao et al. [66] concluded that controlling SO_2 and/or H_2O concentration in flue gas during incineration favoured the transformation of toxic chlorides into less hazardous sulphates, reducing the toxicity of combustion residues. They investigated experimentally the effect of HCl, SO_2 and H_2O on the condensation distribution of Pb, Cd, Zn and Cu vapours in a lab-scale rotary kiln furnace coupled with a multi-cooling zone. The results indicated that Pb, Cd and Zn condensed as their chlorides, whereas Cu deposited as a mixture of CuO and $CuCl_2$ at the temperature range of 853 – 473 K in the presence of HCl in the $N_2/O_2/CO_2$ mixture. The presence of SO_2 and/or steam in flue gas facilitated the conversion of chlorides into sulphates, thereby improving the deposition propensity formed at the temperatures above 853 K. Coexistence of the four metal vapours in flue gas caused the increase of Cd, Zn and Cu sulphates fraction as a consequence of the heterogeneous nucleation of metal vapours on the pre-existing $PbSO_4$ nuclei. Super-cooling lowered the condensation temperature of the metal vapour species, which was greatly compensated by the heterogeneous nucleation once SO_2 and/or H_2O were present in the flue gas. The condensation mechanisms of metal vapour species during flue gas cooling were clarified through the comparison of the experimental results with the prediction of a thermodynamic pseudo-equilibrium model.

The behaviour of trace elements in pollution control systems downstream of the combustor or gasifier was also reviewed by Clarke [67]. During combustion or gasification, coal particles undergo complex charges that lead to the vaporization of volatile elements. Trace elements are partitioned into several output streams, including solid coal residues and flue gases which enter downstream pollution control devices. They concluded that, because volatile trace elements are enriched in the fine particulate material carried downstream of the combustor or gasifier, the emission of these trace elements depends more on the efficiency of the gas cleaning systems than on the method of coal conversion. High-efficiency particulate controls, such as electrostatic precipitators (ESP) or bag houses, can reduce emissions of particulate-bound trace elements to low levels. Scrubbing systems can effective control the emissions of the more volatile trace elements, although they are less effective for B, Hg and Se. Although flue gas cleaning systems may successfully prevent emissions of trace elements to the atmosphere, they do concentrate elements in residue and waste water streams.

Díaz-Somoano et al. [68] ascertained the ability of fly ashes to retain As, Se, Cd and Zn species in hot gas from gasification systems in different conditions. The influence of temperature (550 and 750 °C) and gas composition (with and without H_2S and HCl) on retention capacity was evaluated. The retention of Cd in the fly ash in the experimental conditions was very low compared with the retention of arsenic and selenium, and was lower in a gas atmosphere containing HCl. The retention capacities for Zn at 750 °C were higher in an atmosphere free of HCl and H_2S. It was concluded that this fly ash was an efficient sorbent for retaining As, Se, and Zn compounds in the gas phase from a coal gasification flue gas, retention capacities varying with tem-

perature and gas composition. The use of fly ashes, which are a sub-product of coal utilization processes, is of great interest for this application from the point of view of cost and availability.

The review of the literature on the behaviour of trace metals under gasification conditions shows the lack of quantitative analysis of TE´s emissions. Several works have been conducted to date to investigate the vaporization of heavy metals at high temperature processes and their distribution in flue gas. Nevertheless, studies on the impact of flue gas impurities on the condensation of heavy metal vapours are still scarce. Little is known regarding the condensation behaviours of metallic vapours during flue gas cooling and its variation with a variety of parameters including cooling rate and flue gas composition. Experimental data from gasification systems is limited. Therefore, thermodynamic equilibrium studies using different computer programs have been carried out to gain an initial insight into trace element partitioning in gasifiers and to compensate the lack of data on chemical and physical forms on trace elements during coal gasification. However, this can only serve as a guide to what might happen under the conditions that are studied. Experimental validation of the predictions is therefore very important.

For this purpose, it is of great interest to elucidate the condensation behaviour of heavy metal vapour species during the flue gas cooling stage. Besides, there are also a lot of open questions regarding the release mechanisms. Hence, it is pivotal to clarify the effect of H_2O, HCl and H_2S on the release and on the condensation of the heavy metals vapours, aiming to better understand the gasification process and to gain an insight into optimizing the gasification process to achieve a reduction of the trace metal emissions.

3. Experimental setup and methods

3.1. Experimental setup

Two different experimental setups were used to carry out the experiments: An atmospheric flow channel reactor with a cooling zone for the condensation experiments and an atmospheric flow channel reactor coupled to an MBMS system for the release experiments.

The initially considered atmospheric conditions were a real output gas composition from a coal gasifier and a gas composition before the water-gas shift reaction (WGSR) with a steam to CO ratio of 1.5 (see Table 3).

However, due to the goal of avoiding the use of CO in the laboratory, the search of alternative atmospheric conditions was necessary. The so-called lab conditions should replace the use of CO for the use of Ar or He. For these more fundamental investigations a CO-free gas mixture was used having the same hydrogen content and oxygen partial pressure after entrained flow gasification of coal and in the water-gas-shift reaction.

These conditions were obtained by curve-fitting the oxygen partial pressure evolution of the real conditions in FactSage. It was also required to keep the same hydrogen concentration. The results of the curve-fitting for both atmospheres are shown in Figure 8 and Figure 9. The corresponding conditions are given in Table 3.

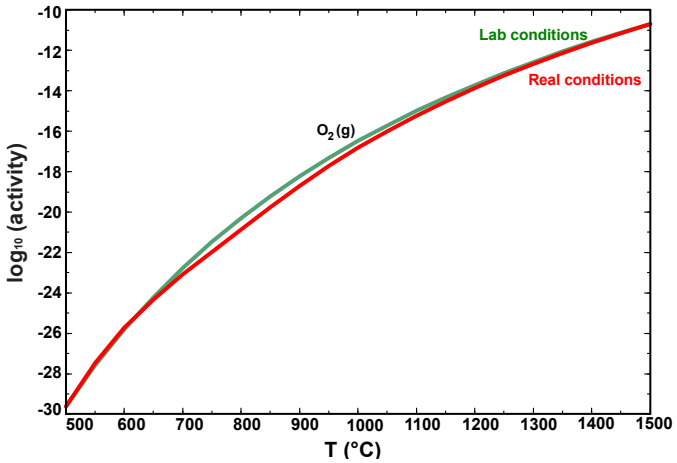

Figure 8. Oxygen partial pressure curve-fitting for the WGS lab conditions and the WGS real conditions.

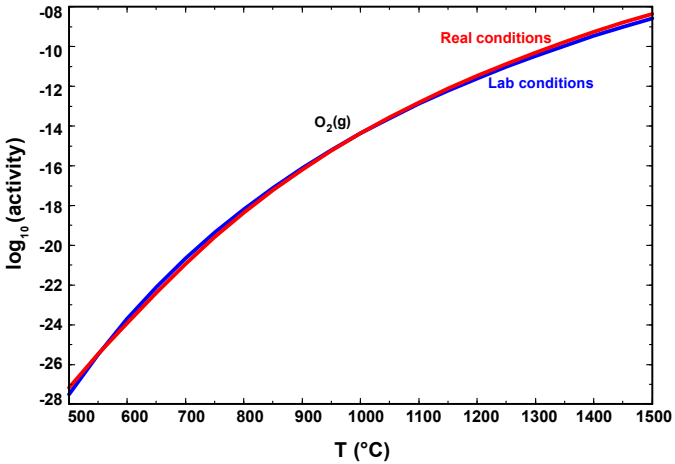

Figure 9. Oxygen partial pressure curve-fitting for the gasification lab conditions and the gasification real conditions.

Table 3. Overview of the experimental conditions that most closely described the real conditions.

Atmosphere	H_2 (%)	H_2O (%)	CO (%)	CO_2 (%)	Ar (%)
Water-gas-shift (real)	15	51	34		
Gasification (real)	29	2	66	3	
Water-gas-shift (lab)	**14**	**17**			**69**
Gasification (lab)	**28**	**3**			**69**

In order to validate this simplification some equilibrium calculations with zinc were carried out in FactSage to see the influence of the CO-free conditions on the experimental results. In the equilibrium calculations the same species were found in the real and laboratory conditions. The results showed only slight differences between the real and the laboratory conditions for both atmospheres. Therefore, the simplification was considered as valid and the so-called laboratory conditions without CO were taken as experimental conditions for all the experimental runs.

The gas flows for both experimental setups were calibrated with a DryCal Gas Flow Calibrator. They were specified with a Westphal WMR 4000 Flow Computer and controlled by Brooks mass flow controllers 5850 during the experiments.

3.1.1. Atmospheric flow channel reactor with a cooling zone

The condensation behaviour (temperature and speciation) of the heavy metal vapours was investigated in a heated flow channel reactor housed in a furnace with a cooling zone. The experimental setup is depicted in Figure 10.

The furnace had 13 independent heating zones. Eight of them were necessary for setting up the temperature gradient in the cooling zone of the furnace. Eight quartz glass filters were placed at different positions along the cooling zone for the deposition of the metal compounds. The metal species deposited in the filters were firstly dissolved and afterwards determined by means of ion chromatography (IC) and inductively coupled plasma optical emission spectrometry (ICP-OES).

Figure 10. Atmospheric flow channel reactor with a cooling zone.

A detailed description of the experimental setup and the temperature profile of the experimental setup are given in Figure 11 and in Figure 12.

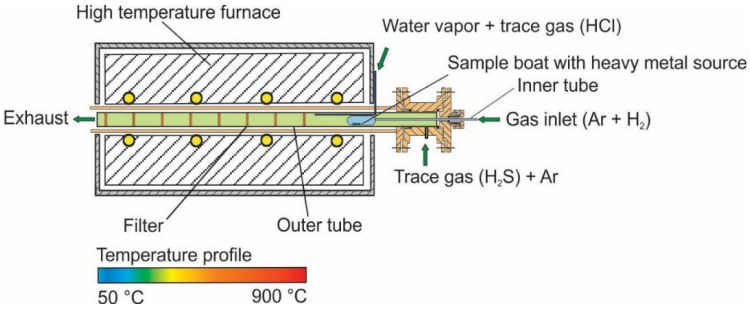

Figure 11. Schematic of the experimental setup for the condensation experiments.

The experimental setup for the condensation experiments consisted of two different parts: the reaction zone and the cooling zone. The reaction zone had an inner tube and an outer tube. The inner tube was used for introducing the heavy metal source and the "synthesis" gas (H_2 and Ar) into the experiments. The outer tube, however, was necessary for the introduction of H_2O and the trace gases HCl and H_2S.

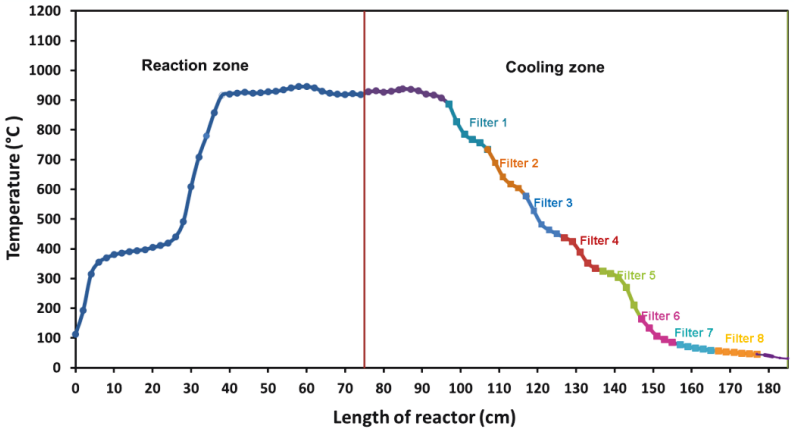

Figure 12. Temperature profile in the condensation experiments.

Both tubes were made of quartz glass. The outer tube had a total length of 210 cm. 75 cm of them corresponded to the reaction zone and 110 cm to the cooling zone. The inner diameter of the outer tube was 2.7 cm. The inner diameter of the inner tube was 1.4 cm and the total length was 77 cm. This tube also had a 5 cm gap in order to hold the sample boat for the introduction of the heavy metals. The sample boat was also made of quartz glass and had a total length of 4.5 cm. The additional cooling zone was necessary for the condensation of the heavy metals.

The temperature and position of each filter in the cooling zone is shown in Table 4. Each filter had a total length of 10 cm and was filled with quartz tube rings.

Table 4. Position and temperature of the eight filters present in the cooling zone.

Filter	T (°C)	Position (cm)
1	886.3 - 734.7	97 - 107
2	734.7 - 577.1	107 - 117
3	577.1 - 437.7	117 - 127
4	437.4 - 324.9	127 - 137
5	324.9 - 163.2	137 - 147
6	163.2 - 77.8	147 - 157
7	77.8 - 55.8	157 - 167
8	55.8 - 44.6	167 - 177

A typical experimental run was as follows: The inner tube with the sample boat containing the heavy metal source was introduced into the heated outer tube causing a slow vaporization of the metal in the synthesis gas. Additionally to the synthesis gas, HCl and H_2S were fed in from the outer tube to determine their influence on the condensation of the heavy metal vapours. The gaseous reaction products flowed to the cooling zone of the reactor where they condensed in the glass filters.

Figure 13. Quartz glass filter for the condensation experiments.

A peristaltic pump (Pumpdrive 5201 Heidolph) was used to introduce the water together with the trace gas HCl in the experiment. The water containing HCl was fed in the experiment through a quartz glass capillary (d = 1 mm) that was fixed to the top of the outer tube. In order to dose H_2S to the experiment, a triple-neck round bottom flask was used, where ferrous sulphide (FeS) reacted with an HCl solution and H_2S could be released. The HCl solution required for the reaction was introduced in the round bottom through a capillary. Argon was used as carrier gas. The desired average concentration of each heavy metal in each experiment was 100 ppm and the duration of each experiment was at least 24 h. The total gas flow was

650 ml/min except for the experiments with zinc, where the total gas flow was 510 ml/min. A summary of the conditions for all condensation experiments is given in Table 5.

During the heating and cooling phases of the experiments, the experimental setup was rinsed with inert gas (Ar). The exhaust gas from the experiments was fed to a gas washing bottle filled with a dilute sodium hydroxide solution for cleaning the gas before releasing it to the atmosphere.

As a safety measure, a flow controller was installed at the end of the experiment in order to measure the exhaust gas flow. In the event of a lower gas flow at the end of the experiment than at the entrance, the supply of H_2 and Ar as well as the kiln heating automatically stopped.

Table 5. Overview of the experimental conditions in the condensation experiments

Experimental run	Atmosphere	H_2 (%)	H_2O (%)	Ar (%)	HCl (ppm)	H_2S (ppm)
Influence of H_2O	Water-gas-shift	14	17	69	0	0
Influence of H_2O	Gasification	28	3	69	0	0
Influence of HCl	Gasification	28	3	69	50	0
Influence of HCl	Gasification	28	3	69	500	0
Influence of H_2S	Gasification	28	3	69	0	50
Influence of H_2S	Gasification	28	3	69	0	500

3.1.2. Atmospheric flow channel reactor coupled to an MBMS

Experiments on the release of the inorganic vapours were carried out in a heated flow channel reactor coupled to an MBMS in order to analyse the gas in-situ. The main aim of these experiments was to determine the species present in the gas phase and their behaviour under different experimental conditions. The channel was housed in a furnace with four heating zones. The total length of the outer tube was 90 cm and the inner diameter 2.7 cm. The inner tube had the same dimensions as the inner tube of the condensation experiments.

A detailed description of the experimental setup is given in Figure 14 and Figure 15.

Figure 14. Atmospheric flow channel reactor coupled to an MBMS.

The experimental setup for the release experiments was identical to the experimental setup for the condensation experiments. The only difference was that it only consisted of a reaction zone and did not include a cooling zone. The total gas flow was 4300 ml/min and the average heavy metal concentration was 100 ppm.

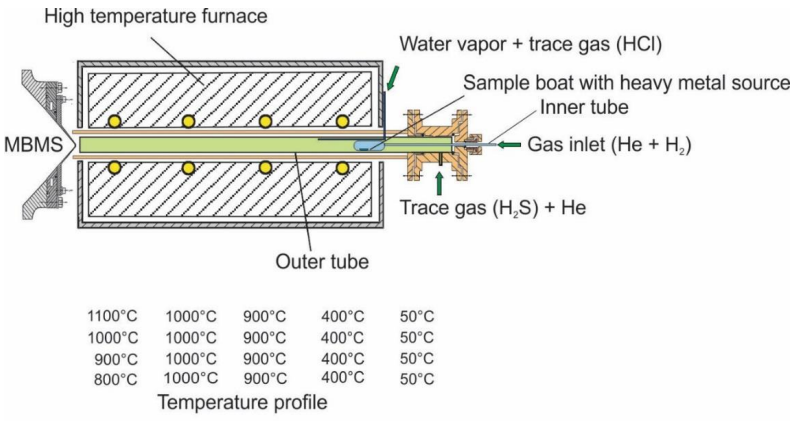

Figure 15. Schematic of the experimental setup for the release experiments.

An experimental run started, like it was in the condensation experiments, with the vaporization of the heavy metal in the synthesis gas. The end of the outer tube was coupled to the sampling orifice of the MBMS in order to sample the high-temperature products. The orifice of the MBMS needed to be placed at the end of the tube for maintaining the high temperature of it

and thus, avoiding the gas-phase species to condense at the nozzle of the MBMS. The gaseous reaction products entered the MBMS nozzle (diameter 0.3 mm) and were analysed. The fraction of non-analysed synthesis gas by the MBMS was discharged to a ventilation system.

The release experiments were carried out with different gas compositions and temperatures. The experimental conditions were exactly as in the condensation experiments (see Table 5). However, each experiment was carried out at two or three different temperatures at the end of the reactor. In this case, argon was replaced by helium, since its low atomic mass leads to high signal intensities in the MBMS. The temperature profile of the release reactor with different temperatures at its end is shown in Figure 16.

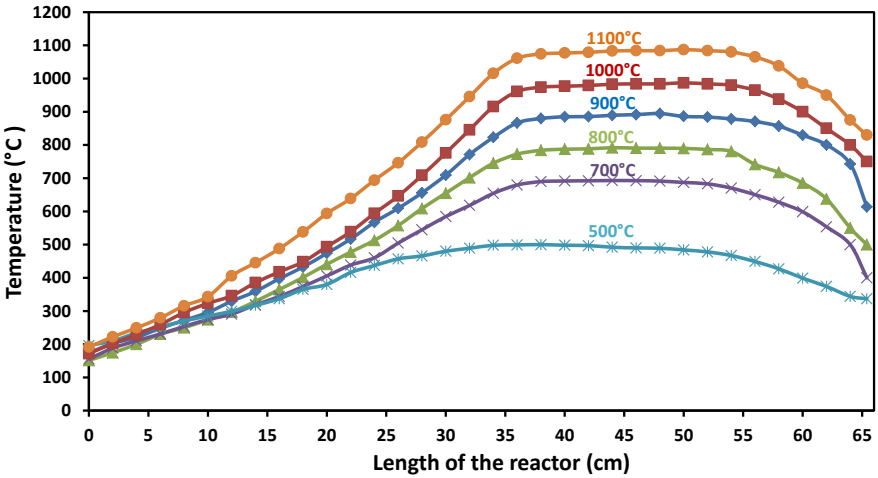

Figure 16. Temperature profile in the release experiments.

For the measurements, mass spectra from 10 to 400 amu were scanned and 10 scans per second were acquired. The monitored species for each experiment varied according to the heavy metal investigated. Thus, for every metal all the possible chlorine, oxygen and sulphur containing species that the metal could form were considered. This is explained in detail in the corresponding results chapter. The qualitative information of the spectra was transformed into quantitative data for every experiment. This required a calibration before the experiments. Therefore, the considered species were evaporated at different temperatures and monitored within the time. The averaged isotope signal intensities and the species concentrations were correlated. The species concentrations were calculated with the weight difference of the species before and after the experiment. Thereby it was possible to quantify the released amount of a species (ppm) in an experiment just knowing the signal intensity of the species.

Nevertheless, due to the strong temperature gradient in the reaction zone of the furnace, the concentration of the trace metals in the gas phase varied from experiment to experiment. Therefore, only a qualitative study of the gas species could be achieved.

3.2. Determination and quantification of the condensed metal species

The outer tube used in the condensation experiments as well as the eight quartz filters present in the cooling zone of the condensation experiments were analysed after each experiment. The metal species deposited in the filters and in the tube were firstly dissolved and afterwards determined by means of ion chromatography (IC) and inductively coupled plasma optical emission spectroscopy (ICP-OES). These analyses were carried out by the central division of analytical chemistry (ZEA-3) of the Forschungszentrum Jülich. The results of the analyses were compared with the weight gain of the filters during the experiments. Thus, the filters were weighed before, after the experiments and after dissolving the metal compounds that deposited in them during the experiments.

The ICP-OES method enables a multi-element determination in solutions or after appropriate sample preparation of solid samples brought into solution. The precision is 1 – 3 % for major elements and ± 10 – 30 % for traces. IC allows a rapid simultaneous multi-ion determination in aqueous solution. The solid samples, which are insoluble in aqueous solutions can be analysed after extraction or combustion.

Since the condensation experiments were carried out with different metals, also different metal compounds were expected to appear and condense. Therefore, for each metal considered, it was required to find a suitable method to dissolve and separate the possible condensing compounds. The metals considered in this study were Zn, Cd, Pb, Sn, As and V.

The systematic procedure to separate the metal compounds in the filters was as it follows [69-74]. In the experiments with zinc, $ZnCl_2$, ZnO and ZnS were dissolved in water, acetic acid (30 %) and hydrochloric acid (25 %), respectively. The determination of Zn^{2+} and Cl^- by ICP-OES and IC of the solutions allowed the quantification of the zinc compounds in every filter. In the experiments with cadmium, $CdCl_2$, CdO, CdS and Cd were dissolved in water, sulphuric acid (25 %), hydrochloric acid (25 %) and nitric acid (20 %), respectively. In this case the amount of Cd^{2+} was determined. Knowing the solubility of each compound in every acid, a good separation of the cadmium compounds was achieved. In the experiments with lead the sequence followed was: $PbCl_2$/PbS and PbO_2-PbO were dissolved in hydrochloric acid (25 %) and nitric acid (20 %). The elements analysed in this case were Pb^{2+} and Cl^-. Due to the similar solubility of the different arsenic compounds in water, hydrochloric acid, nitric acid, acetic acid, sulphuric acid, and sodi-

um hydroxide solutions, among others, the dissolution and separation of the metal compounds could not be achieved. Therefore, in the experiments with arsenic, the concentration of the condensed compounds was calculated with the difference of weight of the filters before and after the experiments.

The different coloration of the arsenic compounds was found to be a good tool for the identification of the compounds in every filter. In the experiments with tin two different sequences were followed depending on the trace gas present in the experiment. In the experiments with HCl, $SnCl_2$, SnO and Sn were dissolved in water, hydrochloric acid (25 %) and nitric acid (20 %). In the experiments containing H_2S, Sn/SnO and SnS were dissolved in nitric acid (20 %) and hydrochloric acid (25 %), respectively. In both cases, the remaining tin corresponded to SnO_2 and its concentration was calculated considering the weight loss of the filters after the separation of the above mentioned compounds. In all the cases a good agreement between the elemental analysis and the gained weight of the filters during the experiments was attained.

The relative error of the ICP-OES and IC analysis was ± 5 – 20 %. Furthermore, the relative error of the separation methods was approximately ± 0 – 20 %.

3.3. Molecular beam mass spectrometry

3.3.1. Principles of mass spectrometry

Mass spectrometry is an analytical technique that enables the determination of gaseous ionised species based on their mass-to-charge ratios (m/z) in an electromagnetic field.

Figure 17 shows a general scheme that every mass spectrometer follows. A mass spectrometer always consists of the following elements: a sample inlet to introduce the compound that is analysed, an ionisation source to produce ions from the sample, one or several mass analysers to separate the various ions, a detector to count the ions emerging from the mass analyser and a data processing system that produces the mass spectrum in a suitable form.

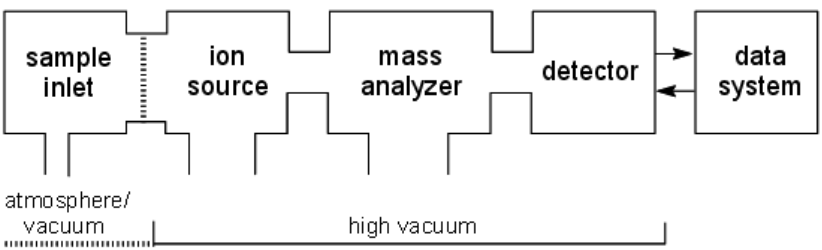

Figure 17. General scheme of a mass spectrometer [75].

Mass spectrometers always perform the following processes [76]:

1) Production of ions from the sample in the ionisation source.
2) Separation of these ions according to their mass-to-charge ratio in the mass analyser.
3) Detection of the ions emerging from the analyser and measure their abundance with the detector that converts the ions into electrical signals.
4) Processing the signals from the detector that are transmitted to the computer.

The use of a scale of atomic mass per number of elementary charges, termed *mass-to-charge ratio*, m/z, was adopted for the use of mass spectrometers. It must be understood as the ratio of the numerical value of ionic mass on the atomic mass scale and the number of elementary charges of the respective ion. Very often the number of elementary charges is equal to one. Therefore, as long as only singly charged ions are observed (z = 1), the m/z scale directly reflects the atomic mass scale. By definition, m/z is dimensionless.

A mass spectrum is a two dimensional representation of signal intensity versus m/z. The position of a peak in the abscissa reflects the m/z of an ion and the intensity of this peak correlates to the abundance of that ion [75].

3.3.2. Molecular beam mass spectrometer

A schematic diagram of the MBMS utilized for the release experiments is given in Figure 18. Molecular beam mass spectrometry is a reliable method for analysing gases under high temperatures and pressures [8, 77-79]. Gases can be analysed in a broad range of different conditions. The temperature of the gas can be 1700 °C high and pressurized gas can be analysed at up to 12 bar [79, 80]. An MBMS permits a parallel analysis of different species, as well as an analysis of condensable gas species. The sensitivity of the MBMS was determined by Wolf [78] after measuring the amount of Kr and Xe in air. The measurements indicated that the detection limit of the mass spectrometer was 20 ppb_{vol}.

The principal advantage of the molecular beam mass spectrometry is that the integrity of the sampled high-temperature gases is preserved during the free-jet expansion, because chemical reactions are effectively quenched and condensation is inhibited [81]. A detailed speciation can be performed by the MBMS scanning a broad range of mass-to-charge ratios in a quasi-simultaneous way. The high vacuum of the chamber system and the large distance between the molecules in the so-called molecular beam inhibit the interaction with underground molecules. The released species are cooled down to room temperature in microseconds. The non-equilibrium nature of the free-jet expansion and the subsequent formation of a molecular beam allow reactive and condensable species to remain in the gas phase at temperatures far below their condensation point for long periods of time, comparing to their reaction rates. Us-

ing the mass spectrometer, comprehensive detection of all gas-phase species can be achieved with high sensitivity [8, 81].

A more detailed description of the Molecular Beam Mass Spectrometer (MBMS) used for the online analysis of the gaseous reaction products in the release experiments was given by Wolf, Rieß and Stemmler [78, 82, 83].

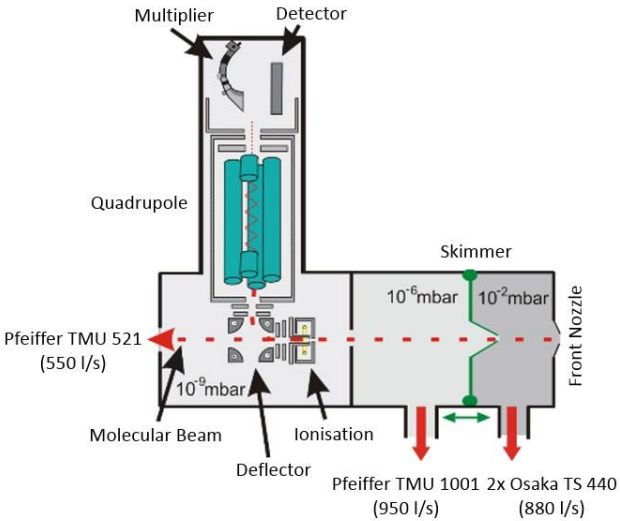

Figure 18. Schematic representation of the molecular beam mass spectrometer (adapted from [77]).

For the experiments with the MBMS a stainless steel cone with a length of 35 mm, an interior angle of 108° and an orifice diameter of 0.3 mm was utilized to sample the gas. This cone was fitted to a water-cooled stainless steel flange connecting it with the MBMS recipient. This front orifice cone was linked to the flow channel tube by moving the furnace toward the MBMS and sealing the gap between the tube and cone with a high-temperature insulation. That way the species were prevented from condensing on the sampling cone [81].

As shown in Figure 18, the MBMS system consists of three pumped chambers that are connected by small orifices. A so-called skimmer divides the first stage from the second. During the measurements pressures of 10^{-2} mbar in the first stage, 10^{-6} mbar in the second stage and 10^{-8} mbar in the third stage are achieved. The first stage is evacuated by two Osaka Helical Groove turbo molecular pumps. The second chamber is used as a pressure stage to reach the high vacuum conditions in the third chamber and the second and third stages are connected to four Pfeiffer turbo molecular pumps. Chamber three contains the ionisation unit, the deflector, the quadrupole and the multiplier [8, 78].

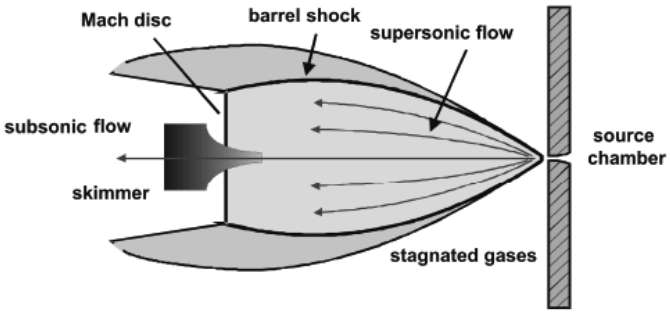

Figure 19. Schematic of the free-jet expansion [8].

The gas enters the first chamber through the front nozzle. As the ratio of the pressure before the nozzle to the pressure in the first chamber exceeds the critical value, the sample gas undergoes a free-jet expansion. Within the flow beyond the nozzle, the Mach number is higher than one. The initial expansion is nearly adiabatic and isentropic. Therefore, extreme collisional and internal energy state cooling occurs. With the transition to the molecular flow, collisions between the molecules of the sample gas are minimized. The hot gas is effectively cooled down to a temperature far below room temperature, in such a way that rotational and vibrational transitions are minimized. As a result, the integrity of the sampled high-temperature gases is preserved and chemical reactions are quenched [8, 84]. About ten orifice diameters downstream from the front nozzle, the expansion attains free molecular flow [79]. The core of the expanded gases is extracted by a conical skimmer (diameter of 1 mm) at the entrance of the second stage forming a molecular beam. The skimmer is constructed to be moveable along the recipient's main axis from the outside during a running experiment. This way, the optimum skimmer position, depending on the sampled gases, can be found and the beam performance as well as the resulting signal intensity can be maximised [81]. The second chamber is needed as a pressure stage in order to reach a very high vacuum in the third chamber. The mass analyser requires an ultra-high vacuum with $\lambda \geq 1$ km, which is reached in the third chamber. The core of the expanding flow is unaffected by the absolute pressure in the chamber. Outside of this zone, the molecular flow is extracted by a skimmer. Skimmers serve as high intensity, low temperature sources of molecular beams [85]. With the right pressure in the first vacuum chamber and with the proper placement of the skimmer, the supersonic flow enters the skimmer without shock formation. This is of great importance since it suppresses several mass transfer effects (see Figure 19) that would otherwise exert a significant influence on the molecular beam [8].

The molecular beam enters the ionisation region inside stage 3 by passing through another small aperture (diameter of 1.5 mm). There, the ions are formed by electron impact ionisation.

The ionisation energy for the release experiments was 70 eV [81]. The electrons are accelerated by a negative current and they cross the molecular beam, where collision leads to the formation of ions. Electron ionisation occurs when an electron abstracts an electron from a gas molecule. When the excess energy in the ion exceeds the bond energies that hold the molecular ion A^+ together, fragmentation occurs. After passing the deflector, the ions are filtered with a quadrupole mass analyser (ABB Extrel) and detected with an off-axis channeltron electron multiplier. The deflector consists of four poles placed in the angles of a square, with each set at the same potential (from 30 to 70 V or from -150 to -250 V). Uncharged molecules and anions are not deflected, which helps to prevent contamination of the detector and mass analyser. The quadrupole mass analyser consists of four rods of preferably hyperbolic shape that act as the poles of an electromagnetic field. The quadrupole filters the ions according to their mass-to-charge ratio. Since mass selection is accomplished by varying voltages or frequencies, the quadrupole analyser is able to scan very quickly and to switch very fast, with negligible dead time between settings for a number of different ions. In the detector, the “electron shower” hits an anode, and the current is recorded by the software and computer package [8]. Control of the scanning parameters and collection of the multiplier signal, as a function of time and the mass-to-charge ratio, were performed using ABB Extrel’s Merlin Automation Data System.

3.3.3. Quantification and calibration of the gaseous metal species by means of MBMS

As it has been previously mentioned, an MBMS was used for the online analysis of the gas species during the release experiments. Qualitative and quantitative analyses of the hot gas were achieved.

In order to quantify the released amounts of the heavy metal species during the experiments it was necessary to carry out a calibration before the experimental runs. A correlation between the signal intensities of the mass spectrometer and the corresponding species concentration in the gas phase was required.

For the purpose of simulating an experimental run, at preliminary measurements single trace metals were vaporised under the same atmospheric conditions as in the experiments. Mass spectra from 30 to 400 amu were scanned to determine the species that were present in the gas phase. This was carried out for every trace metal individually under the different experimental conditions considered. Table 6 shows the species that were found in the gas phase during the experiments with the respective metals considered.

Table 6. Summary of the metal species present in the gas phase during the experiments.

Trace metal	Species in the gas phase
Zn	Zn, ZnO, $ZnCl_2$, ZnS
Cd	Cd, CdO, $CdCl_2$, CdS
Pb	Pb, PbO, PbO_2, $PbCl_2$, PbS
As	As, As_2O_3, As_2O_5, $AsCl_3$, As_2S_2
Sn	Sn, SnO, SnO_2, $SnCl_2$, SnS
V	V_2O_3, V_2O_5, VO_2, VO

During the zinc measurements Zn, ZnO, $ZnCl_2$ and ZnS could be observed in the gas phase as Zn-containing gases. Cd, CdO, $CdCl_2$, CdS were observed in the Cd-measurements and Pb, PbO, PbO_2, $PbCl_2$ and PbS were the Pb-containing gases present in the Pb experiments. In the experiments of As and Sn the only metal-containing gases detected were As, As_2O_3, As_2O_5, $AsCl_3$, As_2S_2 and Sn, SnO, SnO_2, $SnCl_2$ and SnS. Although the release experiments with vanadium could not be implemented due to the high temperature necessary for evaporating vanadium, in preliminary experiments V_2O_3, V_2O_5, VO_2 and VO were detected in the gas phase in an atmosphere containing water vapour.

In order to carry out the calibration (arb. units / ppm_v) of each species found in the preliminary experiments, the furnace was heated up to exactly the same temperature as it was required for the experiments. This temperature was different for each metal considered. As soon as the desired temperature was attained, the inner tube containing the sample boat with the metal source was inserted into the outer tube of the experiment. Afterwards, the gas flow with the same gas composition as in the release experiments was turned on. In order to be able to monitor the process with sufficient temporal resolution, 10 scans per second were required. After the experiment, the metal source was removed.

Considering the weight difference of the metal before and after the experiment and the experiment´s duration, the total concentration of the metal in the gas phase could be calculated. The metal concentrations were determined in the same way at different temperatures in separate runs. The temperature at which the boat sample with the metal source was positioned varied according to the desired concentration of the metal in the gas phase. As the desirable concentration of a trace metal in gas was 100 ppm, the sample was placed at temperatures where approximately 100 ppm was obtained. The duration of the calibrations depended on the selected temperature. Due to the low concentrations required, the calibration experiments had a duration of maximum 4 hours.

According to the spectrums recorded over the calibration time, the metal sources provided a constant metal concentration in the gas stream. Therefore, the correlation curve of the ion signal intensities of the metal species and the corresponding concentrations in the gas phase showed a linear trend.

The monitored isotopes for each metal species, the temperature at which the calibrations were carried out and the results of the calibrations are explained in detail in the results section of this work.

The utilization of calibration curves was a simple method to enable the determination of the concentrations of heavy metal compounds in the gas phase (ppm_{vol}) by simply knowing the signal intensities of the isotopes considered.

3.4. Scheil-Gulliver cooling calculations

Cooling calculations were performed in order to evaluate the release and the condensation behaviour of trace metals during gasification. The calculations were performed using the Scheil-Gulliver cooling model from FactSage 6.3 Software. The model calculations were compared with the experimental results.

The *Equilib* module enables the performance of cooling calculations and display the phase transitions and compositions during equilibrium cooling and Scheil-Gulliver cooling. This module of FactSage employs the Gibbs energy minimization algorithm. It calculates the concentrations of chemical species when specified elements or compounds react or partially react to reach a state of chemical equilibrium. With this module it is possible to calculate all equilibrium (or Scheil-Gulliver non equilibrium) phase transitions as a multicomponent mixture is cooled [86, 87].

Thermodynamic equilibrium assumes that reactions are reversible when the temperature is increasing or decreasing. However, due to the temperature gradient that the gas go through when it leaves the reactor, condensation reactions are not likely to be reversible when temperature is decreasing. The Scheil-Gulliver cooling model is usually used to predict the solid/liquid alloys composition during solidification in metallurgy. This model assumes a non-equilibrium solidification path by calculating stepwise a succession of equilibrium states. For each step the model assumes a complete mixing of the solute and the gas phase. No diffusion to the solid phase takes place. The calculations consider the composition of the gas phase given at high temperature and then the temperature decreases step by step. At every step, the equilibrium state is calculated and then all the solid phases are removed from the calculation. Once an element appears in the condensed phase, the amount of this element is removed and is not present in the following calculations. That means, after each calculation any phase that precipi-

tates is dropped from the total mass balance. The remaining phase is then cooled by another incremental step and the process is repeated. Therefore, the initial composition of each step starts with a 100 % gaseous phase [88]. With the Scheil-Gulliver cooling model results reasonably close to reality can be achieved [89]. The Scheil-Gulliver Cooling tool from FactSage 6.3 has been used in some other research works [88, 89]. The nonequilibrium Scheil-Gulliver solidification model was explained in detail by Laughlin et al. [90].

The calculations to determine the release and the condensation behaviour (temperature and speciation) of Zn, Cd, Pb, As, Sn and V were carried out at decreasing temperature steps of 25 °C starting from 1000 °C to room temperature. The calculations with vanadium started at 2000 °C. The calculations were carried out at atmospheric pressure. As input data for the calculations the same atmospheric conditions as in the experiments were considered. Thus, the main aim was to evaluate the influence of H_2O, HCl and H_2S on the release of gaseous species and condensation behaviour of the condensable metal species.

The results of the calculations are presented as the speciation of the gaseous and condensed phase versus temperature and are shown in the Results and discussion section.

3.5. Thermodynamic pseudo-equilibrium model

Extensive work has been done to clarify the temperature-dependence of the condensation behaviour of heavy metal vapours upon flue gas cooling during municipal solid waste (MSW) incineration [66, 91, 92]. For this purpose, experiments with lead (Pb), cadmium (Cd), zinc (Zn) and copper (Cu) were carried out in a lab-scale rotary kiln reactor coupled with a multiple-stage cooling zone. The gaseous compounds HCl, SO_2 and H_2O were doped into the flue gas to investigate their influence on the condensation distribution of inorganic vapours in a cooling zone. It was found that, due to the rapid cooling rate of flue gas and short residence time of metal vapours in the cooling section, the conventional thermodynamics equilibrium software could not appropriately predict the experimental results. Therefore, in order to understand the condensation mechanisms of metal vapour species during flue gas cooling, a thermodynamic pseudo-equilibrium model was developed using ChemApp linked with the FactSage 6.2 database (FACT, Fact 53, FToxid and FTsalt). This model was able to predict the condensation behaviour of metal vapours under the influence of cooling rate and chemical reaction control. The schematic of the model is shown in Figure 20.

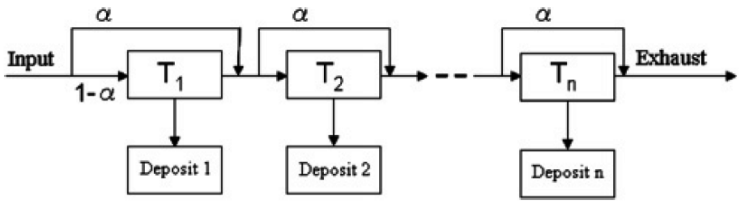

Figure 20. Schematic of the thermodynamic pseudo-equilibrium model [66].

A variable, α, was introduced in the model to describe the proportion of a metallic vapour which does not condense on a certain cooling stage. According to that, 1 – α are the metal vapours that condense in a specific cooling stage. An alpha value of zero at a certain cooling stage indicates that all the species reach an equilibrium state, i.e. there is no super-cooling or thermodynamic reaction control. In agreement with the model, the flue gas quenching rate is also influential in terms of the deposition of a metallic vapour at a given temperature. A rapid quenching of flue gas, "super-cooling", has the potential to cause super-saturation of a vapour. Thus, only a little deposition of the vapour takes place. Thereby, alpha reflects the effect of super-cooling on the condensation of metal vapour species. Super-cooling phenomenon decreases the condensation temperature of the gaseous species, causing them to condensate at far lower temperatures than the temperatures predicted by thermodynamic equilibrium modelling. A detailed description of this model was given by Jiao et al. [66, 92].

For the purpose of getting a better understanding of the condensation mechanisms of the inorganic metal vapours during flue gas cooling, thermodynamic pseudo-equilibrium calculations were performed to predict the condensation behaviour of the heavy metals under the influence of super-cooling and chemical reaction control. The model provided information about the global kinetics of the experiments. This model was applied to the atmospheric conditions of the condensation experiments in order to verify its validity under gasification conditions. The value of alpha was optimized by curve-fitting the results of the condensation experiments. This was carried out for all the atmospheric conditions considered, to wit, H_2O, HCl and H_2S in the atmosphere. The flue gas compositions and the amount of inorganic vapours determined under the experiments were used as input for the modelling. The output included the metallic species in both gas and solid phases. For the calculations, a temperature range from 2000 °C to room temperature with an interval of 100 °C and atmospheric pressure was considered.

4. Results and discussion

4.1. Zinc

4.1.1. Condensation experiments

The total gas flow in the condensation experiments was 510 ml/min and the duration of each experiment was 72 h. In order to reach a concentration of 100 ppm of zinc in each experiment, the sample boat with the heavy metal source needed to be placed at an exact position with the right temperature in the reaction zone. This temperature was first estimated with FactSage (see Figure 21) and afterwards experimentally proved (Figure 22). FactSage predicted a temperature of 400 °C in order to evaporate 100 ppm of zinc under the experimental conditions.

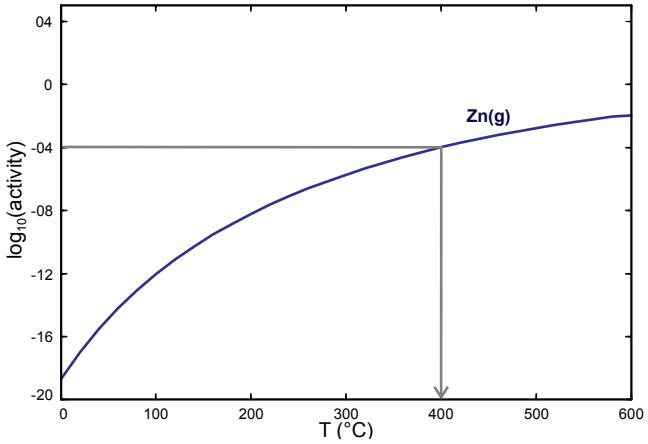

Figure 21. FactSage´s estimation of the necessary temperature for the vaporization of 100 ppm of zinc.

This temperature was experimentally proved by evaporating zinc at different temperatures between 420 – 600 °C and determining the amount of zinc that went to the gas phase in each case.

For carrying out the tests, the furnace was heated up to the same temperature as required for the condensation experiments. The inner tube with the metal source was inserted into the outer tube and the gas flow was turned on. The gas composition was the same as in the condensation experiments and the duration of the tests was 24 hours. Considering the weight loss of zinc

during the experiments and the experiment´s duration, the total amount of evaporated zinc could be calculated. The zinc source for all the experimental runs was metallic zinc.

The results showed that at 492 °C the concentration of zinc was 98 ppm. Although this temperature was higher than the predicted temperature by FactSage due to kinetics, the sample boat containing the metal was positioned at 28 cm (500 °C) in all the condensation experiments of zinc. This would ensure a similar concentration of zinc in every experiment and thereby, facilitate the comparison of the experimental results.

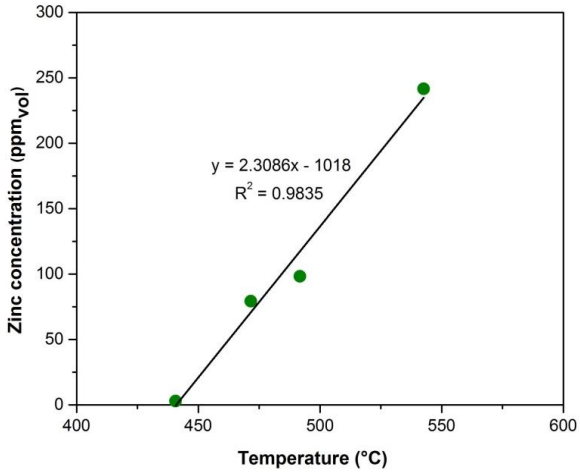

Figure 22. Correlation of zinc concentration (ppm) and temperature (°C).

The results obtained in the condensation experiments of zinc are shown in the next section. The influence of H_2O, HCl and H_2S on the condensation behaviour of zinc was investigated.

Influence of H_2O

Figure 23 shows the condensation distribution of zinc in the filters and in the outer tube when the atmosphere contained H_2O(g). The graph depicts the fraction of zinc species that condensed in the outer tube and in each filter from the condensation zone. The abscissa represents the temperature range in each filter. The first temperature range on the left corresponds to the last filter placed in the condensation zone. This is the filter located at the lowest temperature of the cooling zone. Moving to the right the temperatures increase. The zinc fraction that condensed in the outer tube is represented by “tube”. The reason zinc condensed in the outer tube was a small gap between the filters and the tube. The fraction that condensed in the tube predominantly corresponded to fractions that condensed at the temperature ranges where the majority of the species condensed. In other words, the fraction condensed in the tube could be

considered as a fraction that condensed at the filters where most species were deposited. In this experiment (see Figure 23), the fraction in the tube condensed at the temperature ranges of the second and the third filter. Thus, it is safe to say, that the fraction in the outer tube condensed at temperatures between 735 and 438 °C. The two bars for each temperature range represent the results with different amounts of water vapour. More precisely, the bars on the left represent the results with 3 % vol H_2O and the bars on the right represent the results with a higher amount of water vapour, 17 % vol. The condensed fractions of ZnO, $ZnCl_2$ and ZnS are depicted in red, blue and green, respectively.

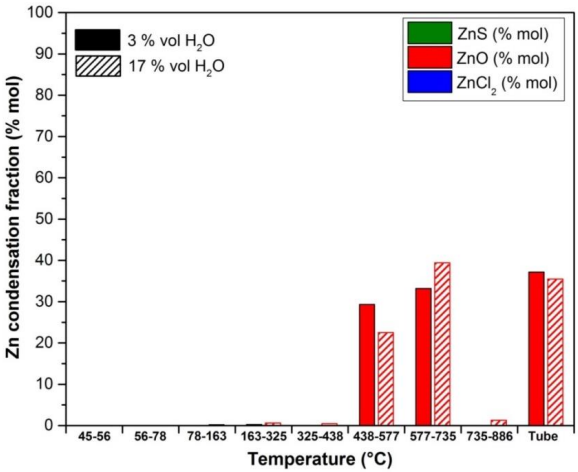

Figure 23. Condensation distribution of zinc in the outer tube and in the filters placed along the cooling zone in an atmosphere containing 3 % vol and 17 % vol water vapour.

The experimental results show that zinc condensed entirely as ZnO at temperatures below 886 °C when the atmosphere only contained water vapour. With 3 % vol of water vapour in the atmosphere ZnO condensed in the second (735 – 577 °C) and third filter (577 – 438 °C) of the cooling zone. However, with 17 % vol of H_2O, ZnO began to condense in the first filter (886 - 735 °C). Thus, the increase of the water vapour amount induced the condensation of ZnO at slightly higher temperatures.

Influence of HCl

Figure 24 shows a comparison between the condensation behaviour of zinc when the atmosphere did not contain HCl and when it contained 50 and 500 ppm HCl. The gas composition in these experiments consisted of 28 % H_2, 3 % H_2O and 69 % Ar. The results depictions follow the same format as in the previous section. In this case the three bars for each temperature range represent the results with different amounts of HCl. The bars on the left show the results for an

atmosphere containing 0 ppm HCl. The bars in the middle represent the results for 50 ppm HCl and the bars on the right the results with 500 ppm HCl in the experiment.

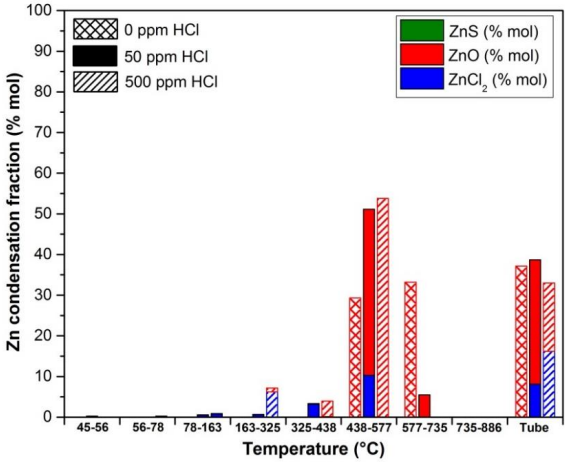

Figure 24. Condensation distribution of zinc in the outer tube and in the filters placed along the cooling zone in an atmosphere containing 0 ppm HCl, 50 ppm HCl and 500 ppm HCl.

As it has been explained above, zinc condensed as ZnO when the atmosphere did not contain HCl or H_2S. In an atmosphere containing 3 % vol of water vapour, ZnO condensed at temperatures between 735 – 438 ° C, in the second and third filters of the cooling zone. The introduction of HCl in the atmosphere promoted the condensation of zinc as a mixture of ZnO and $ZnCl_2$. ZnO condensed generally at higher temperatures (735 – 163°C) than $ZnCl_2$ (577 – 163 °C).

In an atmosphere containing 50 ppm HCl, ZnO condensed in the second and third filter (735 – 438 °C). However, $ZnCl_2$ condensed in the third and fourth filter (577 – 325 °C). When the atmosphere contained 500 ppm HCl, ZnO condensed predominantly in the third and fourth filter (577 – 325 °C). $ZnCl_2$ could only be detected in the fifth filter (325 – 163 °C).

As it can be seen in Figure 24, a larger amount of HCl influenced the condensation behaviour of zinc by promoting the condensation of ZnO at lower temperatures. With 0 ppm HCl, ZnO condensed entirely in the second and third filter, while with 50 ppm HCl, only a small amount of ZnO condensed in the second filter. Thereby, with 500 ppm of HCl, ZnO started to condense in the third filter. With 500 ppm HCl a large amount of $ZnCl_2$ condensed in the tube. This $ZnCl_2$ corresponded to $ZnCl_2$ that condensed in the third and fourth filter. Therefore, $ZnCl_2$ condensed in both cases at the same temperatures. Thus, it can be concluded that the condensation behaviour of $ZnCl_2$ did not seem to be affected by the amount of HCl. The only observed difference was that the zinc amount which condensed as $ZnCl_2$ was a little higher with 500 ppm than

with 50 ppm HCl. The total amount condensed as $ZnCl_2$ with 50 ppm and 500 ppm was 22.8 % and 24 % from the total zinc species condensed in each experiment.

Influence of H_2S

The condensation distribution of zinc in the tubes and in the outer tube when the gas atmosphere contained H_2S is depicted in Figure 25. A comparison between the condensation behaviour of zinc when the atmosphere did not contain H_2S and when it contained 50 and 500 ppm of H_2S it is shown. As well as in the experiments with HCl, the gas composition in these experiments was 28 % H_2, 3 % H_2O and 69 % Ar. In this case the three bars for each temperature range represent the results with different amounts of H_2S. The bars on the left represent the results for an atmosphere containing 0 ppm H_2S. The bars in the middle and on the right represent the results with 50 and 500 ppm H_2S.

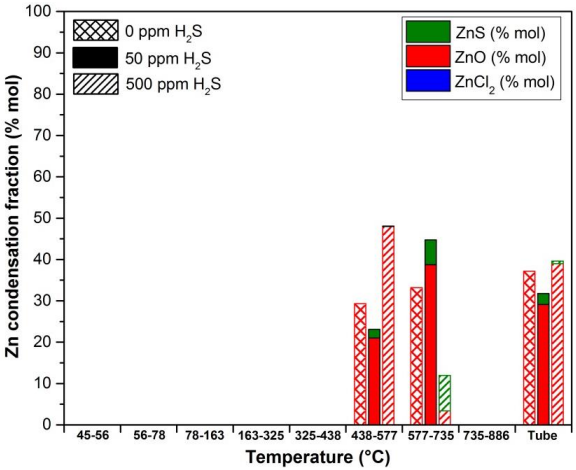

Figure 25. Condensation distribution of zinc in the outer tube and in the filters placed along the cooling zone in an atmosphere containing 0 ppm H_2S, 50 ppm and 500 ppm H_2S.

Zinc condensed as ZnO when the atmosphere did not contain HCl or H_2S. In an atmosphere containing 3 % vol of water vapour, ZnO condensed at temperatures between 735 – 438 °C. The introduction of H_2S in the atmosphere caused zinc to condense as a mixture of ZnO and ZnS. Both components condensed at 735 – 438 °C. ZnO condensed in the second (735 – 577 °C) and third filter (577 – 438 °C) under both experimental conditions. With 50 ppm of H_2S in the atmosphere ZnS also condensed in the second and third filter while with 500 ppm of H_2S, it predominantly condensed in the second filter. The total amount of zinc that condensed as ZnS did not vary much. It was in both cases approximately 10 % of all the total zinc condensed.

In summary, the increase of the H_2S concentration promoted the condensation of ZnS at higher temperatures, causing ZnS to condense at higher temperatures when more H_2S was present in the atmosphere. On the other hand, the amount of H_2S seemed not to affect the condensation temperature of ZnO. This species condensed at 735 – 438 °C regardless of the amount of H_2S.

4.1.2. Thermodynamic pseudo-equilibrium model

Figure 26 shows the comparison between the model calculations and the experimental results of the condensation of zinc in an atmosphere containing H_2O (3 – 17 % vol), HCl (50 – 500 ppm) and H_2S (50 – 500 ppm).

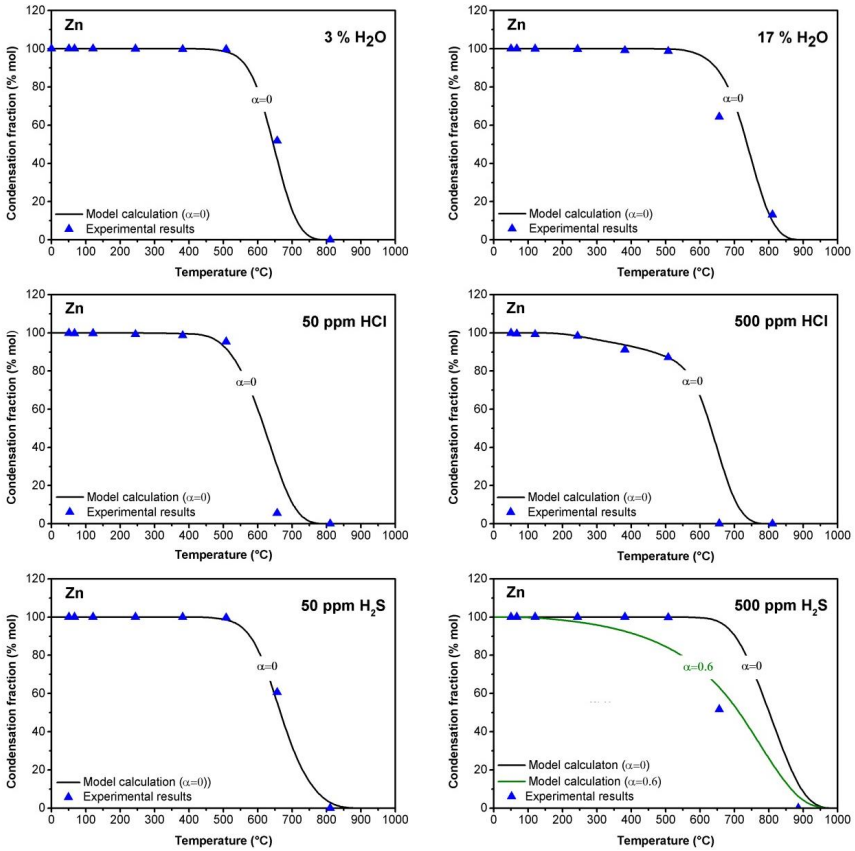

Figure 26. Comparison between the calculated and the experimental results of the condensation of zinc vapours in the presence of H_2O (3 – 17 % vol), HCl (50 – 500 ppm) and H_2S (50 – 500 ppm).

The curve-fitting of the experimental results indicate an alpha value of zero for all experimental conditions except for the experiment with 500 ppm of H_2S, where an alpha value of 0.6 fit well the experimental results. An alpha value of zero assumes that the species have reached the equilibrium and therefore there is not any reaction or cooling control. In these cases the model calculations predicted very well the experimental results. In the case with 500 ppm of H_2S, as it can be observed in Figure 26, the deposition fraction predicted by the model was far higher than the observed in the experimental results. Thus, it is reasonable to consider that super-cooling plays an important role in the partitioning of heavy metal vapours. Due to it, a portion of the ZnO and ZnS vapours were possible saturated and they barely deposited at high temperatures. They quickly diffused across the high temperature cooling zone in gas form and preferred to condense at lower temperatures.

According to the model, super-cooling affects the saturation extent and therefore, the condensation of the heavy metal vapours. However, its influence can be balanced by the presence of H_2S and H_2O, which causes the condensation of metal vapours at higher temperatures due to the formation of sulphides. Thus, the deposition of heavy metal vapours at high temperature is favoured by H_2S and H_2O. Consequently, formation of new compounds through chemical reactions in flue gas is an important factor that affects the condensation distribution and can greatly compensate the negative effect of super-cooling.

In this case, as only the experiment with 500 ppm of H_2S was influenced by super-cooling, any firm conclusions cannot be drawn about the influence of the chemical reactions in the condensation behaviour of zinc.

4.1.3. Scheil-Gulliver cooling calculations for the solid phase

The condensation calculations performed with the Scheil-Gulliver cooling model are presented in this section. The target was to predict the condensation behaviour of zinc using the thermochemical software FactSage 6.3. The calculations were carried out at decreasing temperature steps of 25 °C starting at 1000 °C and going down to room temperature. The results are presented in graphs depicting the amount of zinc species (in mol) that condense at certain temperatures. Like in the condensation experiments, the influence of H_2O, HCl and H_2S in the condensation behaviour of zinc was investigated.

Influence of H_2O

Figure 27 shows the speciation of the condensed phase predicted by the Scheil-Gulliver cooling calculations in an atmosphere containing water vapour and zinc. The graph shows a comparison between the results obtained with 3 and 17 % vol of water vapour in the atmosphere. The results obtained with 3 % vol of water are depicted with a solid line and the results obtained with 17 % vol of water vapour are depicted with a dashed line.

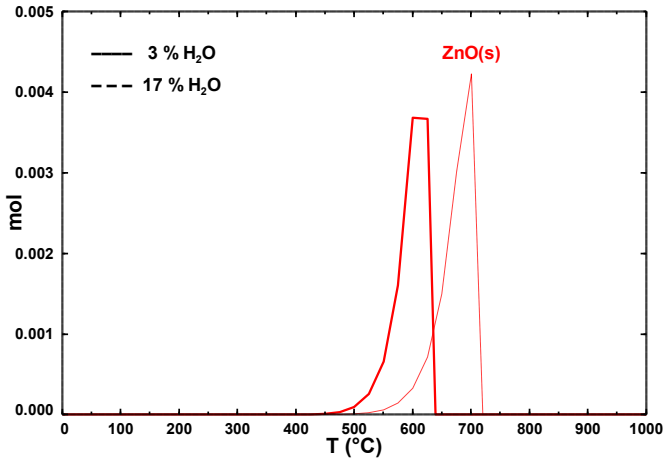

Figure 27. Speciation of the condensed phase during cooling from 1000 to 0 °C predicted by the Scheil-Gulliver cooling model in an atmosphere containing water vapour and zinc.

The model calculations showed that under both atmospheric conditions zinc condensed as ZnO. When the atmosphere contained 3 % vol of H_2O, ZnO condensed at temperatures between 640 – 450 °C. However, when the amount of introduced water was 17 % vol, ZnO began to condense at 725 °C.

In summary it can be said that an increase of the water vapour induced the condensation of ZnO at higher temperatures.

Influence of HCl

Figure 28 shows the results obtained from the Scheil-Gulliver cooling model when 50 ppm and 500 ppm of HCl were considered in the atmospheric conditions. In this case, the results for 50 ppm of HCl in the atmosphere are depicted with a solid line and the results for 500 ppm of HCl are depicted with a dashed line.

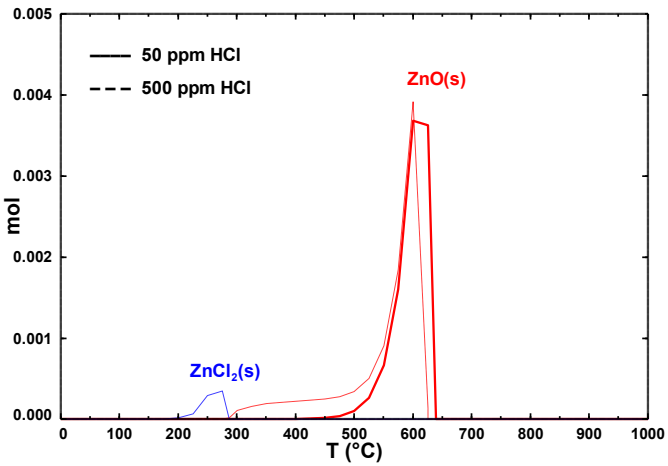

Figure 28. Speciation of the condensed phase during cooling from 1000 to 0 °C predicted by the Scheil-Gulliver cooling model in an atmosphere containing HCl and zinc.

The cooling calculations showed that zinc condensed as a mixture of $ZnCl_2$ and ZnO when HCl was introduced into the experiment. With 50 ppm of HCl in the atmosphere, the simulation predicted the deposition of ZnO at temperatures between 640 and 450 °C. No $ZnCl_2$ was supposed to condense under these atmospheric conditions. The calculations showed the deposition of ZnO and $ZnCl_2$ when 500 ppm of HCl were in the atmosphere. The condensation temperature of this species was 625 – 275 °C for ZnO and 280 – 200 °C for $ZnCl_2$. The amount of zinc condensed as $ZnCl_2$ was very low in comparison to the ZnO deposit.

In general, an increase of HCl amount led to the deposition of ZnO at lower temperatures. With 50 ppm of HCl in the atmosphere, ZnO began to condense at 640 °C while with 500 ppm of HCl, ZnO preferably started to condense at 625 °C. In addition, a higher amount of HCl caused zinc to condense as $ZnCl_2$. With 50 ppm of HCl in the atmosphere, the amount of zinc that condensed as $ZnCl_2$ was insignificant. With 500 ppm of HCl, the amount of zinc condensed as $ZnCl_2$ was appreciable although the amount of ZnO was much higher than the amount condensed as $ZnCl_2$.

Influence of H_2S

Figure 29 shows the condensation behaviour of zinc predicted by FactSage when H_2S was introduced in the atmosphere. A comparison between the results with 50 ppm H_2S and 500 ppm H_2S is displayed.

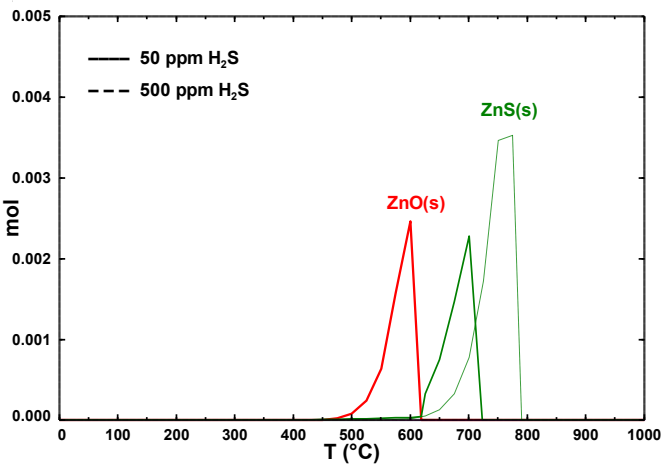

Figure 29. Speciation of the condensed phase during cooling from 1000 to 0 °C predicted by the Scheil-Gulliver cooling model in an atmosphere containing H_2S and zinc.

The cooling calculations predicted the condensation of zinc as a mixture of ZnO and ZnS. As it can be observed in the graph, when the atmosphere had 50 ppm of H_2S, zinc condensed as ZnO at 620 – 450 °C and ZnS at 725 – 625 °C. The amount deposited of both species was similar. When the atmosphere contained 500 ppm of H_2S, zinc only condensed as ZnS and at slightly higher temperatures (790 – 600 °C) than with only 50 ppm of H_2S. The amount of ZnS condensed increased too.

Summing up, the increase of H_2S shifted the condensation of ZnS to higher temperatures and induced ZnO not to condense. The condensed amount of ZnS also increased in an atmosphere containing more ppm of H_2S.

4.1.4. Release experiments

The influence of water vapour, HCl and H_2S on the gas phase concentration and speciation of zinc was investigated by MBMS. The gas flow was 4.3 l/min. The experiments were carried out four times, each with different temperatures at the end of the furnace. They were conducted at 900, 800, 700 and 500 °C. As the mass spectrometer only determines the gaseous ionized species based on their mass-to-charge ratios (m/z), it was necessary to carry out a calibration before starting the experiments. With this calibration it was possible to correlate the intensities of the isotopes present in the experiments with the heavy metal vapour concentration (ppm) obtained. In the experiments of zinc the monitored species were $^{64}Zn^+$, $^{80}ZnO^+$, $^{134}ZnCl_2^+$ and $^{96}ZnS^+$. The correlation between the ion signal intensities of the monitored species and the obtained concentration (ppm) in the gas phase is shown in Figure 30.

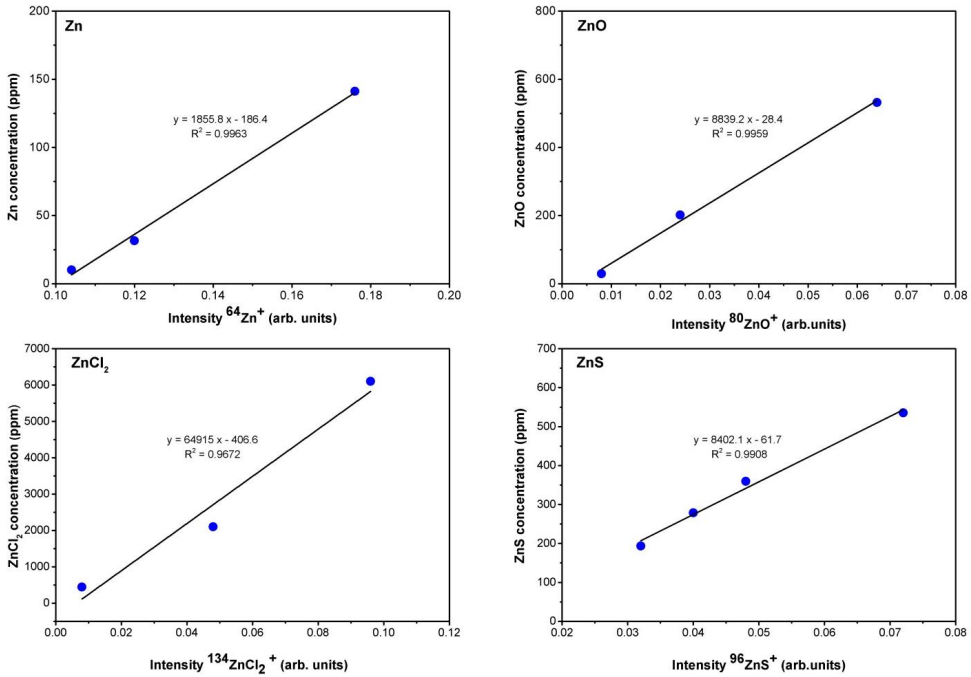

Figure 30. Calibration curves for the release experiments with zinc.

The results of the MBMS measurements are provided in Figure 31, Figure 32 and Figure 33. The graphs show the gas phase behaviour of zinc under the influence of H_2O, HCl and H_2S at different temperatures. That means, the concentration of each zinc containing species that were present at 900, 800, 700 and 500 °C. For each temperature, a comparison between the results obtained with a different amount of H_2O, HCl and H_2S is shown.

In the experiments, some difficulties were found in measuring the total Zn(g) present in the gas phase. A share of zinc was remaining in the MBMS. That is why the total amount of zinc in the gas phase could not be measured accurately. Therefore, only the concentration of the minor species present in the gas phase is shown in the results. However, it should be highlighted that Zn(g) was the major species present in the gas phase in all experiments.

A summary of the concentrations of the minor zinc species in the gas phase is given in the tables on the right of the experimental results.

Influence of H_2O

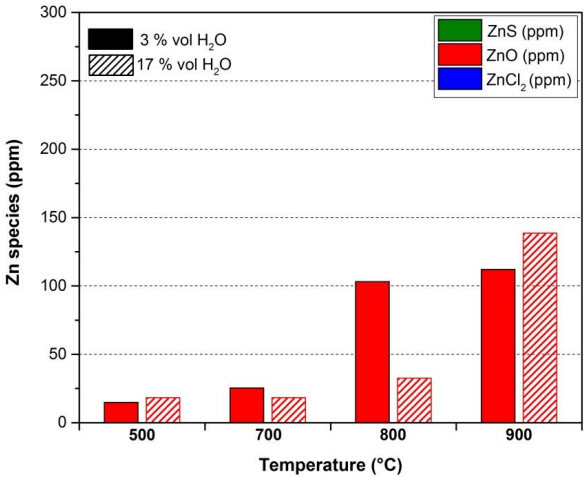

Minor gaseous Zn-species (ppm)		
	3 % vol H_2O	17 % vol H_2O
	ZnO	ZnO
900 °C	112.0	138.6
800 °C	103.2	35.2
700 °C	25.4	18.4
500 °C	14.8	18.4

Figure 31. Concentration of minor gaseous zinc species at 900, 800, 700 and 500 °C when the atmosphere contained water vapour (3 – 17 % vol). Note that Zn(g), the major species in the gas phase, is not represented.

The release experiments showed that Zn and ZnO were the only compounds present in the gas at the experiments with H_2O. The amount of Zn present in the gas phase was much larger than the amount of ZnO in every experiment. The amount of ZnO was similar at 900 and 800 °C, but decreased significantly at 700 °C and 500 °C when 3 % vol of water vapour was introduced into the outer tube. With 17 % vol of water vapour the concentration of ZnO decreased abruptly at 800 °C and then kept constant.

As it can be observed in Figure 31, under both experimental conditions the concentration of ZnO increased significantly with the temperature. Furthermore, it seemed that the concentration of ZnO was slightly higher with 17 % vol of H_2O than it was with 3 % vol of H_2O, especially at 900 °C.

Influence of HCl

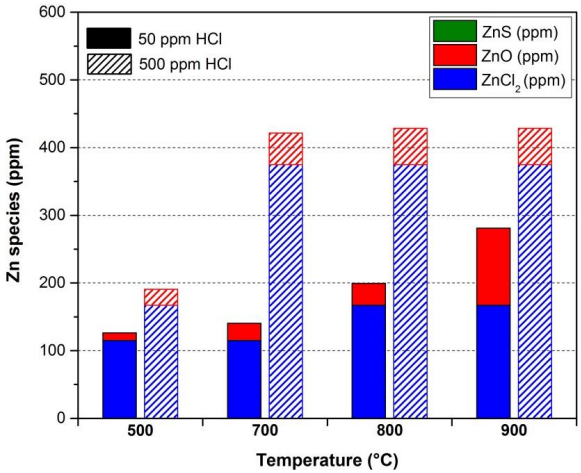

Minor gaseous Zn-species (ppm)				
	50 ppm HCl		500 ppm HCl	
	ZnO	$ZnCl_2$	ZnO	$ZnCl_2$
900 °C	114	167	54	375
800 °C	33	167	54	375
700 °C	25	115	47	375
500 °C	11	115	24	167

Figure 32. Concentration of minor gaseous zinc species at 900, 800, 700 and 500 °C when the atmosphere contained HCl (50 – 500 ppm). Note that Zn(g), the major species in the gas phase, is not represented.

The release experiments with HCl showed that zinc was present in the gas phase as a mixture of Zn, $ZnCl_2$ and ZnO. The amount of Zn present in the gas phase was much larger than the amount of ZnO and $ZnCl_2$ in every experiment. In both experiments the amount of ZnO increased with the temperature. Besides, the concentration of $ZnCl_2$ was in both cases larger than the one of ZnO. With 50 ppm of HCl the amount of $ZnCl_2$ increased until 800 – 900 °C, where the concentration was constant. In the case with 500 ppm of HCl, the concentration of $ZnCl_2$ was constant at temperatures from 700 – 900 °C. Thereby, the only difference between both experiments was the concentration of $ZnCl_2$. In general, with 500 ppm of HCl, the concentration of $ZnCl_2$ was much larger.

Influence of H_2S

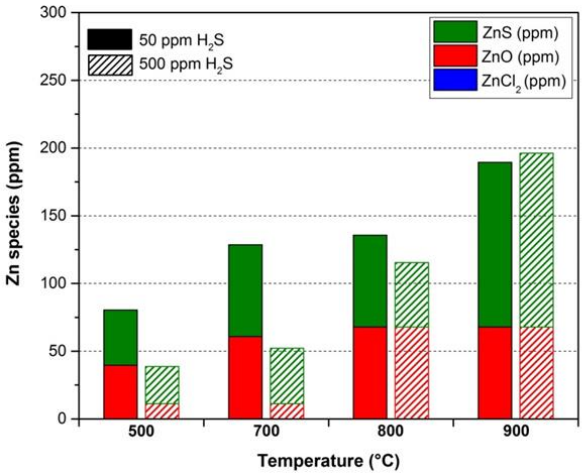

Minor gaseous Zn-species (ppm)				
	50 ppm H_2S		500 ppm H_2S	
	ZnO	ZnS	ZnO	ZnS
900 °C	68	122	68	128
800 °C	68	68	68	48
700 °C	61	68	11	41
500 °C	40	41	11	27

Figure 33. Concentration of minor gaseous zinc species at 900, 800, 700 and 500 °C when the atmosphere contained H_2S (50 – 500 ppm). Note that Zn(g), the major species in the gas phase, is not represented.

The release experiments with H_2S showed that zinc was present in the gas phase as a mixture of Zn, ZnS and ZnO. Zn was the major species present in the gas phase in every experiment. In both experiments the concentration of ZnS and ZnO showed a gradual increase with the temperature. In general, the concentrations of ZnS were higher than the concentrations of ZnO. The only difference between the results of both experiments was that at the lowest temperatures (500 – 800 °C) the concentrations of ZnO and ZnS with 500 ppm of H_2S were very small in comparison with the concentrations obtained with 50 ppm of H_2S in the atmosphere. This was a result of the different total zinc vaporized (ppm) in every experiment.

4.1.5. Scheil-Gulliver cooling calculations for the gas phase

The release behaviour of zinc under the influence of H_2O, HCl and H_2S predicted by the Scheil-Gulliver cooling model is shown in this section. The calculations show the speciation of the main inorganic gaseous species at temperatures between 1000 °C and room temperature.

Influence of H_2O

Figure 34 shows the speciation of the gas phase predicted by the Scheil-Gulliver cooling calculations in an atmosphere containing water vapour and zinc. The graph shows a comparison between the results obtained with 3 and 17 % vol of water vapour in the atmosphere. The results

obtained with 3 % vol of water are depicted with a solid line and the results obtained with 17 % vol of water vapour are depicted with a dashed line.

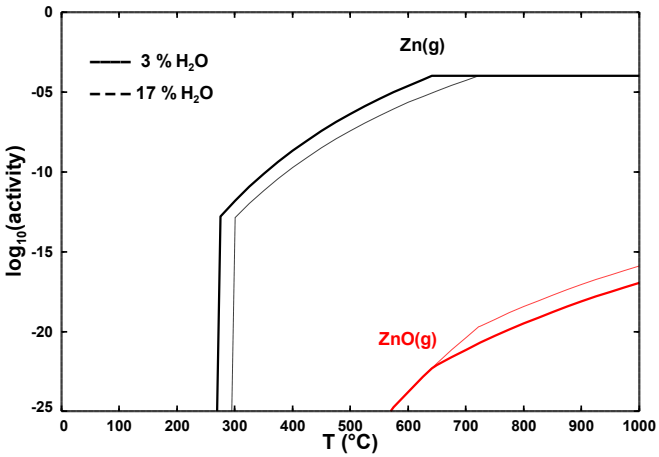

Figure 34. Gaseous zinc-containing species versus temperature in an atmosphere containing 3 – 17 % vol of H_2O calculated by the Scheil-Gulliver cooling model.

As it can be observed from the calculations, Zn(g) was the only gas species that appeared at high concentrations at the temperature range considered. Zn was present between 1000 and 280 °C. The only appreciable difference between both atmospheres was that the concentration of zinc when the atmosphere contained 17 % vol of H_2O started to decrease at slightly higher temperatures. ZnO appeared in the gas phase at 1000 – 570 °C. However, its concentration was lower than 1 ppb ($\log_{10}$ (act) ≈ 10^{-9}) and as it was out of the range of the concentrations mainly addressed in this study, it was not considered.

Influence of HCl

The release behaviour of zinc predicted by the Scheil-Gulliver cooling model when 50 and 500 ppm of HCl were present in the atmospheric conditions is depicted in Figure 35. In this case, the results for 50 ppm of HCl in the atmosphere are depicted with a solid line and the results obtained with 500 ppm of HCl are depicted with a dashed line.

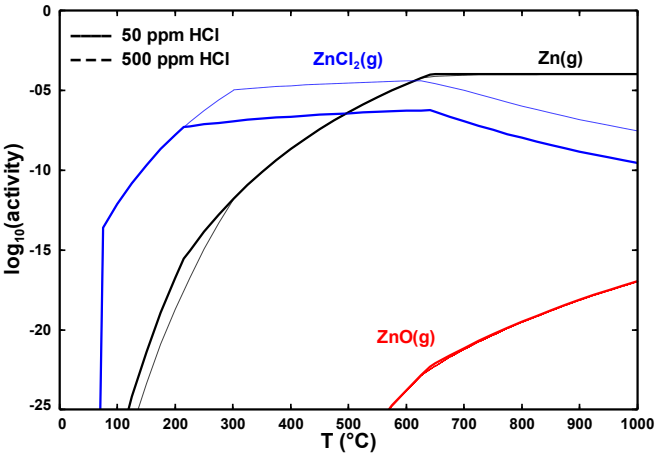

Figure 35. Gaseous zinc-containing species versus temperature in an atmosphere containing 50 – 500 ppm of HCl calculated by the Scheil-Gulliver cooling model.

The main inorganic species present in the gas phase when the atmosphere had HCl were Zn and $ZnCl_2$. ZnO was present at very low concentrations, as in the case with 3 – 17 % vol of H_2O mentioned above. The concentration of $ZnCl_2$ remained constant between 650 and 200 °C. At temperatures higher than 650 °C the concentration of $ZnCl_2$ decreased with the temperature. Zn was only present at high concentrations at 1000 – 650 °C. An increase in the HCl concentration only influenced the behaviour of $ZnCl_2$. The concentration of $ZnCl_2$ when 500 ppm of HCl was in the atmosphere was a little higher than with only 50 ppm of HCl.

Influence of H_2S

Figure 36 shows the release behaviour of zinc predicted by FactSage when H_2S was introduced into the atmosphere. A comparison between the results obtained with 50 ppm H_2S and 500 H_2S is shown. The results for 50 ppm of H_2S in the atmosphere are depicted with a solid line and the results obtained with 500 ppm of H_2S are depicted with a dashed line.

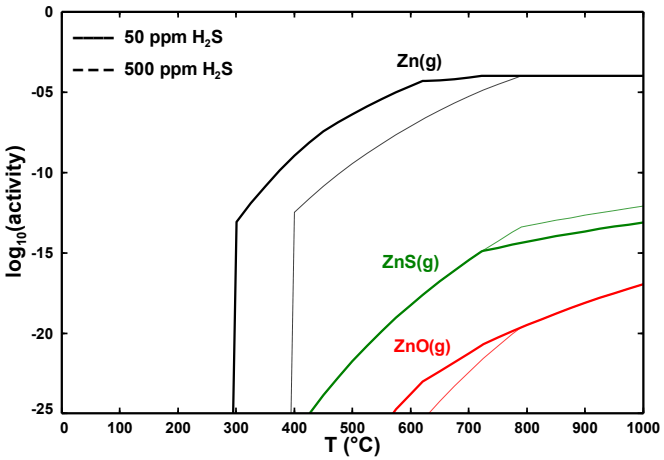

Figure 36. Gaseous zinc-containing species versus temperature in an atmosphere containing 50 – 500 ppm of H_2S calculated by the Scheil-Gulliver cooling model.

The calculations showed that Zn, ZnO and ZnS were present in the gas phase when the atmosphere contained H_2S. The concentrations of ZnO and ZnS were less than 1 ppb and therefore, not considered.

The concentration of Zn increased with the temperature. 100 ppm of Zn was present between 1000 – 620 °C when the atmosphere had 50 ppm of H_2S. However, in an atmosphere containing 500 ppm of H_2S, high concentrations of Zn were in the gas phase only until 780 °C.

4.1.6. Discussion

According to the comparison of the experimental results with the results of the cooling calculations and the thermodynamic pseudo-equilibrium model, the following conclusions of the condensation and release behaviour of zinc could be drawn:

Condensation behaviour of zinc

FactSage 6.3 predicted a temperature of 400 °C for the vaporization of 100 ppm of zinc under the atmospheric conditions considered in the experiments. However, the experiments showed that a concentration of approximately 100 ppm in the gas phase was obtained positioning the zinc sample at 492 °C. The higher temperature required for the vaporization of 100 ppm in the experiments was due to kinetics. The vaporization was not in equilibrium. In all condensation experiments the sample boat containing zinc was placed at 492 °C. This was provided at a distance of 28 cm from the entrance of the reaction zone.

Zinc condensed entirely as ZnO at temperatures between 735 – 438 °C when the atmosphere only contained water vapour (see Figure 23). However, an increase of the water vapour amount induced ZnO to begin condensing at 886 °C. The Scheil-Gulliver calculations (Figure 27) predicted the condensation of zinc as ZnO at 640 – 450 °C when the atmosphere contained 3 % vol water vapour. The model predicted the condensation of ZnO starting at 725 °C when the water vapour amount was 17 % vol. Therefore, it could be concluded that the Scheil-Gulliver calculations matched very well with the experimental results obtained when the atmosphere had water vapour.

In the presence of HCl zinc condensed as mixture of ZnO (735 – 163 °C) and $ZnCl_2$ (577 – 163 °C), as shown in Figure 24. The condensation behaviour of $ZnCl_2$ did not seem to be affected by the amount of HCl. However, a large amount of HCl caused ZnO to condense at lower temperatures (577 – 163 °C). The amount of the total zinc species that condensed as $ZnCl_2$ was 22.8 % with 50 ppm HCl and 24 % with 500 ppm of HCl. The cooling calculations predicted the condensation of zinc as ZnO (640 – 450 °C) when 50 ppm of HCl was present in the experiment (see Figure 28). $ZnCl_2$ was not supposed to condense under these atmospheric conditions. When 500 ppm HCl was considered in the calculations, the model predicted the condensation of zinc as a mixture of ZnO (625 – 275 °C) and $ZnCl_2$ (280 – 200 °C). Thus, the Scheil-Gulliver calculations also predicted the condensation of ZnO at lower temperatures when the amount of HCl increased. In summary, the condensation temperatures of ZnO predicted by the model fit with the experimental results nicely. However, the model did not predict the condensation of $ZnCl_2$ with 50 ppm HCl in the atmosphere. Besides, the temperature at which $ZnCl_2$ condensed with 500 ppm HCl was much higher in the experiments (577 – 163 °C) than in the calculations (280 – 200 °C). For the rest, the model fit very well with the experimental results. Overall, it could be concluded that the cooling calculations predicted the condensation behaviour of zinc properly when HCl was present in the atmosphere.

In an atmosphere containing H_2S, zinc condensed as a mixture of ZnO and ZnS. Both condensed at 735 – 438 °C (Figure 25). The amount of zinc that condensed as ZnS was 10 %, regardless of the amount of H_2S present in the atmosphere. However, a high amount of H_2S in the atmosphere caused ZnS to condense at slightly higher temperatures. In contrast, the condensation of ZnO was not affected by H_2S. The cooling calculations also predicted the condensation of ZnO and ZnS when H_2S was inserted into the atmosphere (Figure 29). ZnO condensed at 620 – 450 °C and ZnS at 725 – 625 °C when 50 ppm of H_2S was considered. These temperatures matched the temperature range at which both compounds condensed in the experimental results. The shift of the condensation of ZnS to higher temperatures (790 – 600 °C) when 500 ppm of H_2S were present in the calculations was also predicted by the calculations. Nevertheless, with 500 ppm of H_2S in the atmosphere the model did not predict the condensation of ZnO as

happened in the experiments. However, without considering the appearance of ZnO in the deposits with 500 ppm of H_2S, the model predicted the experimental results quite good.

According to the results of the thermodynamic pseudo-equilibrium model (Figure 26), all experiments were in equilibrium except that one with 500 ppm H_2S. In this case an alpha value of 0.6 fit the experimental results. ZnO and ZnS were possibly saturated and barely deposited at high temperatures. They diffused across the cooling zone in gas form and condensed at low temperatures. Although it is reasonable to think that super-cooling affected the condensation of the experiment with 500 ppm of H_2S, no conclusions could be drawn as this was the only experiment where super-cooling affected potentially the behaviour of zinc. In the cases with H_2O, HCl and 50 ppm of H_2S, the model was able to predict nicely the total condensation fraction of zinc with the temperature with an alpha value of zero.

Release behaviour of zinc

In the release experiments with zinc some difficulties were found to measure the total Zn(g) present in the gas phase. Zinc was remaining inside the MBMS and the total amount of zinc could not be measured accurately. Therefore, only the concentrations of the minority species were shown in the results although Zn(g) was the major species present in the gas phase in all experiments. Furthermore, it should be emphasized that due to the great temperature gradient in the furnace, the obtainment of a constant zinc concentration in the gas phase in every experiment was complicated. Therefore, the total concentration of zinc differed from experiment to experiment. That is why only a qualitative analysis could be achieved. The speciation and the behaviour of each species present in the gas phase were determined.

The release experiments showed that Zn and ZnO were the only compounds present in the gas phase in the experiments with H_2O. The amount of Zn present was much larger than the amount of ZnO in every experiment. As it can be observed in Figure 31, under both experimental conditions the concentration of ZnO increased significantly with the temperature. Furthermore, it seemed that the concentration of ZnO was slightly higher with 17 % vol H_2O than it was with 3 % vol H_2O, especially at 900 °C. In the calculations (see Figure 34), Zn(g) was the only gas species that appeared in high concentrations at the temperature range considered. Zn was present between 1000 and 280 °C. ZnO appeared in the gas phase at 570 – 1000 °C. As its concentration was lower than 1 ppb ($\log_{10}$ (act) ≈ 10^{-9}) it was not considered. However, although the model predicted a very low concentration of ZnO, this species was found in the gas phase in the experiments in higher concentrations than the predictions. Like in the experiments, ZnO increased significantly with the temperature and its concentration was slightly higher with 17 % vol H_2O than with 3 % vol H_2O. Thus, excluding this difference the model was able to predict reasonably the release behaviour of zinc.

The release experiments with HCl (see Figure 32) showed that zinc was present in the gas phase as a mixture of Zn, $ZnCl_2$ and ZnO. The amount of Zn present in the gas phase was much larger than the amount of ZnO and $ZnCl_2$ in every experiment. In both experiments the amount of ZnO increased with the temperature. Besides, the concentration of $ZnCl_2$ was in both cases larger than the one of ZnO. With 50 ppm of HCl the concentration of $ZnCl_2$ was constant at 800 – 900 °C. With 500 ppm of HCl, the concentration of $ZnCl_2$ was constant at temperatures from 700 – 900 °C. In general, with 500 ppm of HCl, the concentration of $ZnCl_2$ was much higher than with only 50 ppm HCl. The Scheil-Gulliver calculations (see Figure 35) showed that the main inorganic species present in the gas phase were Zn and $ZnCl_2$ when the atmosphere had HCl. ZnO was present at very low concentrations. The concentration of $ZnCl_2$ remained constant between 200 and 650 °C and at temperatures higher than 650 °C the concentration of $ZnCl_2$ decreased with the temperature. Only at 1000 – 650 °C Zn was present in high concentrations. The concentration of $ZnCl_2$ was a little higher when 500 ppm of HCl was in the atmosphere than with only 50 ppm of HCl. Thereby, an increase in the amount of HCl caused the presence of higher concentrations of $ZnCl_2$ in the gas phase. Although in the experimental results only a qualitative analysis was carried out, the calculations predicted the same trend as the one observed in the experimental results. The only appreciable difference was the presence of high concentrations of ZnO in the gas phase. The calculations predicted the existence of ZnO at concentrations out of the range of this study. Except for that, it could be concluded that the speciation and the behaviour of the species was similar in the experiments and in the calculations. Thus, the model could moderately predict the experimental results when HCl was introduced into the atmosphere.

The release experiments with H_2S (see Figure 33) showed that zinc was present in the gas phase as a mixture of Zn, ZnS and ZnO. Zn was the major species in every experiment. In both experiments the concentration of ZnS and ZnO showed a gradual increase with the temperature. In general, the concentrations of ZnS was higher than the concentrations of ZnO. The Scheil-Gulliver calculations (Figure 36) also showed that Zn, ZnO and ZnS were present in the gas phase when the atmosphere had H_2S. However, the concentrations of ZnO and ZnS were less than 1 ppb and therefore not considered. The concentration of Zn increased with the temperature. Besides, the concentration of Zn was lower at high temperatures with 500 ppm of H_2S than with only 50 ppm H_2S. The model calculations had generally the same trend as the experimental results. The only difference observed was that in the calculations ZnS and ZnO were present in the gas phase in very low concentrations. However, the concentrations of these species in the experiments were at ppm level. Besides, the trend of this species was similar in the experiments as in the calculations. For example, the concentration of ZnS was higher than the concentration of ZnO in every experiment. Thereby, although the experimental results were only qualitative, it could be said that the model calculations and the experimental results showed the same trend when the atmosphere had H_2S.

In summary, the Scheil-Gulliver calculations were a good tool for the prediction of the condensation and release behaviour of zinc. In general, a good agreement between the cooling calculations and the experimental results was found. The speciation as well as the temperatures at which the species were released or condensed under the influence of H_2O, HCl and H_2S showed the same trends in the calculations and in the experimental results.

4.2. Cadmium

4.2.1. Condensation experiments

The total gas flow in the condensation experiments with Cd was 645 ml/min and the duration of each experiment was 24 h. In the same way as in the experiments with Zn, the temperature at which the metal boat should be placed in order to obtain 100 ppm of the metal in the gas was first estimated with FactSage (see Figure 37). The program predicted a temperature of 310 °C for the vaporization of 100 ppm of cadmium under the experimental conditions.

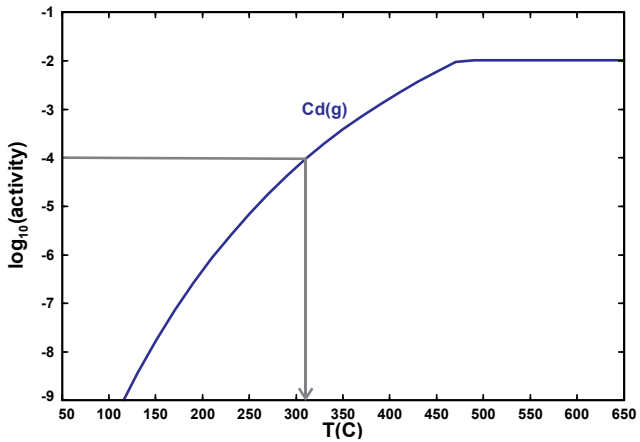

Figure 37. FactSage´s estimation of the necessary temperature for the vaporization of 100 ppm of cadmium.

This temperature was experimentally proved evaporating cadmium at different temperatures between 340 – 380 °C and determining the amount of Cd that went to the gas phase in each case. The concentration of Cd was calculated with the weight loss of cadmium during the experimental runs. The length of the experiments was 24 h and the gas composition was the same as in the condensation experiments. As cadmium source for all the experiments metallic cadmium was used.

The correlation between the cadmium concentration and the temperature is depicted in Figure 38. The results show that placing the sample boat at 368 °C a concentration of 86 ppm of cadmium in the gas was obtained. In the case of placing it at 378 °C the concentration was 133 ppm. Therefore, the necessary temperature to obtain a concentration of 100 ppm was in the temperature range of 368 to 378 °C. The right temperature was obtained with the calibration equation. The temperature at which the metal should be placed in the experiments was 370 °C.

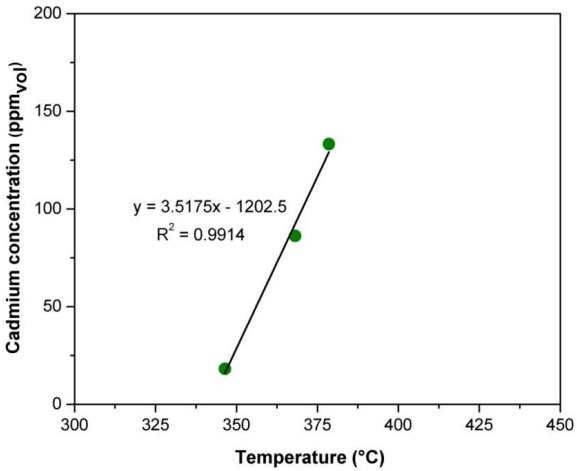

Figure 38. Correlation of cadmium concentration (ppm) and temperature (°C).

The results obtained in the condensation experiments with Cd are shown below. The influence of H_2O, HCl and H_2S in the condensation behaviour of cadmium was investigated.

Influence of H_2O

Figure 39 shows the condensation distribution of cadmium in the tubes and in the outer tube when the atmosphere contained $H_2O(g)$. For this experiments the amount of cadmium condensed as metallic Cd, CdO, $CdCl_2$ and CdS are depicted in purple, red, blue and green colour, respectively.

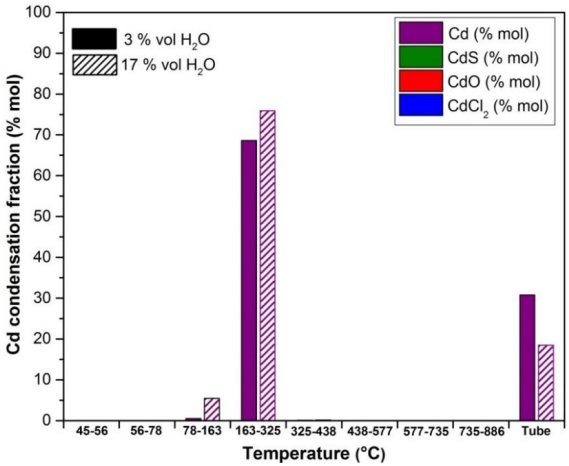

Figure 39. Condensation distribution of cadmium in the outer tube and in the filters placed along the cooling zone in an atmosphere containing 3 % vol and 17 % vol water vapour.

When the atmosphere contained water vapour, cadmium condensed as metallic Cd at temperatures between 325 – 78 °C. Cadmium did not seem to react with oxygen and form cadmium oxide. Under both experimental conditions, with 3 and 17 % vol water vapour, cadmium condensed in the fifth and sixth filters. Therefore, an increase of the water vapour amount did not seem to affect the condensation behaviour of this heavy metal.

Influence of HCl

Figure 40 shows a comparison between the condensation behaviour of cadmium when the atmosphere did not contain HCl and when it contained 50 and 500 ppm HCl. The gas composition in these experiments was 28 % H_2, 3 % H_2O and 69 % Ar. The amount of cadmium condensed as metallic Cd and $CdCl_2$ are depicted in purple and blue colour, respectively. The bars on the left show the results obtained when the atmosphere contained 0 ppm HCl. The bars in the middle represent the results with 50 ppm HCl and the bars on the right the results with 500 ppm HCl.

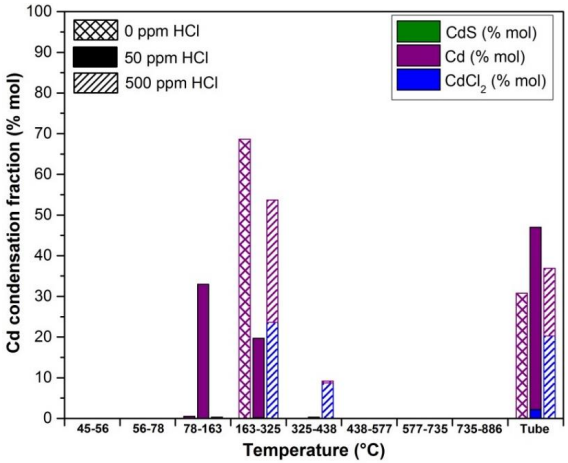

Figure 40. Condensation distribution of cadmium in the outer tube and in the filters placed along the cooling zone in an atmosphere containing 0 ppm HCl, 50 ppm HCl and 500 ppm HCl.

When the atmosphere only had water vapour, cadmium condensed as metallic Cd at temperatures between 325 – 78 °C.

Cadmium condensed as a mixture of $CdCl_2$ and metallic Cd in the presence of HCl. Cadmium condensed as metallic cadmium in the fifth (325 – 163 °C) and sixth filters (163 – 78 °C) when 50 ppm HCl was present in the atmosphere. Thus, Cd condensed at the same temperatures in the experiment with 0 and 50 ppm HCl. However, with 500 ppm HCl in the atmosphere cadmium started to condense preferably in the fourth filter (438 – 325 °C).

$CdCl_2$ condensed in the fourth (438 – 325 °C) and fifth filters (325 – 163 °C) when the atmosphere contained 500 ppm of HCl. The percentage condensed as $CdCl_2$ in this experiment was 52.6 %. However, in the experiment containing only 50 ppm of HCl just a small amount of cadmium (2.7 % of the total) condensed as $CdCl_2$ and this also condensed in the fourth and fifth filter.

In conclusion, both compounds, Cd and $CdCl_2$, condensed at temperatures lower than 438 °C but $CdCl_2$ deposits appeared at higher temperatures than the Cd metallic deposits. Larger amounts of HCl lead Cd to condense at slightly higher temperatures. However, no conclusions could be drawn about the influence of HCl on the condensation temperature of $CdCl_2$ due to the small amount of cadmium that condensed as $CdCl_2$ when only 50 ppm of HCl was available in the atmosphere. It can be said, nevertheless, that the condensed amount of $CdCl_2$ increased considerably with 500 ppm HCl in the atmosphere.

Influence of H_2S

The condensation distribution of cadmium when the gas atmosphere contained the trace gas H_2S is depicted in Figure 41. A comparison between the condensation behaviour of cadmium when the atmosphere did not contain H_2S and when it contained 50 and 500 ppm H_2S is shown. As in the experiments with HCl, the gas composition in these experiments was 28 % H_2, 3 % H_2O and 69 % Ar.

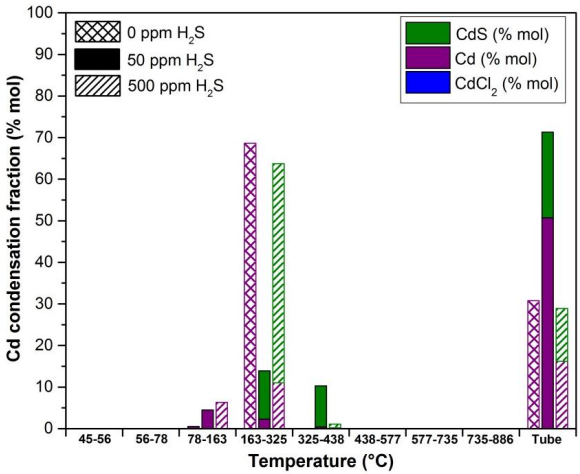

Figure 41. Condensation distribution of cadmium in the outer tube and in the filters placed along the cooling zone in an atmosphere containing 0 ppm H_2S, 50 ppm H_2S and 500 ppm H_2S.

When the atmosphere did not contain H_2S, cadmium condensed as metallic Cd at temperatures between 325 – 78 °C.

Cadmium condensed as CdS and Cd when H_2S was introduced into the outer tube. Cd condensed in both experiments at temperatures between 438 and 78 °C. In other words, Cd condensed in the fourth, fifth and sixth filters, although mostly condensed in the last two ones. Cadmium condensed as CdS in both experiments at 438 – 163 °C, in other words, in the fourth and fifth filters. The main difference was the amount of cadmium condensed as CdS in both experiments. With 50 ppm of H_2S, 42.1 % of the total cadmium condensed as CdS. With 500 ppm H_2S, this amount increased to 66.3 %.

In general, the condensation temperatures of Cd and CdS were not affected by the amount of H_2S introduced into the atmosphere.

4.2.2. Thermodynamic pseudo-equilibrium model

Figure 42 shows the comparison between the model calculations and the experimental results of the condensation of cadmium in an atmosphere containing H_2O (3 – 17 % vol), HCl (50 – 500 ppm) and H_2S (50 – 500 ppm).

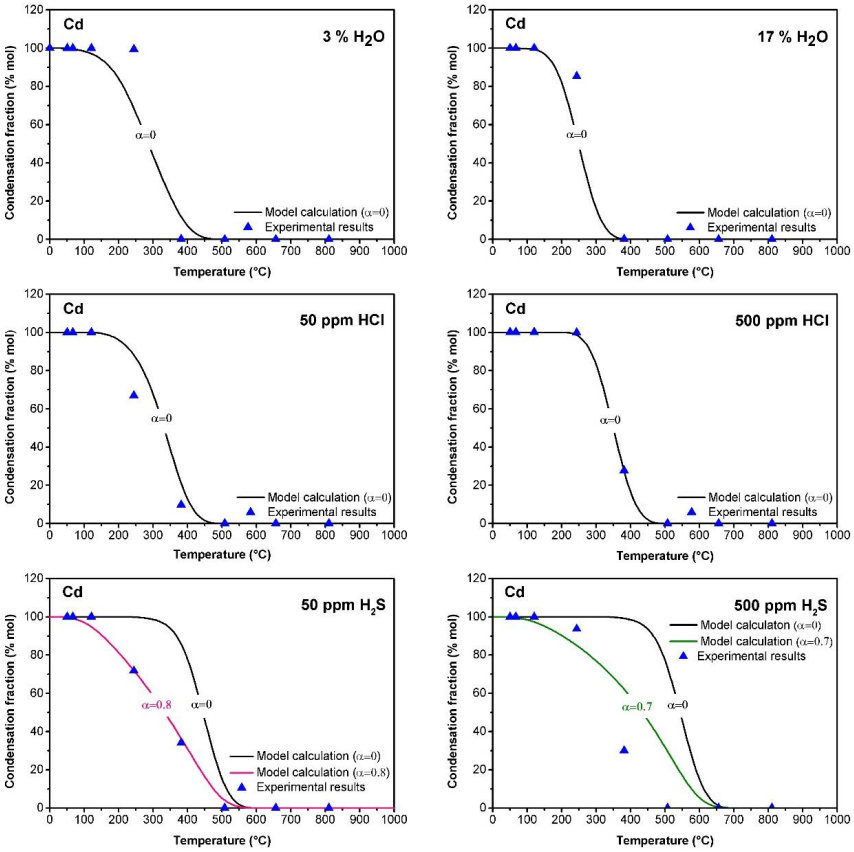

Figure 42. Comparison between the calculated and the experimental results of the condensation of cadmium vapours in the presence of H_2O (3 – 17 % vol), HCl (50 – 500 ppm) and H_2S (50 – 500 ppm).

The curve-fitting of the experimental results indicated an alpha value of zero for all experimental conditions except for the experiments with 50 and 500 ppm of H_2S, where alpha values of 0.8 for the experiment with 50 ppm of H_2S and 0.7 for the one with 500 ppm of H_2S fit nicely the experimental results. As it has been explained elsewhere before, an alpha value of zero as-

sumes that the species have reached the equilibrium and therefore, there is not any reaction or cooling control. For these reason, the model assumes that the experiments containing H_2O or HCl were in equilibrium and hereby, the model calculations predicted very well the experimental results.

In the experiments with H_2S, as it can be observed in Figure 42, the deposition fractions predicted by the model were far higher than the observed in the experimental results. Thus, the experiments did not reach the equilibrium and the condensation of the metallic vapours was affected by the flue gas cooling rate. That means, Cd and CdS vapours were possible saturated and they condensed at lower temperatures than the temperatures predicted by the calculations.

According to the model, the super-cooling effect can be offset by the chemical reaction of inorganic vapours when H_2O and H_2S are introduced into the atmosphere. As it can be seen in the graph, alpha value decreased with the addition of a larger concentration of H_2S. Alpha value was 0.7 with 500 ppm of H_2S and 0.8 with 50 ppm of H_2S. The formation of a higher amount of CdS compensated slightly the negative effect of super-cooling and the condensation was shifted to higher temperatures.

It can be concluded, that chemical reactions had an influence on the condensation behaviour of cadmium when H_2S was present in the atmosphere. However, as the experiments with H_2O and HCl were supposed to be in equilibrium, no conclusions could be drawn about the influence of chemical reactions in the condensation of cadmium when H_2O or HCl were in the atmosphere.

4.2.3. Scheil-Gulliver cooling calculations for the solid phase

The condensation calculations performed with the Scheil-Gulliver cooling model from FactSage 6.3 software in order to predict the condensation behaviour of cadmium are presented in this section. The calculations were carried out at decreasing temperature steps of 25 °C starting from 1000 °C to room temperature. The graphs show the amount of cadmium species that condense (mol) at each temperature. As in the condensation experiments, the influence of H_2O, HCl and H_2S in the condensation behaviour of cadmium was studied.

Influence of H_2O

The cadmium speciation predicted by the Scheil-Gulliver cooling calculations in an atmosphere containing water vapour is depicted in the Figure 43. A comparison between the results with 3 % vol water and the results with 17 % vol water is presented. The species depicted with a solid line are the species that condensed when the atmosphere contained 3 % vol H_2O and the ones depicted with a dashed line are however the species that condensed when the atmosphere contained 17 % vol H_2O.

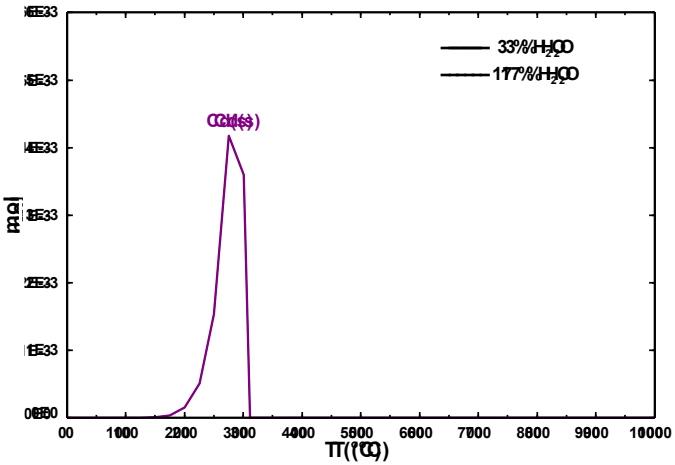

Figure 43. Speciation of the condensed phase during cooling from 1000 to 0 °C predicted by the Scheil-Gulliver cooling model in an atmosphere containing water vapour and cadmium**.**

The model calculations showed that cadmium condensed as metallic Cd at 310 – 150 °C independently of the water vapour amount considered. The results from both simulations overlapped, the program predicted for both atmospheric conditions the condensation of the same amount of metallic cadmium and at the same temperatures. Therefore, according to the cooling calculations, it could be considered that the amount of water vapour introduced in the atmosphere did not influence the condensation behaviour of cadmium.

Influence of HCl

Figure 44 shows the results obtained from the Scheil-Gulliver cooling model when 50 and 500 ppm of HCl were present in an atmosphere containing cadmium. In this case, the results obtained when 50 ppm of HCl was in the atmosphere are depicted with a solid line and the results obtained when the atmosphere contained 500 ppm of HCl are depicted with a dashed line. The amount of cadmium condensed as metallic Cd and $CdCl_2$ are depicted in purple and blue, respectively.

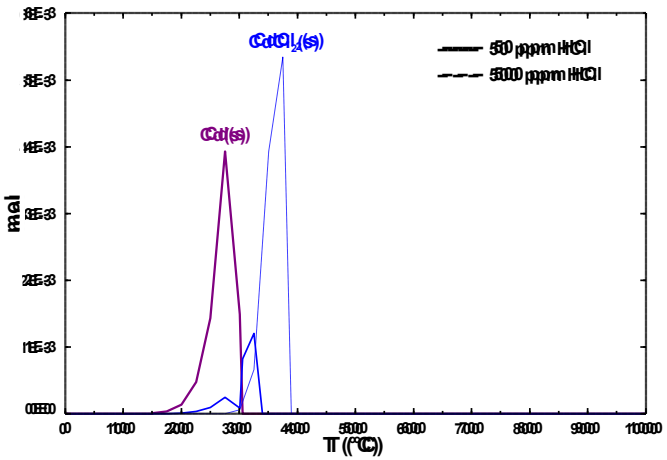

Figure 44. Speciation of the condensed phase during cooling from 1000 to 0 °C predicted by the Scheil-Gulliver cooling model in an atmosphere containing HCl and cadmium.

The cooling calculations show that cadmium condensed as a mixture of $CdCl_2$ and Cd when HCl was introduced in the atmosphere. With an atmosphere containing 50 ppm of HCl, cadmium condensed as $CdCl_2$ (340 – 200 °C) and Cd (310 – 150 °C). The amount condensed as metallic cadmium was larger than the condensed amount of $CdCl_2$. An increase in the amount of HCl to 500 ppm, induced the condensation of $CdCl_2$ at temperatures between 390 and 300 °C. The amount of $CdCl_2$ deposited under these conditions was much larger. In this case, the program did not predict the deposition of metallic cadmium.

In conclusion, the increase in the HCl amount shifted the deposition of $CdCl_2$ to higher temperatures. The amount of $CdCl_2$ deposited also increased. Moreover, with higher concentrations of HCl in the atmosphere, not any cadmium condensed as metallic cadmium.

Influence of H_2S

The results of the cooling calculations obtained with FactSage when H_2S was introduced in an atmosphere containing cadmium are shown in Figure 45. A comparison between the results with 50 ppm H_2S and 500 ppm H_2S is shown. In this case, the amount of cadmium condensed as metallic Cd and CdS are depicted in purple and green, respectively.

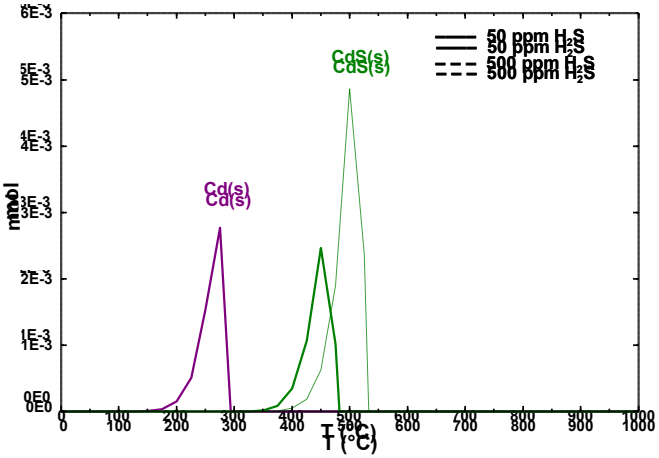

Figure 45. Speciation of the condensed phase during cooling from 1000 to 0 °C predicted by the Scheil-Gulliver cooling model in an atmosphere containing H_2S and cadmium.

The Scheil-Gulliver cooling model predicted the condensation of cadmium as a mixture of metallic Cd and CdS in the presence of H_2S. With 50 ppm of H_2S cadmium condensed as Cd at low temperatures (300 – 150 °C) and CdS at higher temperatures (480 – 350 °C). The amount deposited of both compounds was similar. When 500 ppm of H_2S was considered, only the species CdS condensed. Under these atmospheric conditions, CdS condensed at higher temperatures (530 – 400 °C) than in the simulation with only 50 ppm of H_2S. The amount of CdS condensed was also larger.

Basically, an increase in the H_2S amount considered shifted the condensation of CdS to higher temperatures. The amount of CdS deposited increased with the quantity of H_2S introduced. This probably caused the absence of metallic cadmium in the deposits with 500 ppm of H_2S.

4.2.4. Release experiments

In the same way as in the release experiments with zinc, the influence of water vapour, HCl and H_2S on the gas phase concentration and speciation of cadmium was investigated by MBMS. The gas flow was 4.3 l/min and each experiment was carried out three times, each with different temperatures at the end of the furnace. Experiments were conducted at 1000, 900 and 700 °C. As the mass spectrometer only determines the gaseous ionized species based on their mass-to charge ratios (m/z), it was necessary to carry out a calibration before starting the experiments. With this calibration it was possible to correlate the intensities of the isotopes present in the experiments with the heavy metal vapour concentration (ppm) obtained. In the experiments of cadmium the monitored species were $^{114}Cd^+$, $^{130}CdO^+$, $^{146}CdO_2^+$, $^{184}CdCl_2^+$ and $^{139}CdS^+$. However,

$^{146}CdO_2$ was not found in the gas phase during the experiments. The correlation between the ion signal intensities of the monitored species and the obtained concentration (ppm) in the gas phase is shown in Figure 46.

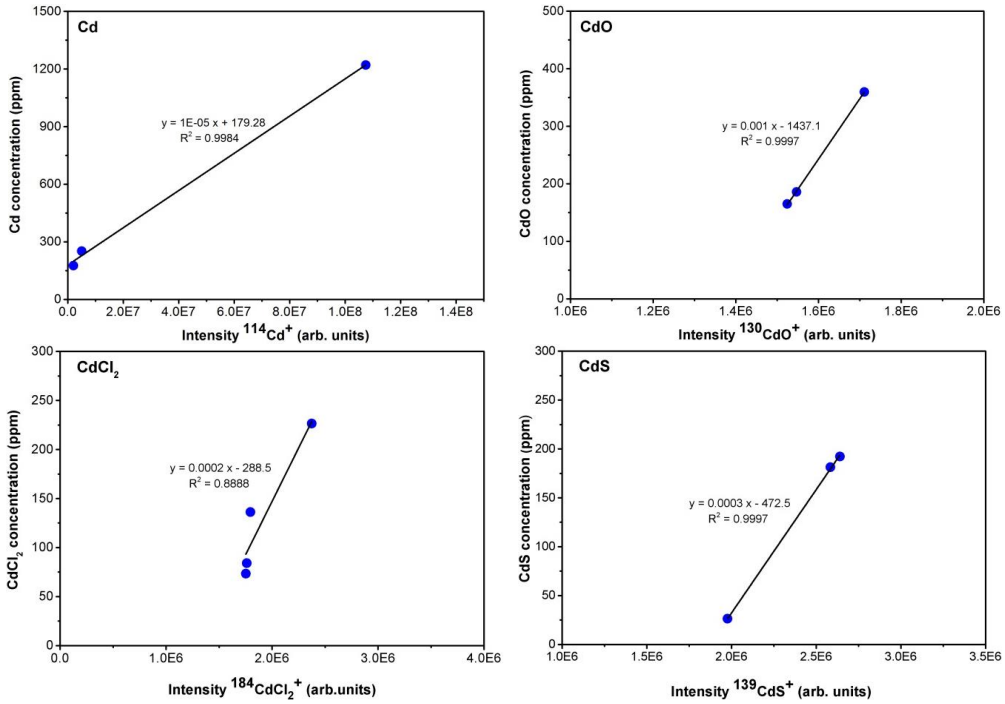

Figure 46. Calibration curves for the release experiments with cadmium.

The results of the MBMS measurements are provided in Figure 47, Figure 48 and Figure 49. The graphs show the minor cadmium species present in the gas phase at 1000, 900 and 700 °C. Cd(g) was the major species in all experiments. Its concentration in the gas phase during the experiments was much higher than the amounts of the other Cd-species present in the gas phase. Due to the difficulty of vaporizing the same amount of cadmium in every experiment and therefore, obtaining similar concentrations of cadmium in the experiments, only a qualitative analysis could be achieved. The speciation of cadmium and the behaviour of each species present in the gas phase were studied. An overview of the percentage concentrations of all the species detected in the gas phase is given in the tables present on the right of the experimental results.

Influence of H_2O

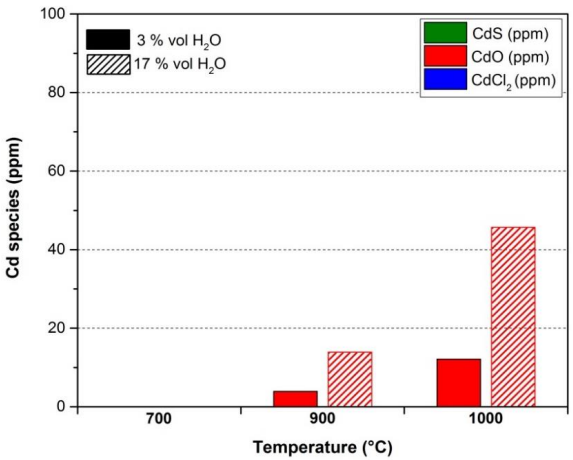

Concentration of gaseous Cd-species (%)				
	3 % vol H_2O		17 % vol H_2O	
	Cd	CdO	Cd	CdO
1000 °C	99.0	1.0	84.6	15.4
900 °C	97.8	2.2	98.1	1.9
700 °C	100.0	0.0	100.0	0.0

Figure 47. Concentration of minor gaseous cadmium species at 1000, 900 and 700 °C when the atmosphere contained water vapour (3 – 17 % vol). Note that Cd(g), the major species in the gas phase, is not represented.

The release experiments showed that during the experiments with H_2O, Cd and CdO were the only compounds present in the gas phase. As it can be seen in the table, Cd was the dominant species in all experiments. It represented approximately 98 – 99 % of the total cadmium present in the gas phase. The concentration of CdO in both experiments increased with the temperature. However, at 700 °C no CdO was present in the gas phase.

As it can be seen in the table, the concentration of CdO was considerably higher in the experiments with 17 % vol of H_2O than in the experiments with 3 % vol of water. Thus, it seemed that with a high amount of H_2O, higher concentrations of CdO were present in the gas phase.

Influence of HCl

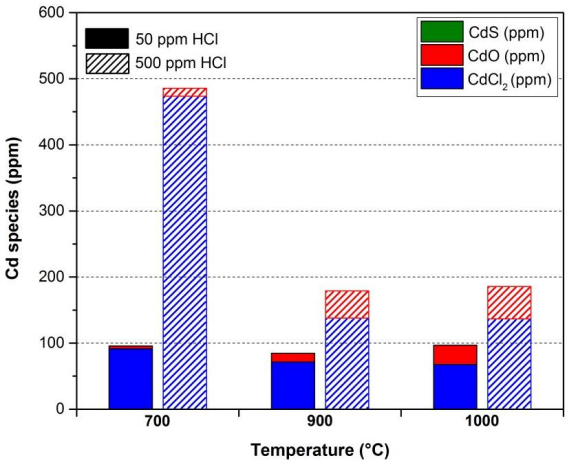

Concentration of gaseous Cd-species (%)						
	50 ppm HCl			500 ppm HCl		
	Cd	CdO	$CdCl_2$	Cd	CdO	$CdCl_2$
1000°C	79.3	6.2	14.5	46.2	14.2	39.6
900 °C	96.3	0.6	3.2	56.2	10.0	33.7
700 °C	87.4	0.5	12.1	67.4	0.8	31.8

Figure 48. Concentration of minor gaseous cadmium species at 1000, 900 and 700 °C when the atmosphere contained HCl (50 – 500 ppm). Note that Cd(g), the major species in the gas phase, is not represented.

The release experiments with HCl showed that cadmium was in the gas phase as a mixture of Cd, $CdCl_2$ and CdO (see Figure 48). Cd was the major species in every experiment. In both experiments the amount of CdO was generally low and increased gently with the temperature. The concentration of $CdCl_2$ was higher than the concentration of CdO and it also increased with the temperature. Furthermore, it could be noticed that the concentrations of the minor species, CdO and $CdCl_2$, were higher in the experiments with 500 ppm HCl than in the experiments with only 50 ppm HCl. The high concentration of $CdCl_2$ at 700 °C with 500 ppm HCl was the result of a high vaporization of cadmium in the experiment. That means, due to the temperature gradient in the reaction zone a great amount of cadmium was vaporized and therefore, the total concentration of cadmium in the experiment was high. However, as it can be seen in the table, the overall percentage of the species was in concordance with the other experimental results.

Influence of H_2S

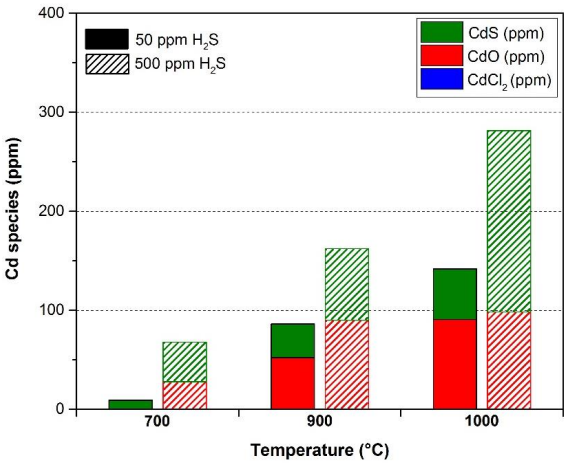

Concentration of gaseous Cd-species (%)						
	50 ppm H_2S			500 ppm H_2S		
	Cd	CdO	CdS	Cd	CdO	CdS
1000°C	97.6	1.5	0.9	52.5	16.5	30.9
900 °C	93.2	4.1	2.7	66.6	18.6	14.8
700 °C	97.1	0.0	2.9	85.3	6.1	8.6

Figure 49. Concentration of minor gaseous cadmium species at 1000, 900 and 700 °C when the atmosphere contained H_2S (50 – 500 ppm). Note that Cd(g), the major species in the gas phase, is not represented.

The results of the release experiments with H_2S are depicted in Figure 49. Cadmium was present in the gas phase as a mixture of Cd, CdS and CdO. The major species in the gas phase was Cd. The concentration of the minor species, CdO and CdS, increased with the temperature. In general, the concentration of CdS was higher than the concentration of CdO, especially with 500 ppm H_2S. As it can be observed in the table, only in the experiments with 500 ppm H_2S the concentrations of CdO and CdS were significant. In the experiment with 50 ppm H_2S they represented less than 7 % of the total Cd-species present in the gas phase.

4.2.5. Scheil-Gulliver cooling calculations for the gas phase

The release behaviour of cadmium under the influence of H_2O, HCl and H_2S predicted by the Scheil-Gulliver cooling model is shown in this section. The calculations show the speciation of the main inorganic gaseous species at temperatures between 1000 °C and room temperature.

Influence of H_2O

The speciation of the gas phase predicted by the Scheil-Gulliver cooling calculations in an atmosphere containing water vapour and cadmium is shown in Figure 50. The graph shows a comparison between the results obtained with 3 and 17 % vol water vapour in the atmosphere. The results obtained with 3 % vol water are depicted with a solid line and the results of an atmosphere containing 17 % vol water vapour are depicted with a dashed line.

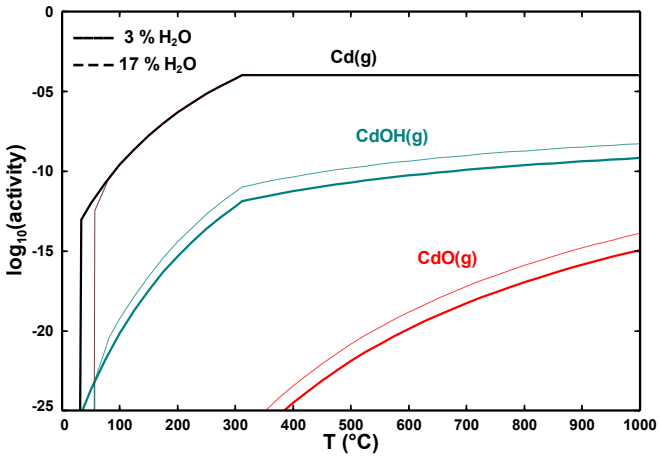

Figure 50. Gaseous cadmium-containing species versus temperature in an atmosphere containing 3 – 17 % vol of H_2O calculated by the Scheil-Gulliver cooling model.

According to the calculations, Cd, CdOH and CdO were the only species that were present in the gas phase at temperatures between 1000 and 50 °C when the atmosphere had water vapour. The concentration of CdO was less than 1 ppb and therefore, out of the range considered in this study. The concentration of Cd was 100 ppm ($\log_{10}(act) \approx 10^{-4}$) at temperatures between 1000 – 50 °C. At temperatures less than 50 °C the concentration of Cd decreased significantly. CdOH was in the gas phase at concentrations considerably smaller than Cd. Besides, the concentration of CdOH increased with the temperature and with the amount of water considered.

Influence of HCl

The release behaviour of cadmium when 50 and 500 ppm of HCl were present in the atmospheric conditions predicted by the Scheil-Gulliver cooling model is depicted in Figure 51. In this case, the results for 50 ppm of HCl in the atmosphere are depicted with a solid line and the results obtained with 500 ppm of HCl are depicted with a dashed line.

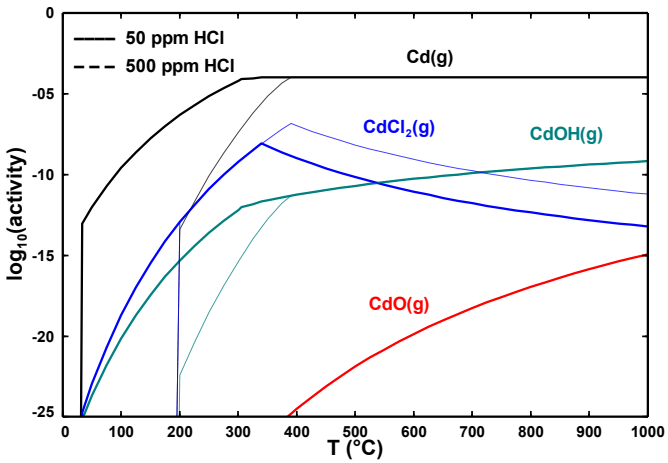

Figure 51. Gaseous cadmium-containing species versus temperature in an atmosphere containing 50 – 500 ppm of HCl calculated by the Scheil-Gulliver cooling model.

When the atmosphere had HCl the main inorganic species present in the gas phase were Cd, CdOH, $CdCl_2$ and CdO. However, CdO was present in concentrations smaller than those addressed in this investigation. 100 ppm of Cd was present at temperatures between 1000 and 350 °C. The concentration of $CdCl_2$ decreased with the temperature and a higher concentration of the species was supposed to be in the gas phase with high amounts of HCl. At temperatures below 350 °C the concentration of $CdCl_2$ decreased abruptly. The concentration of CdOH increased with the temperature. The amount of HCl did not influence the concentration of CdOH present in the gas phase at high temperatures.

Influence of H_2S

Figure 52 shows the release behaviour of cadmium predicted by FactSage when H_2S was introduced into the atmosphere. A comparison between the results with 50 ppm H_2S and 500 H_2S is shown. The results for 50 ppm of H_2S in the atmosphere are depicted with a solid line and the results for 500 ppm of H_2S are depicted with a dashed line.

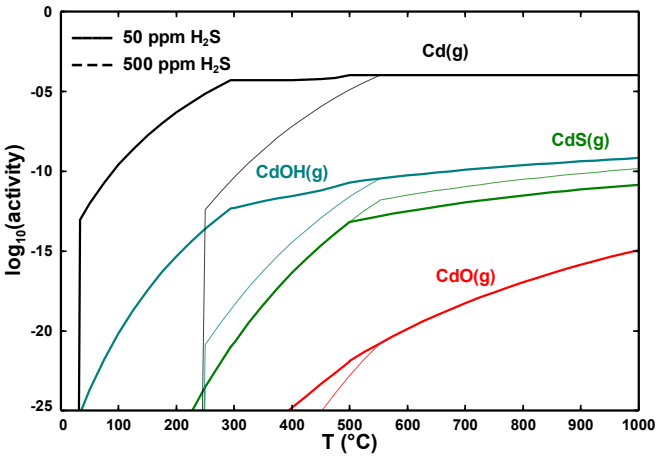

Figure 52. Gaseous cadmium-containing species versus temperature in an atmosphere containing 50 – 500 ppm of H_2S calculated by the Scheil-Gulliver cooling model.

The calculations predicted the speciation of the main inorganic gaseous species when H_2S was introduced into the atmosphere. According to the calculations, Cd, CdOH, CdS and CdO were the only cadmium-containing species present in the gas phase. Like in the calculations with H_2O and HCl, the concentration of CdO was out of the concentrations considered in this study. With 50 ppm H_2S, 100 ppm of Cd were in the gas phase at temperatures between 1000 and 250 °C. However, in the calculation with 500 ppm H_2S, the concentration of Cd started to decrease at 550 °C. The concentrations of CdOH and CdS increased with the temperature and the amount of H_2S influenced their behaviour. The concentration of CdS between 500 and 1000 °C was higher when 500 ppm of H_2S was present in the atmosphere. Furthermore, at temperatures between 280 – 550 °C, a higher concentration of CdOH was found in the gas phase with 50 ppm H_2S than with 500 ppm H_2S.

4.2.6. Discussion

According to the comparison of the experimental results with the results of the cooling calculations and the thermodynamic pseudo-equilibrium model, the following conclusions of the condensation and release behaviour of cadmium could be drawn:

Condensation behaviour of cadmium

FactSage 6.3 predicted a temperature of 310 °C for the evaporation of 100 ppm of cadmium under the atmospheric conditions considered in the experiments. However, the experiments showed that positioning the cadmium sample at 368 °C a concentration of approximately 86 ppm in the gas phase was obtained. Placing the sample at 378 °C a concentration of

133 ppm of cadmium was achieved. The calibration equation predicted a temperature of 370 °C to evaporate 100 ppm. Consequently, in all experiments the metal source was placed at 370 °C.

When the atmosphere contained water vapour, cadmium condensed as metallic Cd at temperatures between 325 – 78 °C (see Figure 39). Cadmium did not react with oxygen to form cadmium oxide. An increase of the water vapour amount did not seem to affect the condensation behaviour of this heavy metal. As it can be seen in Figure 43, the model calculations showed that cadmium condensed as metallic Cd at 310 – 150 °C independently of the water vapour amount considered. Thus, the results of the cooling calculations were in concordance with the experimental results.

In the presence of HCl, cadmium condensed as a mixture of $CdCl_2$ and metallic Cd (Figure 40). When 50 ppm HCl was present in the atmosphere, cadmium condensed as metallic cadmium at 325 – 78 °C. However, with 500 ppm HCl in the atmosphere cadmium preferably condensed at 438 – 163 °C. The deposits of $CdCl_2$ condensed at 438 – 163 °C when the atmosphere contained 500 ppm of HCl. Nevertheless, no $CdCl_2$ was observed during the experiments with 50 ppm of HCl. In general, larger amounts of HCl lead Cd to condense at slightly higher temperatures. The cooling calculations displayed in Figure 44 show that cadmium also condensed as a mixture of $CdCl_2$ and Cd when HCl was introduced into the atmosphere. With 50 ppm of HCl, cadmium condensed as $CdCl_2$ (340 – 200 °C) and Cd (310 – 150 °C). An increase of the amount of HCl to 500 ppm, induced the condensation of $CdCl_2$ at temperatures between 390 and 300 °C. However, with higher concentrations of HCl in the atmosphere, not any cadmium condensed as metallic cadmium. In summary, the experimental results showed that cadmium condensed at higher temperatures with high amounts of HCl. On the other side, the calculations predicted the condensation of $CdCl_2$ at higher temperatures with 500 ppm of HCl. No metallic cadmium condensed under these conditions. However, no comparison could be done with the condensation temperature of $CdCl_2$ as this species did not appear in the experiments with 50 ppm of HCl. Also the prediction of the Cd condensation did not fit perfectly with the model calculations. Hence, in this case, the cooling calculations were not able to predict accurately the experimental results.

In the experiments containing H_2S, cadmium condensed as CdS (438 – 163 °C) and Cd (438 – 78 °C) (see Figure 41) regardless the amount of the trace metal introduced. In the experiment with 500 ppm of H_2S, a larger amount of CdS condensed than in the experiment with only 50 ppm. The Scheil-Gulliver cooling model also predicted the condensation of cadmium as a mixture of metallic Cd and CdS in the presence of H_2S (Figure 45). With 50 ppm of H_2S cadmium condensed as Cd at 300 – 150 °C and CdS at 480 – 350 °C. However, when 500 ppm of H_2S was considered, only the species CdS condensed. An increase of the H_2S amount shifted the condensation of CdS to higher temperatures (530 – 400 °C). The amount of CdS deposited also in-

creased with the quantity of H_2S introduced. In the experiments, as well as in the calculations, the amount of CdS deposited increased with the amount of H_2S introduced into the atmosphere. However, no increase of the condensation temperature of CdS was observed with 500 ppm of H_2S in the experiments. Thus, the cooling calculations could predict quite well the results with 50 ppm of H_2S. With 500 ppm of H_2S some discrepancies were found.

According to the results of the thermodynamic pseudo-equilibrium model (see Figure 42), all experiments were in equilibrium except the experiments with H_2S. Alpha values of 0.8 and 0.7 fit the experimental results nicely. The model assumed that the experiments containing water and HCl were in equilibrium and hereby, the calculations with an alpha value of zero predicted well the experimental results. In the experiments with H_2S, Cd and CdS were probably saturated and condensed at lower temperatures than the predictions. Alpha decreased with larger concentrations of H_2S, which means that a larger formation of CdS compensated the super-cooling effect and the condensation was slightly shifted to higher temperatures. In this way, the model confirmed the importance of the chemical reactions in the condensation behaviour of cadmium. In the graphs it can be observed that cadmium started to condense at around 400 – 500 °C when H_2O and HCl were considered. However, in the experiments with H_2S, the condensation started at 550 and 650 °C.

Release behaviour of cadmium

Due to the difficulty of vaporizing the same amount of cadmium in every experiment only a qualitative analysis could be achieved. The main target of these experiments was the determination of the cadmium-species in the gas phase and their behaviour under different experimental conditions.

The results of the MBMS measurements showed that Cd(g) was the major species in all experiments. Its concentration in the gas phase during the experiments was much higher than the amounts of the other Cd-species present in the gas phase.

The release experiments showed that during the experiments with H_2O, Cd and CdO were the only compounds present in the gas phase (see Figure 47). Cd was the dominant species in all experiments and represented approximately 98 – 99 % of the total cadmium present in the gas phase. The concentration of CdO increased with the temperature and with the amount of water vapour. The results of the Scheil-Gulliver calculations predicted the existence of high concentrations of Cd and CdOH in the gas phase when the atmosphere had water vapour (see Figure 50). The concentration of CdO was lower than 1 ppb. However, in the experiments the concentration of CdO was at ppm level. Besides, no CdOH was detected in the gas phase. In conclusion, the speciation, as well as the behaviour of the species found in the gas phase were different in

the calculations and in the experiments. Thus, the calculations could not predict appropriately the behaviour of cadmium when H_2O was considered in the calculations.

The experiments with HCl showed that cadmium was in the gas phase as a mixture of Cd, $CdCl_2$ and CdO (see Figure 48). Cd was the major species in every experiment. The amount of CdO and $CdCl_2$ increased gently with the temperature. Besides, the concentration of $CdCl_2$ was higher than the concentration of CdO. It could be noticed that the concentrations of CdO and $CdCl_2$, the minor species, were higher in the experiments with 500 ppm HCl than in the experiments with only 50 ppm HCl. The calculations predicted the existence of Cd, CdOH, $CdCl_2$ and CdO (see Figure 51). CdO was present in the gas phase in concentrations smaller than those addressed in this investigation (1 ppb). The concentration of $CdCl_2$ decreased with the temperature and a higher concentration of the species was supposed to be in the gas phase with high amounts of HCl. The concentration of CdOH increased with the temperature and HCl did not influence its behaviour at high temperatures. Although the major species in the experiments and in the calculations concurred, their behaviour was different. The concentration of $CdCl_2$ increased with rising temperatures and a higher amount of HCl. However, in the calculations the concentration of $CdCl_2$ decreased with the temperature. Furthermore, in the experiments the concentration of CdO was appreciable. No CdOH was detected. The results of the Scheil-Gulliver calculations definitely did not show the same tendency as observed in the experiments.

The results of the experiments with H_2S showed that cadmium was present in the gas phase as a mixture of Cd, CdS and CdO (see Figure 49). The major species in the gas phase was Cd. The concentration of the minor species, CdO and CdS, increased with the temperature. In general, the concentration of CdS was higher than the concentration of CdO, especially with 500 ppm H_2S. According to the Scheil-Gulliver calculations, Cd, CdOH, CdS and CdO were the only cadmium-containing species present in the gas phase (see Figure 52). The concentration of CdO was out of the range considered in this study. The concentrations of CdOH and CdS increased with the temperature and the amount of H_2S influenced their behaviour. Thus, the concentration of CdS between 1000 and 500 °C was higher when 500 ppm of H_2S was present in the atmosphere. The behaviour of CdO and CdS in the calculations and in the experiments was found to be similar. However, in the experiments the concentration of CdO was higher than in the calculations. Besides, in the experiments no CdOH was found in the gas phase. For this reason, it could not be concluded that the Scheil-Gulliver model predicted accurately the experimental results.

To sum up, the Scheil-Gulliver calculations could be considered a good tool for the prediction of the condensation behaviour of cadmium. In general, a good agreement between the cooling calculations and the experimental results was found. The speciation as well as the temperatures at which the species condensed under the influence of H_2O, HCl and H_2S had the same trend in the calculations as in the experimental results. Only in the condensation experiments

with HCl and H_2S some differences were observed. These differences could be explained by the difficulty of evaporating the same amount of ppm in each experiment and by the error associated to the analytical methods for determining the species present in the filters of the cooling zone. Nevertheless, for the gas phase, the Scheil-Gulliver calculations did not predict the experimental results accurately. Although for some species the behaviour in the calculations and in the experiments showed the same trend, the model predicted the existence of species that were not found in the gas phase during the experimental runs.

4.3. Lead

4.3.1. Condensation experiments

The total gas flow in the condensation experiments with lead was 645 ml/min and the duration of each experiment was 24 h. Similar to the experiments with zinc and cadmium the temperature at which the metal boat should be placed in order to obtain 100 ppm of the metal in the gas was first estimated with FactSage (see Figure 53). The program predicted a temperature of 810 °C for the vaporization of 100 ppm of lead under the experimental conditions.

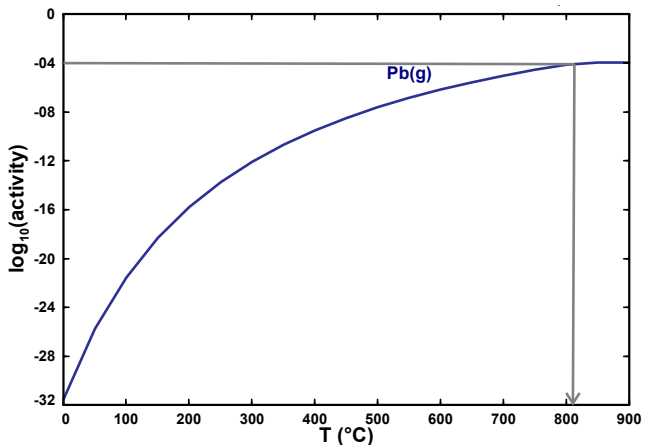

Figure 53. FactSage´s estimation of the necessary temperature for the vaporization of 100 ppm lead.

This temperature was experimentally proved evaporating lead at different temperatures between 780 – 900 °C and determining the amount of lead that went to the gas phase in each case. The length of the experiments was 24 h and the gas composition was the same as in the condensation experiments. As lead source for all the experiments metallic lead was used.

The correlation between the obtained lead concentration and the temperature is depicted in Figure 54. Placing the sample boat at 851 °C, 112 ppm of lead was evaporated. The location of the furnace´s reaction zone at which the temperature was 846 °C, was the position at which the sample boat with the source was placed during the experiments with lead.

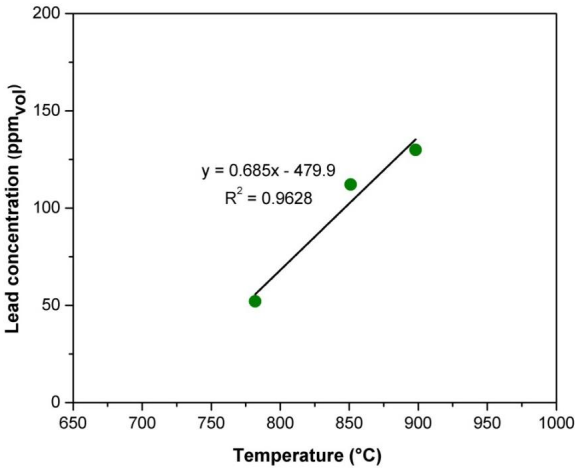

Figure 54. Correlation of lead concentration (ppm) and temperature (°C).

The condensation experiments carried out with lead and the corresponding obtained results are explained and shown in the following sections. In the experiments the influence of H_2O, HCl and H_2S on the condensation behaviour of lead was investigated.

Influence of H_2O

Figure 55 shows the condensation distribution of lead species in the tubes and in the outer tube when the atmosphere contained H_2O(g). The amount of lead condensed as metallic Pb, PbO-PbO_2, $PbCl_2$ and PbS are depicted in purple, red, blue and green colour respectively.

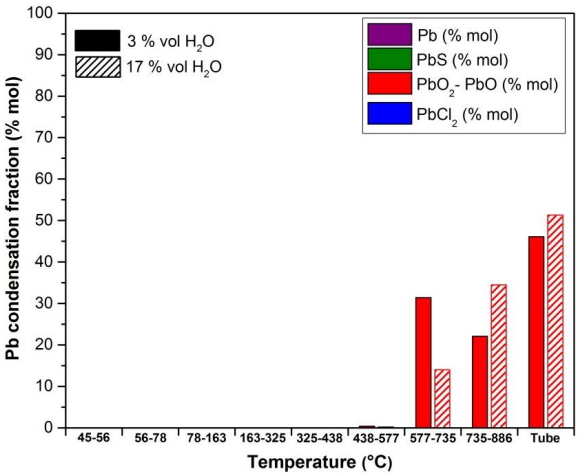

Figure 55. Condensation distribution of lead in the outer tube and in the filters placed along the cooling zone in an atmosphere containing 3 % vol and 17 % vol of water vapour.

Lead condensed as a mixture of PbO_2 and PbO in the first and second filters, i.e. at temperatures between 886 – 577 °C regardless of the volume of water vapour in the atmosphere. Therefore, an increase of the $H_2O(g)$ amount did not influence the condensation behaviour of lead.

Influence of HCl

Figure 56 shows the condensation behaviour of Pb when HCl was introduced into the outer tube. A comparison between the experiments with 0 ppm HCl, 50 ppm HCl and 500 ppm HCl is shown. The amounts of lead that condensed as metallic PbO-PbO_2 and $PbCl_2$ are depicted in red and blue colour, respectively. The bars on the left show the results obtained when the atmosphere contained 0 ppm HCl. The bars in the middle and on the right are the results with 50 and 500 ppm HCl.

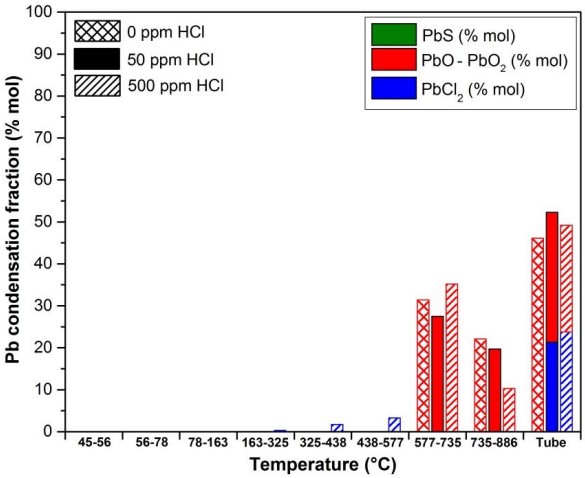

Figure 56. Condensation distribution of lead in the outer tube and in the filters placed along the cooling zone in an atmosphere containing 0 ppm HCl, 50 ppm HCl and 500 ppm of HCl.

Lead condensed as a mixture of PbO_2 and PbO in the first and second filter when no HCl was introduced into the atmosphere.

Lead condensed as a mixture of PbO-PbO_2 and $PbCl_2$ when HCl was introduced into the experiment. PbO-PbO_2 condensed in both experiments in the first and second filters (886 – 577 °C) from the cooling zone. In the experiment with 50 ppm of HCl, $PbCl_2$ condensed mostly in the outer tube. As it can be observed in the graph, 0.5 % of the total percentage condensed as $PbCl_2$ deposited in the fifth filter. In total, 21.8 % condensed as $PbCl_2$ in the experiment with 50 ppm HCl but it mostly condensed in the outer tube. The fraction condensed in the tube could be considered as $PbCl_2$ that condensed in the fifth filter. This was confirmed observing the experimental outer tube after the experiment. When 500 ppm of HCl was introduced into the experiment, $PbCl_2$ however condensed in the third, fourth and fifth filters. Therefore, the condensation of $PbCl_2$ started at higher temperatures than with only 50 ppm HCl in the atmosphere. In this case, the total percentage condensed as $PbCl_2$ corresponded to 29.2 %.

Thereby, an increase in the HCl amount increased the amount of lead condensing as $PbCl_2$. It seemed that $PbCl_2$ condensed at higher temperatures when 500 ppm of HCl was introduced into the experiment than when only 50 ppm of HCl was present. No change was observed in the condensation temperature of PbO-PbO_2 when the HCl introduced increased.

Influence of H_2S

Figure 57 shows the condensation behaviour of the heavy metal when H_2S was introduced into the outer tube. A comparison between the experiments with 0, 50 and 500 ppm H_2S is shown. Like in the experiments with HCl, the bars on the left represent the results obtained when the atmosphere contained 0 ppm H_2S. The bars in the middle and on the right are the results with 50 and 500 ppm H_2S.

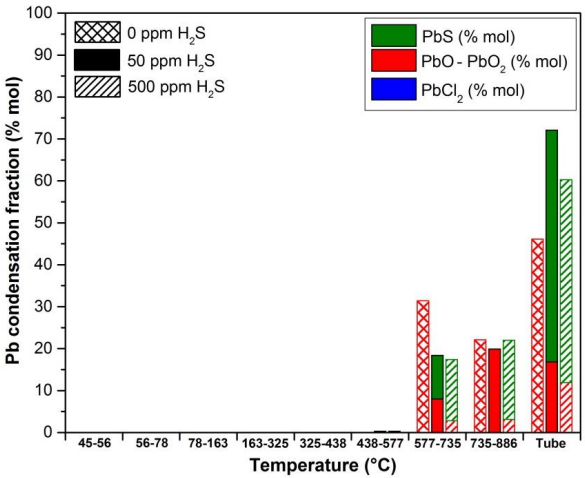

Figure 57. Condensation distribution of lead in the outer tube and in the filters placed along the cooling zone in an atmosphere containing 0 ppm H_2S, 50 ppm H_2S and 500 ppm of H_2S.

Lead condensed as a mixture of PbO_2 and PbO in the first and second filter when no H_2S was introduced into the atmosphere.

The experiments with lead showed that Pb condensed as PbS and PbO-PbO_2. Both did condense in the first and second filters (886 – 577 °C). PbS condensed with 500 ppm of H_2S in the atmosphere at 886 – 577 °C while with only 50 ppm of H_2S, it started to condense at 735 °C. The amount of lead condensed as PbS under both experimental conditions was 53.3 % and 82.3 %, respectively.

Definitely, the introduction of 500 ppm of H_2S promoted the condensation of PbS at higher temperatures (886 – 577 °C). An increase in the amount of H_2S also increased the amount of lead condensed as PbS. Nevertheless, the amount of H_2S did not seem to affect the condensation behaviour of PbO-PbO_2. In all cases PbO-PbO_2 condensed at the same temperatures and in the same filters as in the cases shown before with water vapour and HCl present in the experiments.

4.3.2. Thermodynamic pseudo-equilibrium model

Figure 58 shows the comparison between the model calculations and the experimental results of the condensation of lead in an atmosphere containing H_2O (3 – 17 % vol), HCl (50 – 500 ppm) and H_2S (50 – 500 ppm).

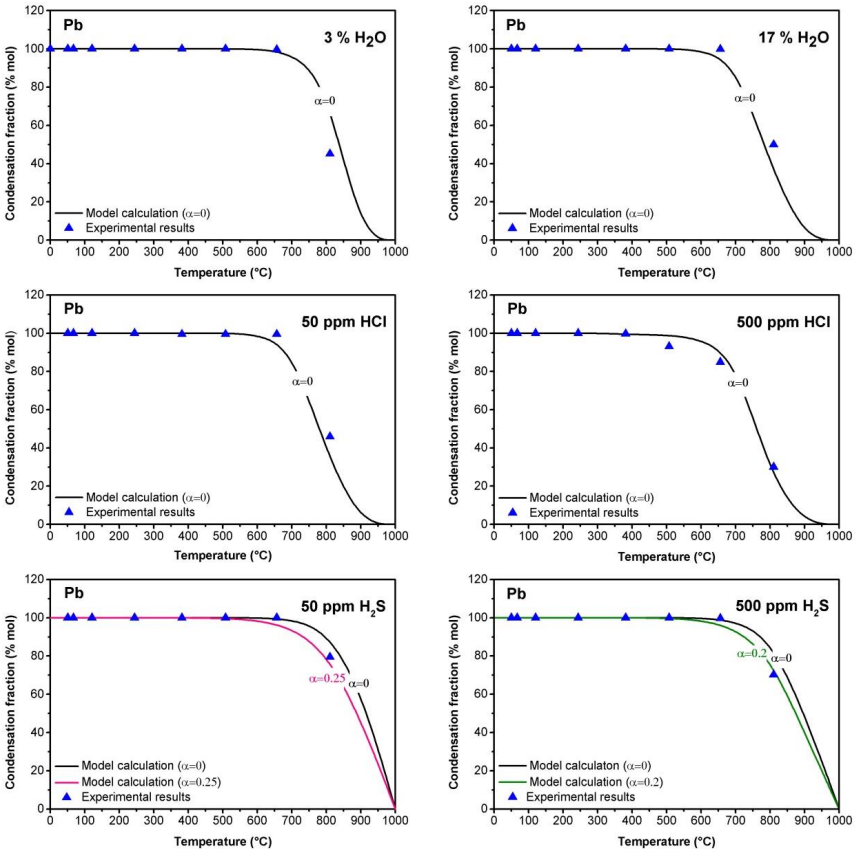

Figure 58. Comparison between the calculated and the experimental results of the condensation of lead vapours in the presence of H_2O (3 – 17 % vol), HCl (50 – 500 ppm) and H_2S (50 – 500 ppm).

In this case, the curve-fitting of the experimental results indicate an alpha value of zero for all experimental conditions except for the experiments with 50 and 500 ppm of H_2S, where alpha values of 0.25 for the experiment with 50 ppm of H_2S and 0.2 for the one with 500 ppm of H_2S fit nicely the experimental results. For this reason, the model assumes that the experiments

containing H_2O or HCl were in equilibrium and hereby, the model calculations predicted very well the experimental results.

In the experiments with H_2S (see Figure 58) the deposition fractions predicted by the model were a little higher than the observed in the experimental results. Thus, the experiments did not reach the equilibrium state and the condensation of the metallic vapours was affected by super-cooling effect. That means, PbO_2-PbO and PbS vapours were possible saturated and they condensed at lower temperatures than the temperatures predicted by the calculations. However, according to the calculations the experimental results were not very far away from an equilibrium state.

As it can be seen in the graph, the alpha value was smaller in the experiments with 500 ppm of H_2S (0.2) than in the experiments with 50 ppm of the trace gas (0.25). The formation of a higher amount of PbS compensated slightly the negative effect of super-cooling and the condensation was shifted to slightly higher temperatures. According to this, the super-cooling effect could be offset by the chemical reaction of inorganic vapours when H_2S was introduced into the atmosphere.

It can be concluded, that chemical reactions had an influence on the condensation behaviour of lead when H_2S was present in the atmosphere. However, as the experiments with H_2O and HCl were supposed to be in equilibrium, no conclusions could be drawn about the influence of chemical reactions in the condensation of cadmium when H_2O or HCl were in the atmosphere.

4.3.3. Scheil-Gulliver cooling calculations for the solid phase

The Scheil-Gulliver cooling calculations performed with FactSage 6.3 in order to predict the condensation behaviour of lead are presented in this section. The calculations were carried out at decreasing temperature steps of 25 °C starting from 1000 °C to room temperature. The results show the condensed cadmium species and their condensation temperature. As well as in the condensation experiments, the influence of H_2O, HCl and H_2S in the condensation behaviour of lead was analysed.

Influence of H_2O

The lead speciation predicted by the Scheil-Gulliver Cooling calculations in an atmosphere containing water vapour is depicted in Figure 59. A comparison between the results with 3 % vol of water and the results with 17 % vol of water is presented. The species depicted with a solid line are the species that condensed when the atmosphere contained 3 % vol of H_2O and the ones depicted with a dashed line are the species that condensed when the atmosphere contained 17 % vol of H_2O.

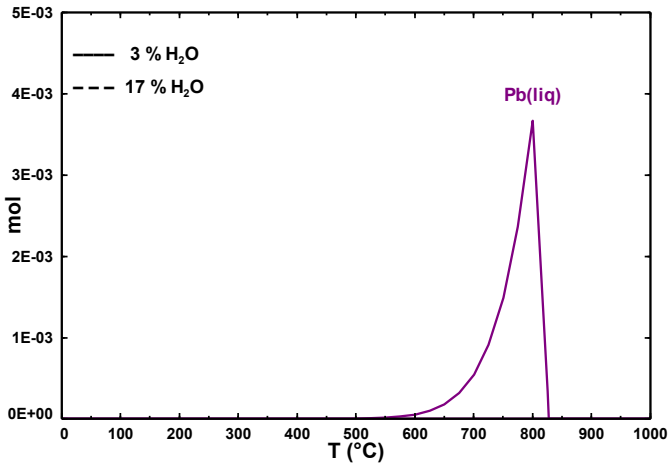

Figure 59. Speciation of the condensed phase during cooling from 1000 to 0 °C predicted by the Scheil-Gulliver cooling model in an atmosphere containing water vapour and lead.

The model calculations show that lead condensed as Pb(liq) at 825 – 550 °C independently of the water vapour amount considered. The results from both simulations overlapped, the program predicted for both atmospheric conditions the condensation of the same amount of Pb(liq) at the same temperatures. The model also predicted the condensation of a very small amount of Pb(s) at 325 – 250 °C. However, its concentration was so low that it cannot be appreciated in the graph. Therefore, according to the cooling calculations, it can be considered that the amount of water vapour introduced into the atmosphere did not have an influence on the condensation behaviour of lead.

Influence of HCl

The results obtained from the Scheil-Gulliver cooling model when 50 and 500 ppm of HCl were present in an atmosphere containing lead are presented in Figure 60. In this case, the results obtained when 50 ppm of HCl was in the atmosphere are depicted with a solid line and the results obtained when the atmosphere contained 500 ppm of HCl are depicted with a dashed line. The amount of lead condensed as Pb(liq) is depicted in purple.

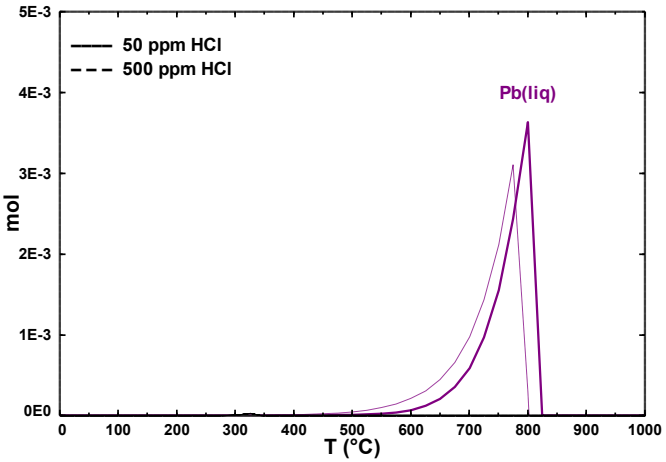

Figure 60. Speciation of the condensed phase during cooling from 1000 to 0 °C predicted by the Scheil-Gulliver cooling model in an atmosphere containing HCl and lead.

The cooling calculations showed that lead condensed basically as Pb(liq) when HCl was taken into account. When the atmosphere contained 50 ppm of HCl, lead condensed as Pb(liq) at 825 – 550 °C. However, when the atmosphere contained 500 ppm of HCl, Pb(liq) condensed at 800 – 500 °C, as shown in Figure 60. A small amount of Pb(s) and $PbCl_2$(s) also condensed under these conditions. However, the condensed amounts of both compounds were so low that they are barely appreciable. Pb(s) condensed at 265 – 200 °C and $PbCl_2$(s) at 350 – 250 °C. Therefore, it could be concluded that the increase of HCl in the atmosphere caused Pb(liq) to condense at lower temperatures.

Influence of H_2S

The cooling calculations carried out with FactSage when H_2S was introduced in an atmosphere containing lead are shown in Figure 61. A comparison between the results with 50 ppm H_2S and 500 ppm H_2S is shown.

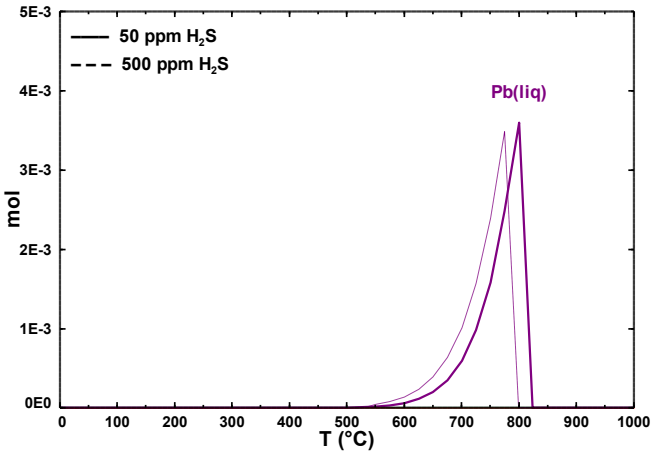

Figure 61. Speciation of the condensed phase during cooling from 1000 to 0 °C predicted by the Scheil-Gulliver cooling model in an atmosphere containing H_2S and lead.

The simulation results for lead showed the condensation of Pb(liq) at temperatures between 800 – 550 °C when 50 ppm H_2S was considered. With 500 ppm of H_2S, Pb(liq) condensed at temperatures between 825 – 550 °C. Hence, the increase in the amount of H_2S induced the condensation of Pb(liq) at lower temperatures. The cooling calculations also showed the condensation of lead as PbS at 525 – 400 °C. However, the amount of PbS deposited was very small in comparison with the deposits of Pb(liq).

4.3.4. Release experiments

The influence of water vapour, HCl and H_2S on the gas phase concentration and speciation of lead was investigated by MBMS. The gas flow was 4.3 l/min and each experiment was carried out four times, each with different temperatures at the end of the furnace. Experiments have been conducted at 1100, 900, 800 and 600 °C. As the mass spectrometer only determines the gaseous ionized species based on their mass-to charge ratios (m/z), it was necessary to carry out a calibration before starting the experiments. With this calibration it was possible to correlate the intensities of the isotopes present in the experiments with the heavy metal vapour concentration (ppm) obtained. In the experiments of lead the monitored species were $^{208}Pb^+$, $^{224}PbO^+$, $^{240}PbO_2^+$, $^{278}PbCl_2^+$ and $^{242}PbS^+$. The correlation between the ion signal intensities of the monitored species and the obtained concentration (ppm) in the gas phase is shown in Figure 62.

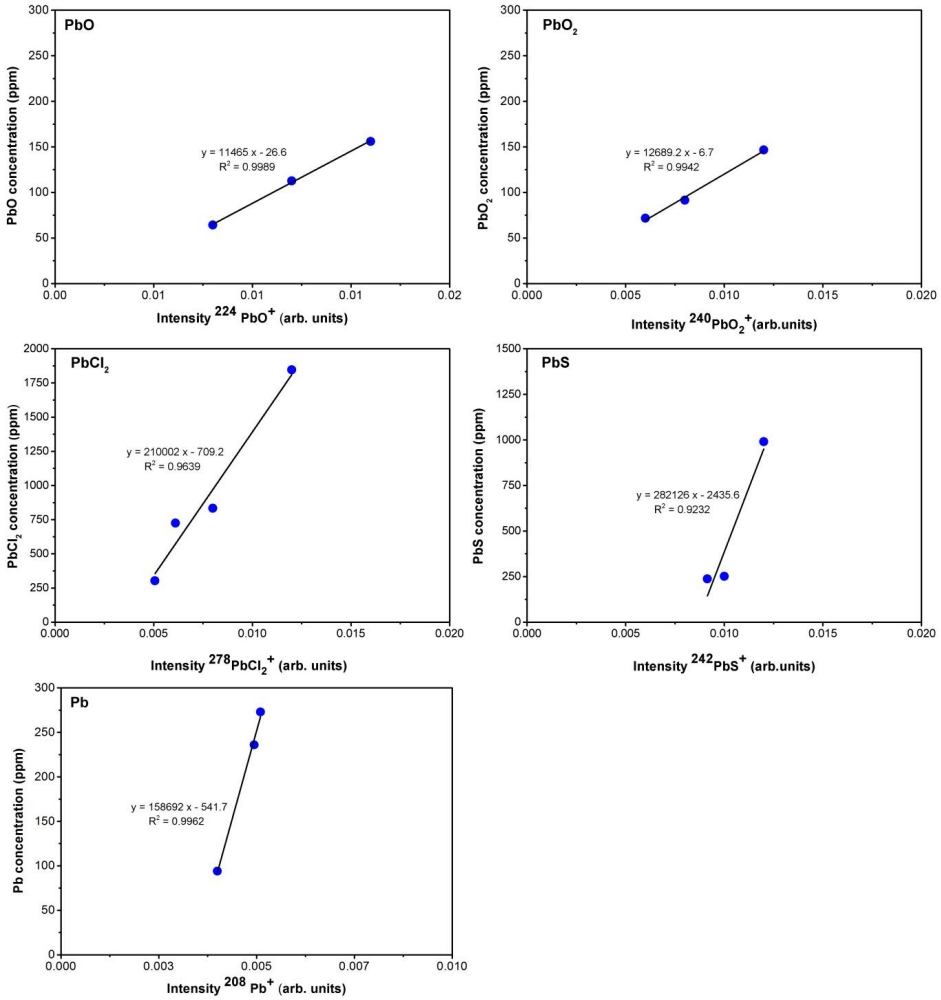

Figure 62. Calibration curves for the release experiments with lead.

The results of the MBMS measurements are provided in Figure 63, Figure 64 and Figure 65. The graphs show the speciation and behaviour of the Pb-species under the influence of H_2O, HCl and H_2S at different temperatures. Pb(g) was the major species in all experiments and its concentration during the experiments was much higher than the amounts of the other Pb-species present in the gas phase. However, in the graphs only the minor lead species present in the gas phase at 1100, 900, 800 and 600 °C are depicted. Due to the difficulty of vaporizing the same amount of lead in every experiment and therefore, obtaining a similar concentration of lead in

the experiments, only a qualitative analysis could be achieved. An overview of the percentage concentrations of all the species detected in the gas phase is given in the tables present on the right of the experimental results.

Influence of H_2O

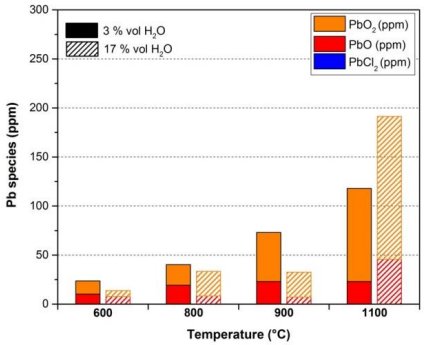

Concentration of gaseous Pb-species (%)						
	3 % vol H_2O			17 % vol H_2O		
	Pb	PbO	PbO_2	Pb	PbO	PbO_2
1100 °C	36.6	12.4	51.1	50.5	11.9	37.6
900 °C	76.4	7.4	16.2	73.0	6.0	21.0
800 °C	87.2	6.1	6.7	53.6	35.6	10.7
600 °C	79.9	8.5	11.6	95.0	2.8	2.2

Figure 63. Concentration of minor gaseous lead species at 1100, 900, 800 and 600 °C when the atmosphere contained water vapour (3 – 17 % vol). Note that Pb(g), the major species in the gas phase, is not represented.

The experimental results showed that Pb, PbO and PbO_2 were present in the gas phase during the experiments with H_2O. As shown in the table, Pb was the dominant species in every experiment. The concentration of the minor species, PbO and PbO_2, increased with the temperature. In general, the concentration of PbO_2 was higher than the concentration of PbO. Considering the results, the amount of water did not have a great influence on the release behaviour of lead.

Influence of HCl

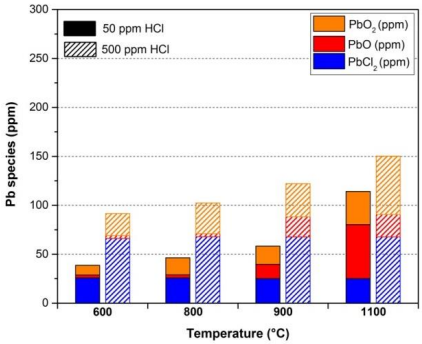

Concentration of gaseous Pb-species (%)								
	50 ppm HCl				500 ppm HCl			
	Pb	PbO	PbO_2	$PbCl_2$	Pb	PbO	PbO_2	$PbCl_2$
1100 °C	56.6	20.8	12.8	9.7	35.3	9.9	26.0	28.8
900 °C	67.3	8.3	10.3	14.2	57.3	7.1	11.8	23.7
800 °C	75.1	10.7	5.8	8.4	57.4	1.3	13.0	28.2
600 °C	96.4	0.3	0.9	2.4	55.2	1.4	10.8	32.6

Figure 64. Concentration of minor gaseous lead species at 1100, 900, 800 and 600 °C when the atmosphere contained HCl (50 – 500 ppm). Note that Pb(g), the major species in the gas phase, is not represented.

The experiments with HCl showed that lead was released as a mixture of Pb, PbO, PbO_2 and $PbCl_2$. As it can be observed in the table, the dominant species was Pb. In general, the concentration of the oxides in the gas phase increased with the temperature. However, the concentration of $PbCl_2$ did not seem to change much with the temperature. In general terms, the concentration of PbO_2 was higher than the concentration of PbO, especially in the experiments with 500 ppm HCl. Furthermore, an increase in the amount of HCl seemed to influence the behaviour of the lead-species. Thus, with 500 ppm HCl, higher concentrations of $PbCl_2$ and PbO_2 were present in the gas phase. On the contrary, the concentration of PbO was smaller in the experiments with 500 ppm HCl than in the experiments with only 50 ppm, especially at 1100 °C.

Influence of H_2S

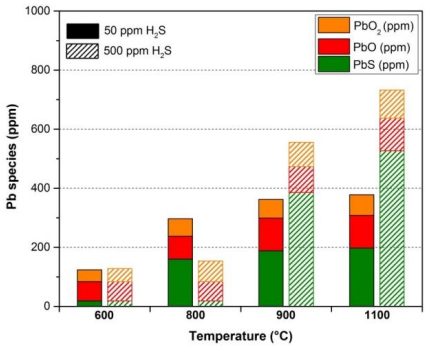

Concentration of gaseous Pb-species (%)								
	50 ppm H_2S				500 ppm H_2S			
	Pb	PbO	PbO_2	PbS	Pb	PbO	PbO_2	PbS
1100 °C	78.6	6.3	3.9	11.2	20.0	12.1	10.4	57.5
900 °C	79.1	6.4	3.6	10.9	16.3	13.3	12.4	58.1
800 °C	54.9	11.8	9.0	24.3	43.1	24.1	25.8	7.1
600 °C	87.9	7.5	4.6	0.0	38.8	31.1	21.1	9.0

Figure 65. Concentration of minor gaseous lead species at 1100, 900, 800 and 600 °C when the atmosphere contained H_2S (50 – 500 ppm). Note that Pb(g), the major species in the gas phase, is not represented.

The experiments with H_2S are shown in Figure 65. The species detected in the gas phase were Pb, PbO, PbO_2 and PbS. Pb was the dominant species in the experiments with 50 ppm H_2S. In all experiments, the concentrations of PbO seemed to be slightly higher than the concentrations of PbO_2. However, their concentrations were too similar to draw conclusions. The concentration of PbS increased strongly with the temperature. Besides, a higher amount of PbS was present in the experiments with 500 ppm H_2S than in the experiments with 50 ppm H_2S. Thus, in the experiments with 500 ppm H_2S, PbS was the major species. Its concentration in the gas phase was higher than the concentration of Pb. Therefore, it could be assumed that H_2S had a slight influence on the release behaviour of PbS.

4.3.5. Scheil-Gulliver cooling calculations for the gas phase

The release behaviour of lead under the influence of H_2O, HCl and H_2S predicted by the Scheil-Gulliver cooling model is shown in this section. The calculations show the speciation of the main inorganic gaseous species at temperatures between 1200 °C and room temperature.

Influence of H_2O

The speciation of the gas phase predicted by the Scheil-Gulliver cooling calculations in an atmosphere containing water vapour and lead is shown in Figure 66. The graph shows a comparison between the results obtained with 3 % vol and 17 % vol water vapour in the atmosphere. The results obtained with 3 % vol water are depicted with a solid line and the results containing 17 % vol water vapour are depicted with a dashed line.

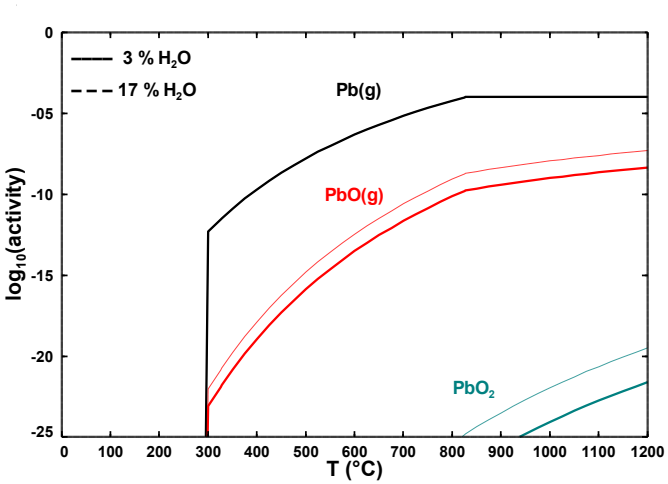

Figure 66. Gaseous lead-containing species versus temperature in an atmosphere containing 3 – 17 % vol of H_2O calculated by the Scheil-Gulliver cooling model.

According to the calculations, Pb, PbO and PbO_2 were the only gaseous species present in the gas phase when the atmosphere contained water vapour. A concentration of 100 ppm of Pb was in the gas phase at temperatures between 1000 – 850 °C. At lower temperatures, the concentration of Pb decreased significantly. The concentration of PbO was much smaller than the concentration of Pb and increased with the temperature. Besides, a higher concentration of PbO was in the gas phase with 17 % vol H_2O than with only 3 % vol H_2O. The amount of PbO_2 was out of the concentrations considered in this study and therefore, not taken into account.

Influence of HCl

The release behaviour of lead when 50 and 500 ppm of HCl were present in the atmospheric conditions predicted by the Scheil-Gulliver cooling model is depicted in Figure 67. In this case, the results for 50 ppm of HCl in the atmosphere are depicted with a solid line and the results for 500 ppm of HCl are depicted with a dashed line.

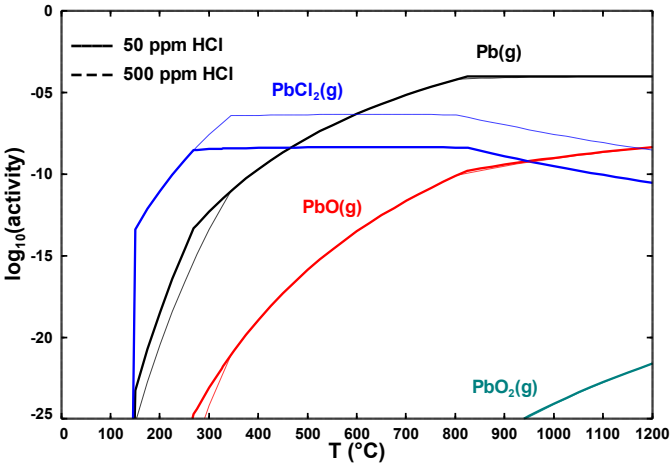

Figure 67. Gaseous lead-containing species versus temperature in an atmosphere containing 50 – 500 ppm of HCl calculated by the Scheil-Gulliver cooling model.

When the atmosphere had HCl, the main inorganic species present in the gas phase were Pb, $PbCl_2$ and PbO. PbO_2 was in the gas phase in very low concentrations. The concentration of Pb began to decrease at 800 °C. At 1000 – 800 °C a constant concentration of Pb was observed. The concentration of $PbCl_2$, the second major species in the gas phase, was, according to the model, constant at temperatures between 800 – 300 °C. At temperatures higher than 800 °C the concentration decreased with the temperature. The concentration of PbO was smaller than the concentration of $PbCl_2$ and increased with the temperature. Furthermore, an increase of the HCl amount introduced induced the presence of higher concentrations of $PbCl_2$. Nevertheless, HCl barely influenced the release of Pb and PbO_2.

Influence of H_2S

Figure 68 shows the release behaviour of lead predicted by FactSage when H_2S was introduced into the atmosphere. A comparison between the results with 50 ppm H_2S and 500 ppm H_2S is shown. The results for 50 ppm of H_2S in the atmosphere are depicted with a solid line and the results for 500 ppm of H_2S are depicted with a dashed line.

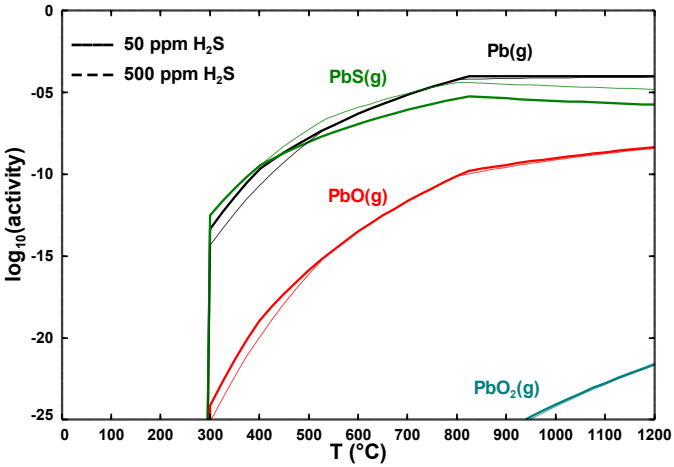

Figure 68. Gaseous lead-containing species versus temperature in an atmosphere containing 50 – 500 ppm of H_2S calculated by the Scheil-Gulliver cooling model.

In this case, the simulations predicted the existence of Pb, PbS, PbO and PbO_2 in the gas phase. The concentrations of all species increased with the temperature. In general, the concentration of Pb was higher than the concentration of PbS. Besides, the concentration of both compounds started to decrease at 825 °C. The concentration of PbO was much smaller than the concentrations of Pb and PbS. The amount of PbO_2 was very small to be considered. As it can be observed in the graph, an increase of the amount of H_2S caused the presence of higher amounts of PbS in the gas phase than when only 50 ppm of H_2S were introduced into the atmosphere.

4.3.6. Discussion

According to the comparison of the experimental results with the results of the cooling calculations and the thermodynamic pseudo-equilibrium model, the following conclusions of the condensation and release behaviour of lead could be drawn:

Condensation behaviour of lead

FactSage 6.3 predicted a temperature of 810 °C for the evaporation of 100 ppm of lead under the atmospheric conditions considered in the experiments. However, the experiments showed that positioning the lead sample at 851 °C a concentration of approximately 112 ppm in the gas phase was obtained. In all experiments the metal source was placed at 846 °C.

As shown in Figure 55, lead condensed as a mixture of PbO_2 and PbO at 886 – 577 °C regardless of the volume of water vapour in the atmosphere. Therefore, an increase of the $H_2O(g)$ amount

did not influence the condensation behaviour of lead. On the contrary, the model calculations predicted the condensation of lead as Pb(liq) at 825 – 550 °C independently of the water vapour amount considered. The model also predicted the condensation of a very small amount of Pb(s) at 325 – 250 °C (see Figure 59). Thus, the Scheil-Gulliver calculations did not match well with the experimental results.

Lead condensed as a mixture of PbO-PbO_2 (886 – 577 °C) and $PbCl_2$ (577 – 163 °C) when HCl was introduced into the experiment (see Figure 56). An increase of the HCl amount increased the amount of lead condensing as $PbCl_2$ as well as the temperature at which it was deposited. No change of the condensation temperature of PbO-PbO_2 was observed when the HCl amount increased. The cooling calculations predicted the condensation of lead as Pb(liq) when HCl was taken into account. When the atmosphere contained 50 ppm HCl, lead condensed as Pb(liq) at 825 – 550 °C. However, when the atmosphere contained 500 ppm HCl, Pb(liq) condensed at 800 – 500 °C, as shown in Figure 60. A small amount of Pb(s) and $PbCl_2$(s) also condensed under these conditions. However, the condensed amounts of both compounds were so low that they were barely appreciable. Pb(s) condensed at 265 – 200 °C and $PbCl_2$(s) at 350 – 250 °C. Thus, the speciation as well as the condensation temperatures of the species in the experiments were different to the ones of the calculations. Besides, the calculations did not predict the condensation of lead oxides at high temperatures. For these reasons, it could not be concluded that the Scheil-Gulliver calculations predicted well the condensation of lead when HCl was introduced into the atmosphere.

The experiments with H_2S showed that Pb condensed as PbS and PbO-PbO_2. Both species condensed at 886 – 577 °C (see Figure 57). An increase of the amount of H_2S raised the amount of lead condensed as PbS as well as its condensation temperature. Nevertheless, the amount of H_2S did not affect the condensation behaviour of PbO-PbO_2. The simulation results for lead showed a similar trend as in the calculations with HCl. Pb(liq) condensed at temperatures between 800 – 550 °C when 50 ppm H_2S was considered. With 500 ppm of H_2S, Pb(liq) condensed at temperatures between 825 – 550 °C. Hence, the increase of the amount of H_2S induced the condensation of Pb(liq) at lower temperatures. The cooling calculations (see Figure 61) also showed the condensation of lead as PbS at 525 – 400 °C. However, the amount of PbS deposited was very small in comparison with the deposits of Pb(liq). The calculations did not predict the deposition of PbO_2-PbO. Furthermore, the condensation of PbS took place at much lower temperatures than in the experiments. Thus, the model calculations did not match with the experimental results well.

According to the results of the thermodynamic pseudo-equilibrium model (Figure 58), all the experiments were in equilibrium except the experiments with H_2S. In these experiments, the metallic vapours were saturated and condensed at lower temperatures than predicted by the

calculations. In other words, the super-cooling effect affected the condensation behaviour of lead. Alpha values of 0.2 and 0.25 fit nicely the experimental results. That is, with 500 ppm of H_2S a greater amount of PbS was formed than in the experiment with only 50 ppm of H_2S. Therefore, the condensation of lead was shifted to higher temperatures. The super-cooling effect was offset by the chemical reaction and the alpha value decreased. In the graphs it could be observed that lead started to condense at 950 °C when H_2O and HCl were in the atmosphere. However, in the experiments with H_2S, the condensation started at 1000 °C, proving the importance of the chemical reactions in the condensation of lead. Due to the chemical reactions, PbS was formed and condensed at higher temperatures than $PbCl_2$ and PbO_2-PbO.

Release behaviour of lead

The results of the MBMS showed the speciation and the behaviour of the Pb-species in the gas phase under the influence of H_2O, HCl and H_2S at different temperatures. Pb(g) was the major species in all experiments. Its concentration in the experiments was much higher than the amounts of the other Pb-species present in the gas phase. Due to the difficulty of vaporizing the same concentration of lead in all experiments, only a qualitative analysis of the gas phase could be achieved.

The experimental results show that Pb, PbO and PbO_2 were present in the gas phase during the experiments with H_2O (see Figure 63). Pb was the dominant species in every experiment. The concentration of the minor species, PbO and PbO_2, increased with the temperature. Besides, the concentration of PbO_2 was higher than the concentration of PbO. In general, the amount of water did not have a great influence on the release behaviour of lead. The calculations predicted the presence of Pb, PbO and PbO_2 in the gas phase when the atmosphere contained water vapour (see Figure 66). The concentration of PbO was much smaller than the concentration of Pb and increased with the temperature. Besides, with 17 % vol H_2O a higher concentration of PbO was in the gas phase than with only 3 % vol H_2O. The amount of PbO_2 was out of the range considered in this study and therefore, not taken into account. The main difference between the calculations and the experiments was the concentration of PbO_2. In the experiments PbO_2 was the second largest species. However, in the calculations it only appeared in very low concentrations. For this reason, it could not be said that the model predicted the experimental results well.

The experiments with HCl showed that lead was present in the gas phase as a mixture of Pb, PbO, PbO_2 and $PbCl_2$ (see Figure 64). The dominant species was Pb. The concentration of the oxides in the gas phase increased with the temperature. However, the concentration of $PbCl_2$ did not seem to change much with the temperature. In general, the concentration of PbO_2 was higher than the concentration of PbO, especially in the experiments with 500 ppm HCl. Furthermore, an increase of the amount of HCl seemed to influence the behaviour of the lead-

species. Thus, with 500 ppm HCl, higher concentrations of $PbCl_2$ and PbO_2 were present in the gas phase. On the contrary, the concentration of PbO was smaller in the experiments with 500 ppm HCl than in the experiments with only 50 ppm, especially at 1100 °C. The cooling calculations (see Figure 67) predicted the existence of Pb, $PbCl_2$, PbO and PbO_2 in the gas phase in an atmosphere containing HCl. PbO_2 was present in the gas phase at very low concentrations. The concentration of $PbCl_2$, the second major species in the gas phase, was, according to the model, constant at temperatures between 800 – 300 °C. The concentration of PbO was smaller than the concentration of $PbCl_2$ and increased with the temperature. Furthermore, an increase of the introduced HCl amount induced the presence of higher concentrations of $PbCl_2$. Nevertheless, HCl barely influenced the release of Pb and PbO_2. In general, the predictions of the calculations matched quite well with the experimental results. The only difference observed was that in the experiments the concentration of PbO_2 was higher than the concentration of PbO. In the calculations PbO_2 was only in the gas phase at very low concentrations. Nevertheless, this difference was important and therefore, it could not be assumed that the Scheil-Gulliver model predicted accurately the experimental results.

The species detected in the gas phase in the experiments with H_2S were Pb, PbO, PbO_2 and PbS (see Figure 65). Pb was the dominant species in the experiments with 50 ppm H_2S. In all experiments, the concentrations of PbO seemed to be slightly higher than the concentrations of PbO_2. In the experiments with 500 ppm H_2S slightly higher concentrations of PbO and PbO_2 were found than in the ones with 50 ppm H_2S. However, their concentrations in the gas phase were too similar to draw conclusions. The concentration of PbS increased strongly with the temperature and with the amount of H_2S. Thus, in the experiments with 500 ppm H_2S, PbS was the major species. The cooling calculations (see Figure 68) predicted the existence of Pb, PbS, PbO and PbO_2 in the gas phase. Like in the experiments, Pb and PbS were the dominant species. The concentrations of all species increased with the temperature. The concentration of PbO was much smaller than the concentrations of Pb and PbS. The amount of PbO_2 was too small to be considered. An increase of the amount of H_2S caused the presence of higher amounts of PbS in the gas phase. However, the calculations predicted a very low concentration of PbO_2. In the experiments, this species was found in the gas phase at concentrations similar to PbO. In conclusion, the Scheil-Gulliver model did not predict accurately the experimental results.

In general, the Scheil-Gulliver calculations predicted the existence of the same species in the gas phase as the species found in the experiments. However, important discrepancies were found between the behaviour and concentrations of these species in the calculations and in the experiments. Thus, the predictions of the Scheil-Gulliver model of the condensation behaviour of lead were very different to the experimental results. Therefore, the model could not be used for the prediction of the condensation of lead. The data base for the lead species should be modified or extended. Perhaps that would improve the capacity of the model for predicting the

condensation of lead under different atmospheric conditions. The relative error of the applied method for analysing the filters should be also taken into account.

4.4. Arsenic

4.4.1. Condensation experiments

The total gas flow in the condensation experiments with arsenic was 645 ml/min and the duration of each experiment was 24 h. The temperature at which the metal boat should be placed in order to obtain 100 ppm of the metal in the gas was first estimated with FactSage (see Figure 69). As it can be observed, the program predicted a temperature of 300 °C for the vaporization of 100 ppm of arsenic under the experimental conditions.

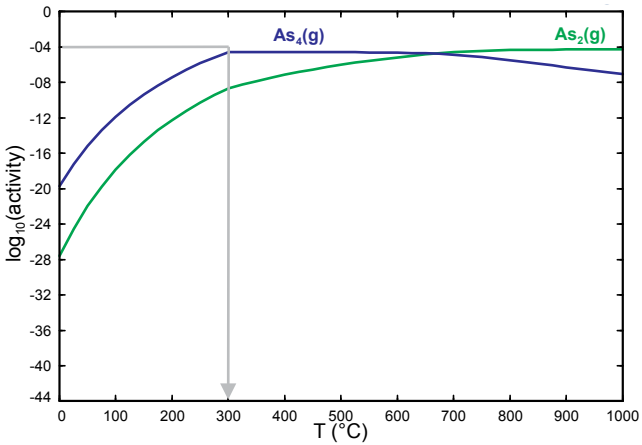

Figure 69. FactSage´s estimation of the necessary temperature for the vaporization of 100 ppm arsenic.

In the same way as in the condensation experiments with the other metals considered, the temperature predicted by FactSage 6.3 to evaporate 100 ppm of the metal was experimentally checked. Thus, arsenic powder was evaporated at different temperatures between 200 °C and 400 °C during 24 h. Three experimental runs were carried out. As arsenic source metallic arsenic was used.

The results obtained from the experiments are depicted in Figure 70. To place the sample boat with the arsenic source at 207 °C lead to a vaporisation of 90 ppm of arsenic. This temperature was a little lower than the predicted temperature by FactSage. In the experiments with arsenic the sample boat was situated at the reaction´s zone where the temperature was 210 °C.

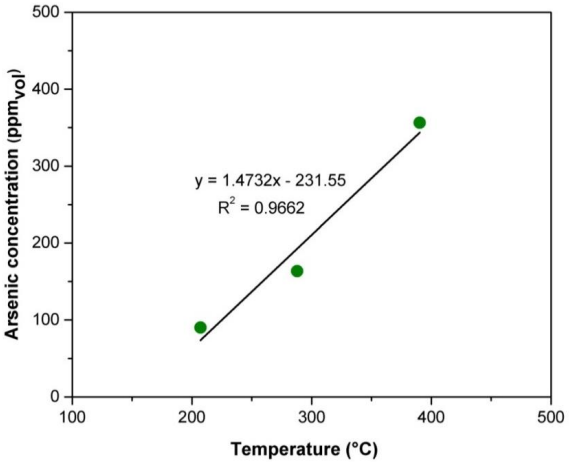

Figure 70. Correlation of arsenic concentration (ppm) and temperature (°C).

The experimental results of the condensation behaviour of arsenic under the presence of H_2O, HCl and H_2S are shown and explained in detail in the next sections.

Influence of H_2O

The condensation distribution of arsenic species in the tubes and in the outer tube when the atmosphere contained H_2O(g) is depicted in Figure 71. In this graph the results with 3 % vol of H_2O and with 17 % vol H_2O in the atmosphere are shown. The percentage of arsenic condensed as metallic As, As_2O_5, $AsCl_3$ and As_2S_2 are depicted in purple, red, blue and green colour, respectively.

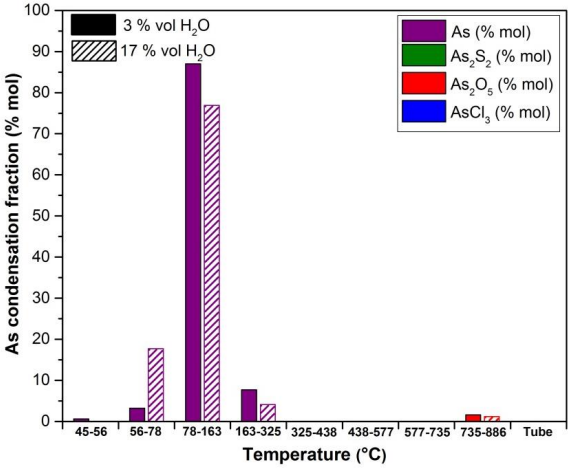

Figure 71. Condensation distribution of arsenic in the outer tube and in the filters placed along the cooling zone in an atmosphere containing 3 % vol and 17 % vol of water vapour.

Arsenic condensed in atmospheres containing water vapour as metallic As and As_2O_5. As condensed for the two amounts of H_2O considered in the fifth, sixth and seventh filters, i.e. at temperatures between 325 – 56 °C. As_2O_5 preferably condensed for both conditions at higher temperatures. It condensed at 886 – 735 °C (first filter of the cooling zone). The total amount of arsenic that was oxidized was 1.6 % and 1.2 % for 3 % vol and 17 % vol of H_2O in the atmosphere, respectively.

In summary, an increase in the amount of H_2O(g) introduced into the experiment did not influence the condensation behaviour of arsenic. At high temperatures deposits of As_2O_5 were found and at temperatures lower than 325 °C the condensation of metallic arsenic was noticeable. As_2O_5 condensed at 886 – 735 °C and As at 325 – 56 °C. Besides, the percentage of oxidized arsenic was in both experiments similar.

Influence of HCl

Figure 72 shows the condensation behaviour of arsenic when HCl was introduced into the outer tube. The results of the experiments with 0 ppm HCl, 50 ppm of HCl and 500 ppm of HCl are shown. The bars on the left show the results obtained when the atmosphere contained 0 ppm HCl. The bars in the middle and on the right are the results with 50 and 500 ppm HCl in the experiment.

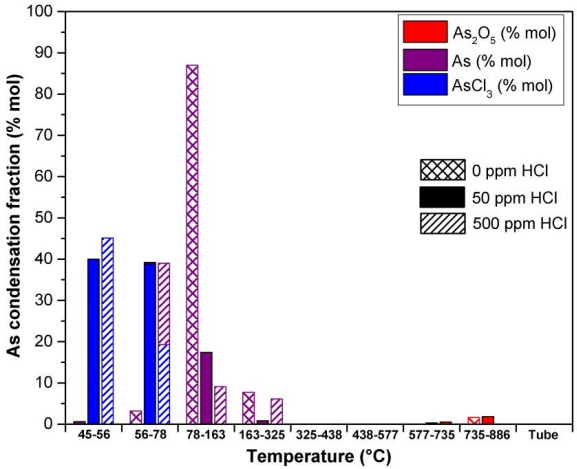

Figure 72. Condensation distribution of arsenic in the outer tube and in the filters placed along the cooling zone in an atmosphere containing 0 ppm HCl, 50 ppm of HCl and 500 ppm of HCl.

Arsenic condensed in an atmosphere containing 0 ppm HCl as metallic arsenic and As_2O_5. As condensed at temperatures between 325 – 56 °C and As_2O_5 at 886 – 735 °C.

Arsenic condensed as As_2O_5, metallic As and $AsCl_3$ when HCl was introduced into the experiment. The deposits of As_2O_5 were found at high temperatures. With 50 ppm of HCl in the experiment as well as with 500 ppm HCl, As_2O_5 condensed in the first and second filters (886 – 577 °C). However, the amount condensed in the first filter in the experiment with 500 ppm HCl was so little that it is not appreciated in the graph. The oxidized percentage of As in each experiment corresponded to 2.1 % and 0.6 % respectively.

As well as in the experiments with water vapour, metallic As condensed in the fifth, sixth and seventh filter at temperatures between 325 and 56 °C. $AsCl_3$ condensed in both experiments in the seventh and eighth filters, i.e. at 78 – 45 °C. In total, 79.3 % of the total arsenic condensed as $AsCl_3$ in the experiment with 50 ppm of HCl. In the experiment with 500 ppm of HCl, however, the percentage condensed as $AsCl_3$ was only 64.4 %. Although the amount condensed as $AsCl_3$ was higher in the case with 50 ppm of HCl in the experiment, the reality is that more quantity of $AsCl_3$ condensed in the case with 500 ppm of HCl than in the case with only 50 ppm of HCl. However, the total arsenic evaporated (ppm) in the experiment with 500 ppm of HCl was higher than in the first experiment and therefore, the total of $AsCl_3$ appeared to be less.

On this basis, it was concluded that the introduction of HCl in the experiments did not have an appreciable influence on the condensation behaviour of arsenic. The condensation of As_2O_5 took place at high temperatures (886 – 577 °C) under all experimental conditions. Independent-

ly of the amount of HCl introduced, As and $AsCl_3$ condensed at low temperatures, at 325 – 56 °C and 78 – 45 °C, respectively.

Influence of H_2S

Figure 73 shows the condensation behaviour of arsenic when H_2S was introduced into the outer tube. The results of the experiments with 0, 50 and 500 H_2S are presented. The bars on the left show the results obtained when the atmosphere contained 0 ppm H_2S. The bars in the middle and on the right are the results with 50 and 500 ppm H_2S in the experiment, respectively.

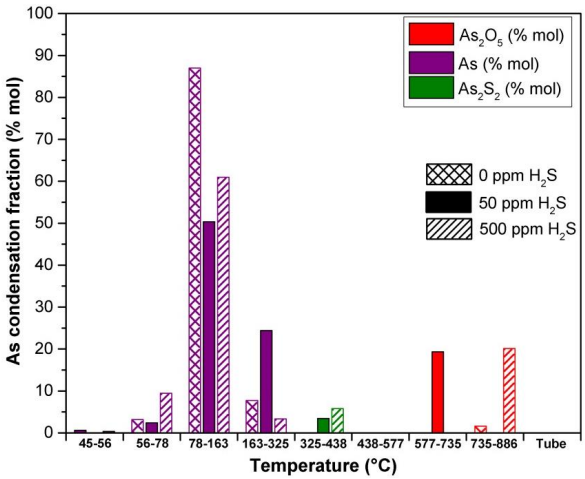

Figure 73. Condensation distribution of arsenic in the outer tube and in the filters placed along the cooling zone in an atmosphere containing 0 ppm H_2S, 50 ppm of H_2S and 500 ppm of H_2S.

Arsenic condensed in an atmosphere containing 0 ppm H_2S as metallic arsenic and As_2O_5. As condensed at temperatures between 325 – 56 °C and As_2O_5 at 886 – 735 °C.

The experiments showed that arsenic condensed as metallic As, As_2O_5 and As_2S_2 when H_2S was introduced into the atmosphere. The deposits of As_2O_5 were found at high temperatures similarly to the As_2O_5 condensed in the experiments with H_2O or HCl in the atmosphere. In more detail, As_2O_5 condensed in the second filter (577 – 735 °C) when 50 ppm of H_2S was present in the atmosphere. When 500 ppm of H_2S was introduced into the experiment, As_2O_5 condensed in the first filter, at temperatures between 886 – 735 °C. The percentage of arsenic that was oxidized was 19.4 % and 20.1 % in the experiments with 50 and 500 ppm of H_2S, respectively.

Moreover, a little percentage of the arsenic condensed as As_2S_2. This species condensed in both experiments at 438 – 325 °C, i.e. in the fourth filter from the cooling zone. In the experiment with 50 ppm of H_2S the percentage of arsenic condensed as As_2S_2 was 3.4 % while in the exper-

iment with 500 ppm of H_2S it increased to 5.8 %. At temperatures between 325 – 56 °C arsenic condensed as metallic arsenic. This means that the condensation of the metallic arsenic took place in the fifth, sixth and seventh filters in the experiment with 50 ppm of H_2S as well as in the experiment with 500 ppm of H_2S.

In summary, an increase in the amount of H_2S introduced in the atmosphere promoted the condensation of As_2O_5 at higher temperatures. In the experiment with 500 ppm of H_2S, As_2O_5 condensed in the first filter (886 – 735 °C) while in the experiment with 50 ppm of H_2S it preferably condensed in the second filter (735 – 577 °C) of the cooling zone. However, the total percentage of As_2O_5 was apparently similar (20 %) in both experiments.

Notwithstanding, the introduction of higher amounts of H_2S into the atmosphere did not influence the condensation temperatures of As_2S_2 and metallic As. As_2S_2 condensed at 438 – 325 °C and As condensed at 325 – 56 °C under the influence of 50 and 500 ppm of H_2S. The only appreciable difference was that the condensed amount of As_2S_2 increased slightly when 500 ppm of H_2S was present in the atmosphere.

As it has been shown in the results, the total amount condensed as As_2O_5 in the experiments with H_2O and HCl was less than 2 % of the total deposition. However, in the experiments with H_2S, the percentage of arsenic condensed as As_2O_5 increased to 20 %. Due to the low concentration of water present in the experiments (3 % vol), the formation of such an amount of oxide was very unlikely.

In order to check this affirmation and to get an explanation for the high amounts of As_2O_5 in the experiments, the oxygen partial pressure in the experiments and a phase diagram for the system As-O_2 was calculated with FactSage.

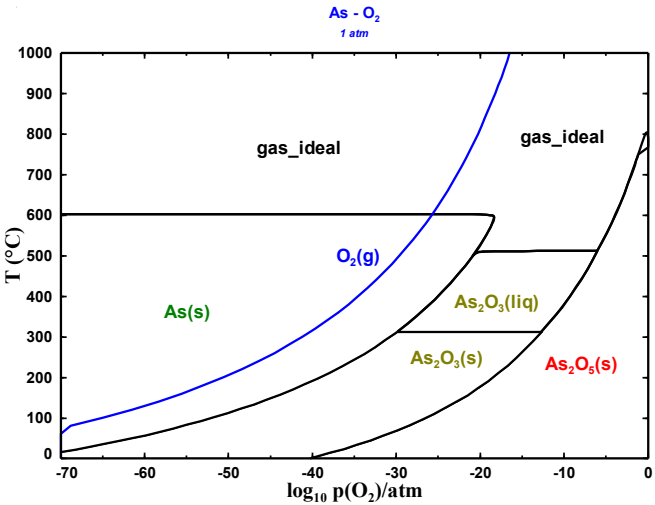

Figure 74. Phase diagram for the As-O_2 system including the equilibrium partial pressure of oxygen.

The graph shows the phase diagram for the As-O_2 system calculated by FactSage. The oxygen partial pressure in equilibrium versus the temperature for the experimental conditions is represented by the blue line. As it can be observed, the partial pressure of oxygen in the experiments was too low for the formation of oxides. Thus, As_2O_5 (s) needed a very high oxygen partial pressure to appear at 886 – 577 °C. For this reason, it could be affirmed that there was an external source of oxygen during the experiments. Most likely oxygen entered the experiment before the cooling phase of the experiments. As explained in the methods section, after the experiments the sample boat containing the metal source was taken out of the inner tube. In doing so a certain amount of air probably entered the experiment and formed As_2O_5 in the first filters during the cooling phase. However, since this small amount of O_2 was consumed in the first filters, the following filters were obviously not affected. Therefore, the condensation of arsenic as As_2O_5 need not be taken into account in the condensation experiments. It can be assumed that As only condensed as As, $AsCl_3$ and As_2S_2.

4.4.2. Thermodynamic pseudo-equilibrium model

Figure 75 shows the comparison between the model calculations and the experimental results of the condensation of arsenic in an atmosphere containing H_2O (3 – 17 % vol), HCl (50 – 500 ppm) and H_2S (50 – 500 ppm). For the calculations the amount of arsenic condensed as As_2O_5 was not considered.

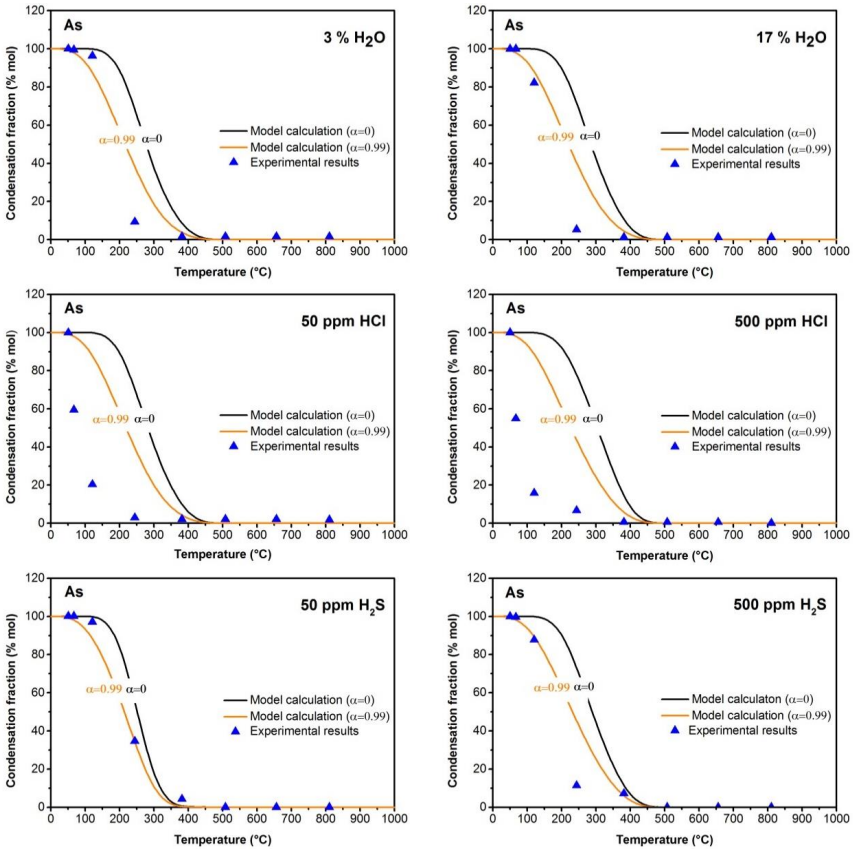

Figure 75. Comparison between the calculated and the experimental results of the condensation of arsenic vapours in the presence of H_2O (3 – 17 % vol), HCl (50 – 500 ppm) and H_2S (50 – 500 ppm).

The curve-fitting of the experimental results indicated an alpha value of 0.99 for all experimental conditions. This value of alpha fit well the experimental results with water vapour and H_2S in the atmosphere. However, according to the model the experimental results with HCl were so far away from the condensation behaviour predicted by the calculations that an alpha value of 0.99 was the value that better fit the experimental results. In line with the model, the condensation experiments with HCl were very far away from reaching an equilibrium stage. Therefore, the model calculations could only predict acceptably the condensation behaviour of arsenic when the atmosphere contained H_2O and H_2S.

In the case with HCl in the atmosphere, as it can be observed in Figure 75, the deposition fraction predicted by the model was far higher than the observed in the experimental results. It

would be reasonable to consider that super-cooling played an important role in this case but the condensation of the arsenic compounds took place at such a low temperature that no alpha value could fit nicely the experimental results.

In conclusion, the condensation behaviour of arsenic predicted by the pseudo-equilibrium model was totally different to the tendency that the experimental results showed when the atmosphere contained HCl. However, the model could predict acceptably the condensation behaviour of arsenic when the atmosphere contained H_2O and H_2S.

4.4.3. Scheil-Gulliver cooling calculations for the solid phase

The Scheil-Gulliver cooling calculations carried out for arsenic are presented in this section. The calculations were carried out at decreasing temperature steps of 25 °C starting from 1000 °C to room temperature. As well as in the condensation experiments, the influence of H_2O, HCl and H_2S in the condensation behaviour of arsenic was studied.

Influence of H_2O

The arsenic speciation predicted by the Scheil-Gulliver cooling calculations in an atmosphere containing water vapour is depicted in Figure 76. The results with 3 and 17 % vol of water are presented. The species depicted with a solid line are the species that condensed when the atmosphere contained 3 % vol of H_2O and the ones depicted with a dashed line are the species that condensed when the atmosphere contained 17 % vol of H_2O.

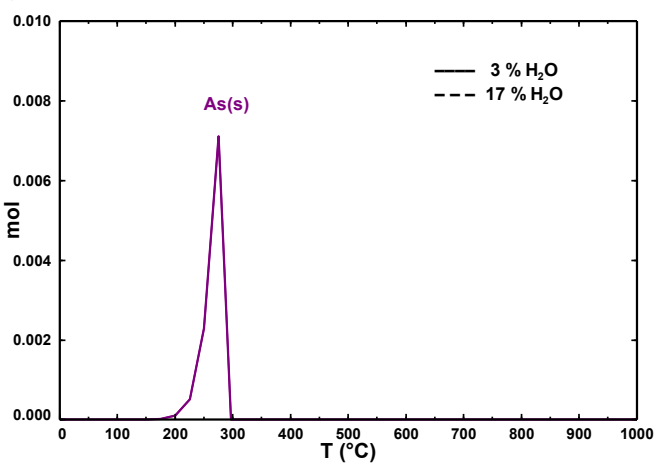

Figure 76. Speciation of the condensed phase during cooling from 1000 to 0 °C predicted by the Scheil-Gulliver cooling model in an atmosphere containing water vapour and arsenic.

The model calculations showed that arsenic condensed as metallic As at 300 – 200 °C regardless of the water vapour amount considered. The results from both simulations overlapped, the program predicted for both atmospheric conditions the condensation of the same amount of metallic arsenic and at the same temperature range. Hence, the amount of water vapour introduced in the atmosphere did not influence the condensation behaviour of arsenic.

Influence of HCl

Figure 77 shows the results obtained from the Scheil-Gulliver cooling model when 50 and 500 ppm of HCl were present in an atmosphere containing arsenic. Once again, the results obtained when 50 ppm of HCl was in the atmosphere are depicted with a solid line and the results obtained when the atmosphere contained 500 ppm of HCl are depicted with a dashed line.

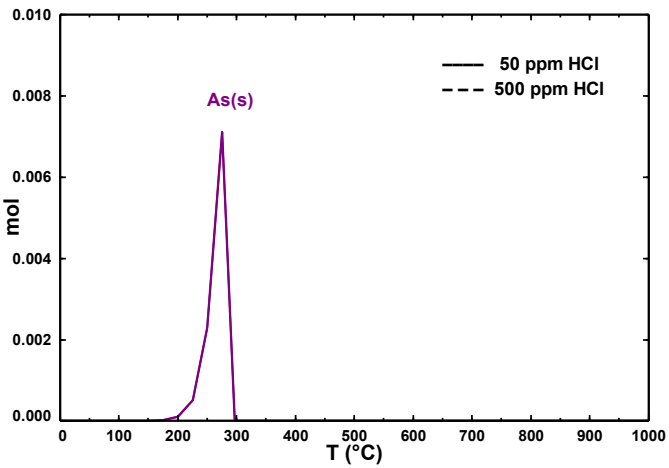

Figure 77. Speciation of the condensed phase during cooling from 1000 to 0 °C predicted by the Scheil-Gulliver cooling model in an atmosphere containing HCl and arsenic.

The results obtained from the cooling calculations showed the same tendency as in the cooling calculations with water vapour. Under both concentrations of HCl, arsenic condensed as metallic arsenic at 300 – 200 °C. In conclusion, the calculations predicted that the amount of HCl considered did not influence the condensation behaviour of arsenic. Furthermore, HCl seemed not to change the condensation of arsenic. The results are identic to the ones obtained under the influence of H_2O and not any compound containing chloride was expected to condense.

Influence of H_2S

The condensation behaviour of arsenic predicted by FactSage when H_2S was introduced into the atmosphere is depicted in Figure 78. A comparison between the results with 50 ppm H_2S and 500 ppm H_2S is shown.

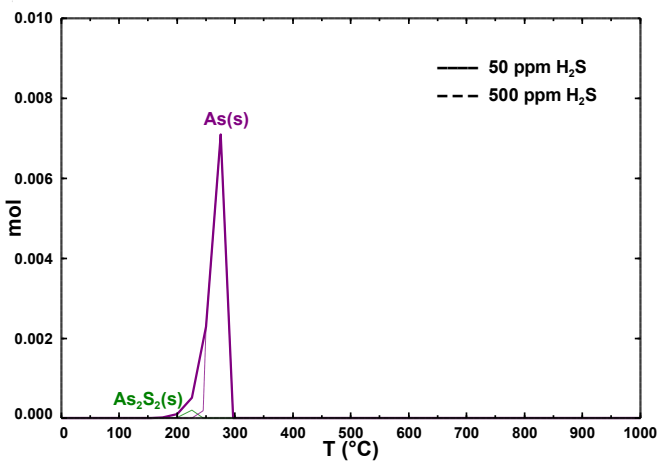

Figure 78. Speciation of the condensed phase during cooling from 1000 to 0 °C predicted by the Scheil-Gulliver cooling model in an atmosphere containing H_2S and arsenic.

The cooling calculations predicted the condensation of metallic As (300 – 200 °C) when 50 ppm of H_2S were in the atmosphere. When 500 ppm of H_2S were considered, arsenic condensed as As_2S_2 (250 – 200 °C) and metallic arsenic (300 – 225 °C). The amount condensed as As_2S_2 was low in comparison with the metallic arsenic deposition. In general, an increase in the amount of H_2S induced the occurrence of As_2S_2 and caused As to condense at slightly higher temperatures.

4.4.4. Release experiments

The influence of water vapour, HCl and H_2S on the gas phase concentration and speciation of arsenic was investigated by MBMS. The gas flow was 4.3 l/min and the experiments were conducted at 1000, 900 and 700 °C. As the mass spectrometer only determines the gaseous ionized species based on their mass-to-charge ratios (m/z), it was necessary to carry out a calibration before starting the experiments. With this calibration it was possible to correlate the intensities of the isotopes present in the experiments with the metal vapour concentration (ppm) obtained. In the experiments of arsenic the monitored species were $^{75}As^+$, $^{198}As_2O_3^+$, $^{230}As_2O_5^+$, $^{180}AsCl_3^+$, $^{214}As_2S_2^+$, $^{91}AsO^+$, $^{107}AsO_2^+$, $^{108}AsS^+$, $^{246}As_2S_3^+$ and $^{428}As_4S_4^+$. However, only the first five species were found in the gas phase during the experiments. The correlation between the ion

signal intensities of the monitored species and the obtained concentration (ppm) in the gas phase is shown in Figure 79.

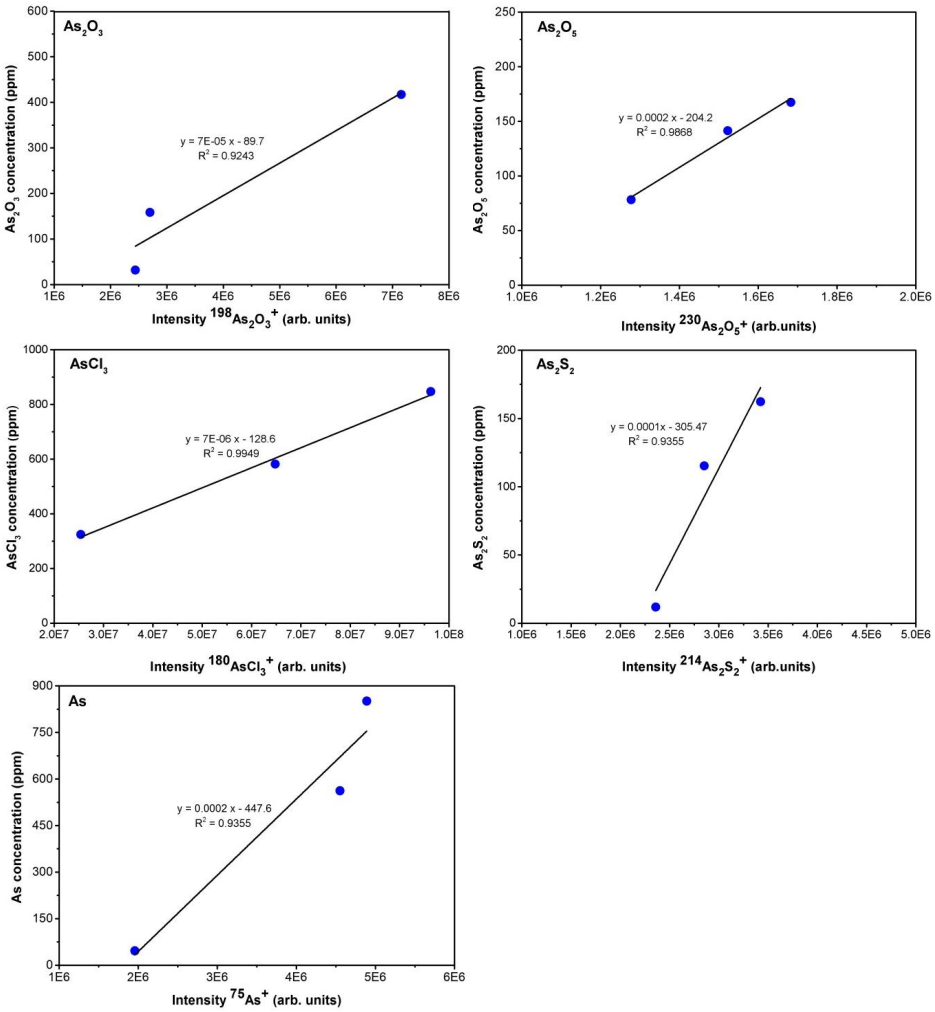

Figure 79. Calibration curves for the release experiments with arsenic.

The results of the MBMS measurements are provided in Figure 80, Figure 81 and Figure 82. The graphs show the speciation and behaviour of the arsenic-containing species that were in the gas phase at 1000, 900 and 700 °C. As(g) was the major species in all experiments and its concentration in the gas phase during the experiments was much higher than the amounts of the

other As-species present. However, in the graphs only the minor arsenic species present in the gas phase at 1000, 900 and 700 °C are depicted. Due to the difficulty of vaporizing the same amount of arsenic in every experiment and therefore, obtaining a similar concentration each time, only a qualitative analysis could be achieved. An overview of the concentrations (in %) of all species detected in the gas phase is given in the tables on the right of the experimental results.

Influence of H_2O

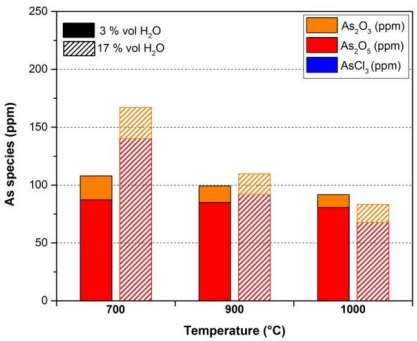

Concentration of gaseous As-species (%)						
	3 % vol H_2O			17 % vol H_2O		
	As	As_2O_3	As_2O_5	As	As_2O_3	As_2O_5
1000 °C	96.5	0.4	3.1	96.2	0.7	3.1
900 °C	90.5	1.4	8.2	84.8	2.4	12.7
700 °C	87.3	2.4	10.3	75.2	4.0	20.8

Figure 80. Concentration of minor gaseous arsenic species at 1000, 900 and 700 °C when the atmosphere contained water vapour (3 – 17 % vol). Note that As(g), the major species in the gas phase is not represented.

The experiments showed that As, As_2O_3 and As_2O_5 were present in the gas phase during the experiments with H_2O. As(g) was the dominant species and represented approximately 90 % of the gaseous species found in the gas phase. In every experiment, the concentrations of As_2O_3 were smaller than the concentrations of As_2O_5. Furthermore, it seemed that the amount of oxides that were detected at high temperatures were smaller than the amounts of oxides at low temperatures. Besides, both species were present in higher concentrations in the experiments with 17 % vol water than in the experiments with 3 % vol water. However, due to the different amounts of total arsenic in the experiments, no firm conclusion could be drawn.

Influence of HCl

Arsenic was present in the gas phase as a mixture of As, $AsCl_3$, As_2O_3 and As_2O_5 in the experiments with HCl (see Figure 81). The major species were As and $AsCl_3$, as it can be observed in the table. In every experiment, the concentrations of As_2O_3 were smaller than the concentrations of As_2O_5. Like in the experiments containing H_2O, the oxides concentration decreased with the temperature. On the contrary, the concentration of $AsCl_3$ seemed to be constant with the

temperature and with the amount of HCl. Therefore, it could not be concluded that HCl had a great influence on the release of arsenic.

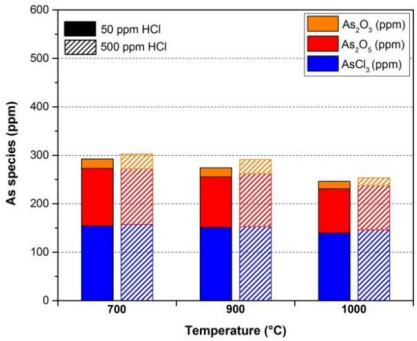

Concentration of gaseous As-species (%)								
	50 ppm HCl				500 ppm HCl			
	As	As_2O_3	As_2O_5	$AsCl_3$	As	As_2O_3	As_2O_5	$AsCl_3$
1000°C	69.5	1.9	11.3	17.3	86.5	0.8	4.9	7.8
900 °C	75.6	1.7	9.3	13.4	69.8	3.0	11.4	15.8
700 °C	61.2	2.6	15.8	20.5	75.1	2.5	9.4	13.0

Figure 81. Concentration of minor gaseous arsenic species at 1000, 900 and 700 °C when the atmosphere contained HCl (50 – 500 ppm). Note that As(g), the major species in the gas phase is not represented.

Influence of H_2S

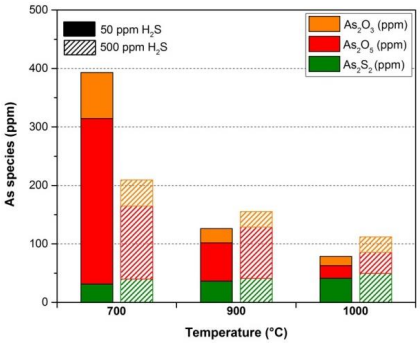

Concentration of gaseous As-species (%)								
	50 ppm H_2S				500 ppm H_2S			
	As	As_2O_3	As_2O_5	As_2S_2	As	As_2O_3	As_2O_5	As_2S_2
1000°C	94.3	1.1	1.6	3.0	90.1	2.2	3.2	4.5
900 °C	91.4	1.6	4.4	2.6	67.9	5.5	18.1	8.5
700 °C	46.7	10.7	38.4	4.3	94.6	1.1	3.2	1.0

Figure 82. Concentration of minor gaseous arsenic species at 1000, 900 and 700 °C when the atmosphere contained H_2S (50 – 500 ppm). Note that As(g), the major species in the gas phase is not represented.

The release experiments with H_2S showed that As, As_2S_2, As_2O_3 and As_2O_5 were the species present in the gas phase. As(g) was the dominant species. Like in the experiments with HCl and H_2O, the oxides concentration decreased with the temperature. In all the experiments, the concentration of As_2O_5 was higher than the concentration of As_2O_3. It seemed that the concentration of both oxides was not influenced by the amount of H_2S. Thus, their concentration was similar under both experimental conditions. The high concentration of both oxides at 700 °C with 50 ppm of H_2S was the result of a high evaporation of the arsenic sample that caused a

higher evaporation of arsenic (ppm) than in the other experiments. On the other hand, the concentration of As_2S_2 increased with the temperature and with the amount of H_2S introduced. Thus, an increase of the amount of H_2S caused the release of slightly higher concentrations of As_2S_2 than in the experiments with a low concentration of H_2S.

4.4.5. Scheil-Gulliver cooling calculations for the gas phase

The release behaviour of arsenic predicted by the Scheil-Gulliver cooling model is shown in this section. The influence of H_2O, HCl and H_2S on the release of arsenic was studied. The calculations show the speciation of the main inorganic gaseous species at temperatures between 1000 °C and room temperature.

Influence of H_2O

The speciation of the gas phase predicted by the Scheil-Gulliver cooling calculations in an atmosphere containing water vapour and arsenic is shown in Figure 83. The graph shows a comparison between the results obtained with 3 and 17 % vol water vapour in the atmosphere. The results obtained with 3 % vol of water are depicted with a solid line and the results containing 17 % vol water vapour are depicted with a dashed line.

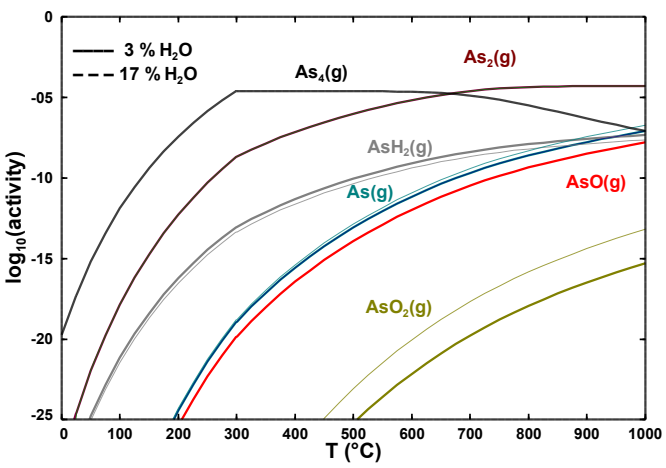

Figure 83. Gaseous arsenic-containing species versus temperature in an atmosphere containing 3 – 17 % vol of H_2O calculated by the Scheil-Gulliver cooling model.

The calculations showed that As_2, As_4, AsH_2, As and AsO were the species appearing in the gas phase when the atmosphere contained water vapour. AsO_2 was present in the gas phase but at lower concentrations than the ones addressed in this study. The concentration of all species, except As_4, increased with the temperature. The amount of As_4 was constant at 700 – 300 °C

and decreased at temperatures higher than 700 °C. According to the calculations, the amount of water did not have a great influence on the behaviour of the arsenic species.

Influence of HCl

The predicted behaviour of arsenic when 50 and 500 ppm of HCl were present in the atmospheric conditions is depicted in Figure 84. In this case, the results for 50 ppm of HCl in the atmosphere are depicted with a solid line and the results containing 500 ppm of HCl are depicted with a dashed line.

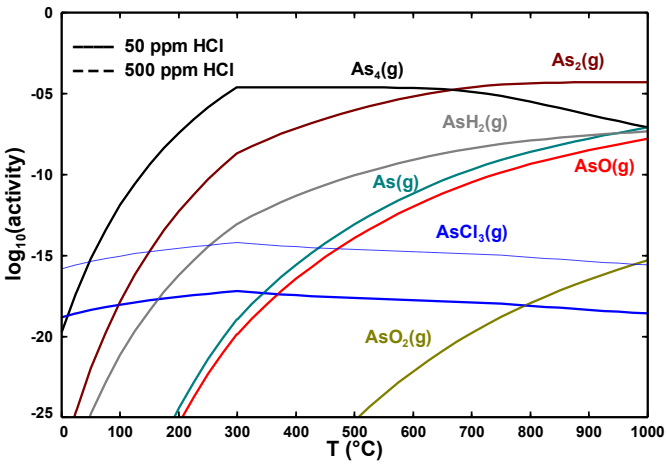

Figure 84. Gaseous arsenic-containing species versus temperature in an atmosphere containing 50 – 500 ppm of HCl calculated by the Scheil-Gulliver cooling model.

When the atmosphere contained HCl, the main inorganic species present in the gas phase were As_2, As_4, AsH_2, As and AsO. $AsCl_3$ and AsO_2 appeared at concentrations lower than 1 ppb and were not considered. As in the case with water vapour, the concentration of all species, except As_4, increased with the temperature. The amount of As_4 was constant at 700 – 300 °C and decreased at temperatures higher than 700 °C. According to the calculations, the amount of HCl did not have any influence on the behaviour of the arsenic species. In all cases, except for $AsCl_3$, the results of both atmospheric conditions overlapped.

Influence of H_2S

Figure 85 shows the behaviour of arsenic predicted by FactSage when H_2S was introduced into the atmosphere. A comparison between the results with 50 ppm H_2S and 500 ppm H_2S is shown. The results for 50 ppm of H_2S in the atmosphere are depicted with a solid line and the results containing 500 ppm of H_2S are depicted with a dashed line.

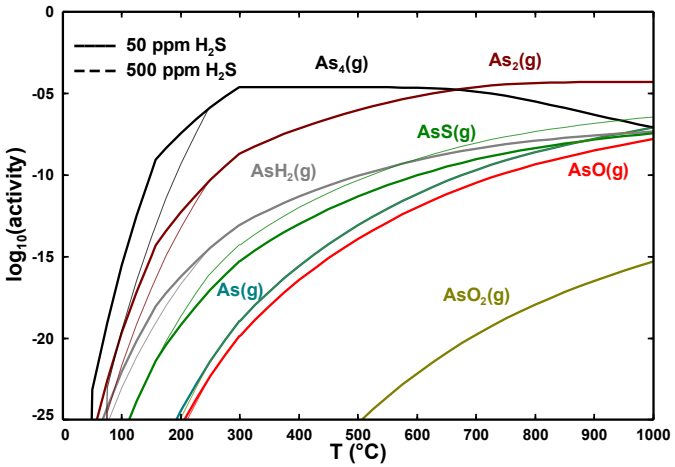

Figure 85. Gaseous arsenic-containing species versus temperature in an atmosphere containing 50 – 500 ppm of H_2S calculated by the Scheil-Gulliver cooling model.

The Scheil-Gulliver cooling model predicted the presence of arsenic in the gas phase as a mixture of As_2, As_4, AsS, AsH_2, As and AsO. AsO_2 was present at very low concentrations and was not considered in this study. The behaviour of all arsenic species was identical to the two other cases considered, i.e. with H_2O and with HCl in the atmosphere. Therefore, neither HCl, nor H_2O nor H_2S had influence on the behaviour of As_2, As_4, AsS, AsH_2, As and AsO. In this case, also AsS was present in the gas phase and its concentration increased with the temperature. Furthermore, an increase of the amount of H_2S caused AsS to be present in the gas phase in higher concentrations. Therefore, it could be concluded that H_2S influenced the behaviour of AsS.

4.4.6. Discussion

According to the comparison of the experimental results with the results of the cooling calculations and the thermodynamic pseudo-equilibrium model, the following conclusions of the condensation and release behaviour of arsenic could be drawn:

Condensation behaviour of arsenic

FactSage 6.3 predicted a temperature of 300 °C for the evaporation of 100 ppm of arsenic under the atmospheric conditions considered in the experiments. The experiments showed that positioning the arsenic sample at 207 °C a concentration of approximately 90 ppm in the gas phase was obtained. Therefore, in all experiments the metal source was placed at 210 °C.

As it is shown in Figure 71, arsenic condensed in atmospheres containing water vapour as metallic arsenic (325 – 56 °C) regardless of the water volume. The model calculations also showed

that arsenic condensed as metallic As at 300 – 200 °C regardless of the water vapour amount considered (Figure 76). Hence, it could be concluded that the Scheil-Gulliver calculations predicted perfectly the condensation behaviour of arsenic when water was present in the atmosphere.

When HCl was introduced into the experiment arsenic condensed as metallic As and $AsCl_3$ (see Figure 72). As and $AsCl_3$ condensed at low temperatures, at 325 – 56 °C and 78 – 45 °C respectively. Approximately 80 % of the deposits were $AsCl_3$. The introduction of a higher concentration of HCl in the experiments did not have an appreciable influence on the condensation behaviour of arsenic. The cooling calculations (see Figure 77) showed the same tendency as the cooling calculations with water vapour. Arsenic condensed as metallic arsenic at 300 – 200 °C and the model did not predict the condensation of any chloride-containing compound. Although the model predicted accurately the condensation behaviour of the metallic arsenic, it did not predict the existence of $AsCl_3$. For this reason, the Scheil-Gulliver model was not appropriate for the prediction of the condensation behaviour of arsenic in an atmosphere containing HCl.

The experiments showed that arsenic condensed as metallic As (325 – 56 °C) and As_2S_2 (438 – 325 °C) when H_2S was introduced into the atmosphere (see Figure 73). The arsenic that condensed as As_2S_2 was generally less than 6 %. The only difference observed between the experiments with 50 and 500 ppm of H_2S was the amount of As_2S_2. With 500 ppm H_2S, 5.8 % of the total arsenic condensed as As_2S_2. However, with 50 ppm H_2S, only 3.4 % condensed as As_2S_2. The cooling calculations predicted the condensation of metallic arsenic (300 – 200 °C) when H_2S was in the atmosphere. This can be seen in Figure 78. With 500 ppm of H_2S, a small amount of arsenic condensed as As_2S_2 (250 – 200 °C). In general, an increase of the amount of H_2S induced the occurrence of As_2S_2 and caused As to condense at slightly higher temperatures. Comparing the calculations with the experimental results, it could be observed that the temperature at which As_2S_2 condensed was higher in the experiments than in the model. Furthermore, the amount of As_2S_2 in the experiments was higher than the amount predicted by the model. Hence, the Scheil-Gulliver model did not predict with exactitude the condensation behaviour of arsenic in an atmosphere containing H_2S.

Furthermore, the experimental results showed the deposition of a small amount of As_2O_5 in all experiments. The concentration of this species represented less than 2 % of the total arsenic deposited. The partial pressure of oxygen in the experiments was proved to be too low for the formation of oxides. Therefore, only an external source of oxygen during the experiments could have built oxygen. Most likely air entered the experiment during the extraction of the metal source from the inner tube. Thus, enough oxygen was available during the cooling phase in the

experiment to form As_2O_5. Hereby, the condensation of arsenic as As_2O_5 was not taken into account and it has not been mentioned in the paragraphs above.

According to the results of the thermodynamic pseudo-equilibrium model (Figure 75), the experiments with HCl were far away from reaching an equilibrium stage. An alpha value of 0.99 fit well the experimental results with water vapour and H_2S in the atmosphere. The model calculation could acceptably predict the condensation behaviour of arsenic when the atmosphere contained H_2O and H_2S. In the experiments with HCl the deposition fraction predicted by the model was far higher than observed in the experimental results. It was reasonable to think that supercooling played an important role in this case. An alpha value of 0.99 was the value that fit the experimental results better. In conclusion, the model calculations could only predict acceptably the condensation behaviour of arsenic when the atmosphere contained H_2O and H_2S. With HCl, the condensation of the arsenic compounds took place at such a low temperature that not even an alpha value of 0.99 fit the experimental results.

Release behaviour of arsenic

Due to the difficulty of vaporizing the same amount of arsenic in every experiment and therefore, obtaining a similar concentration each time, only a qualitative analysis of the gas could be achieved. The main target of these experiments was to determine the speciation of arsenic in the gas phase and the behaviour of the gas species under different atmospheric conditions. The influence of H_2O, HCl and H_2S on the behaviour of arsenic was investigated. The gas analysis was carried out at 1000, 900 and 700 °C. As(g) was the major species in all experiments and its concentration in the gas phase during the experiments was much higher than the amounts of the other As-species present. However, in the results only the minor species were shown.

The experiments showed that As, As_2O_3 and As_2O_5 were present in the gas phase during the experiments with H_2O (see Figure 80). As(g) was the dominant species and represented approximately 90 % of the gaseous species found in the gas phase. In every experiment, the concentrations of As_2O_3 were lower than the concentrations of As_2O_5. The concentration of both species decreased with the temperature and both were released at higher concentrations in the experiments with a higher volume of water. The calculations showed that As_2, As_4, AsH_2, As and AsO were the species appearing in the gas phase when the atmosphere contained water vapour (see Figure 83). AsO_2 was present in the gas phase in very low concentrations. The concentration of all species, except As_4, increased with the temperature. The amount of As_4 was constant at 700 – 300 °C and decreased at temperatures higher than 700 °C. According to the calculations, the amount of water did not have a great influence on the behaviour of the arsenic species. Since the calculations predicted the existence of different arsenic compounds, it could be concluded that the model could not predict the behaviour of arsenic when the atmosphere contained water.

In the experiments with HCl, arsenic was present in the gas phase as a mixture of As, $AsCl_3$, As_2O_3 and As_2O_5 (see Figure 81). The major species were As and $AsCl_3$. In every experiment, the concentration of As_2O_3 was smaller than the concentration of As_2O_5. Like in the experiments containing H_2O, the oxides concentration decreased with the temperature. On the contrary, the concentration of $AsCl_3$ seemed to be constant with the temperature and with the amount of HCl. HCl did not have a great influence on the release of arsenic. According to the calculations, when the atmosphere contained HCl, the main inorganic species present in the gas phase were As_2, As_4, AsH_2, As and AsO (see Figure 84). $AsCl_3$ and AsO_2 appeared at concentrations lower than 1 ppb. Like in the case with water vapour, the concentration of all species, except As_4, increased with the temperature. The amount of As_4 was constant at 700 – 300 °C and decreased at temperatures higher than 700 °C. As in the experiments, the amount of HCl did not have any influence on the behaviour of the arsenic species. In all cases the results of both atmospheric conditions overlapped. Although the model predicted well the behaviour of $AsCl_3$, it also predicted the existence of different arsenic species as found in the experiments. Therefore, the Scheil-Gulliver calculations were not a good method for the prediction of the behaviour of arsenic when the atmosphere contained HCl.

The release experiments with H_2S showed that As, As_2S_2, As_2O_3 and As_2O_5 were the species present in the gas phase (see Figure 82). As(g) was the dominant species. Like in the experiments with HCl and H_2O, the oxides concentration decreased with the temperature. Besides, the concentration of As_2O_5 was higher than the concentration of As_2O_3. It seemed that the concentration of both oxides was not influenced by the amount of H_2S. Thus, their concentration was similar under both experimental conditions. The concentration of As_2S_2 increased with the temperature and with the amount of H_2S introduced. Thus, an increase of the amount of H_2S caused the release of slightly higher concentrations of As_2S_2 than in the experiments with less H_2S. The Scheil-Gulliver cooling model predicted the presence of arsenic in the gas phase as a mixture of As_2, As_4, AsS, AsH_2, As and AsO (see Figure 85). AsO_2 was present in very low concentrations. The behaviour of all arsenic species was identical to the two other cases considered, i.e. with H_2O and with HCl in the atmosphere. Therefore, neither HCl nor H_2O nor H_2S had influence on the behaviour of As_2, As_4, AsS, AsH_2, As and AsO. However, an increase of the amount of H_2S caused AsS to be present in the gas phase in higher concentrations. The concentration of AsS also increased with the temperature. For the same reasons as in the experiments with H_2O and HCl, the Scheil-Gulliver method could not be considered a good method for the prediction of the release of arsenic when H_2S was in the atmosphere.

In general, the Scheil-Gulliver calculations did not match well with the experimental results obtained in the condensation experiments and in the release experiments. Only in the condensation experiments with water a similar trend was found. Therefore, it could be concluded that the Scheil-Gulliver model was not a suitable tool for predicting the behaviour of arsenic under

the influence of H_2O, HCl and H_2S. The data base for the arsenic species should be modified or extended. That would improve the capacity of the model for predicting the behaviour of arsenic under different atmospheric conditions.

4.5. Tin

4.5.1. Condensation experiments

The total gas flow in the condensation experiments with tin was 645 ml/min and the duration of each experiment was 24 h. The temperature at which the metal boat should be placed in order to obtain 100 ppm of the metal in the gas was estimated with FactSage (see Figure 86). FactSage predicted a temperature of 1370 °C for the vaporization of 100 ppm of tin under the experimental conditions.

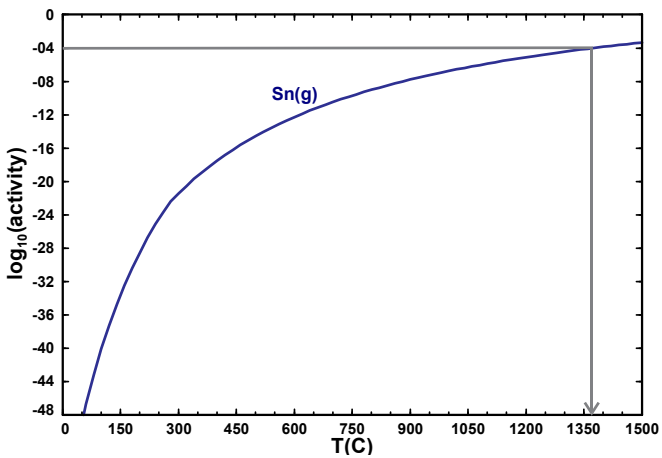

Figure 86. FactSage´s estimation of the necessary temperature for the vaporization of 100 ppm of tin.

The temperature predicted by FactSage 6.3 to evaporate 100 ppm of the metal was experimentally checked as in the condensation experiments with the other metals considered in the previous sections. For it, tin powder was evaporated at different temperatures between 990 and 1100 °C during 24 h. As tin source metallic tin was utilized.

The results obtained from the three experimental runs carried out are depicted in Figure 87. In the experiment in which the sample boat was situated at 1025 °C, the concentration of tin obtained was 72 ppm. Moreover, increasing the temperature at which the sample boat was placed to 1100 °C lead to a total tin concentration in the experiment of 465 ppm. The equation of the calibration curve was utilized for the determination of the necessary temperature to

evaporate 100 ppm of tin. The equation predicted a temperature of approximately 1015 °C for the evaporation of 100 ppm of tin. Thereby, in all the experiments with tin the sample boat containing the metal was placed at that temperature for ensuring the vaporization of 100 ppm.

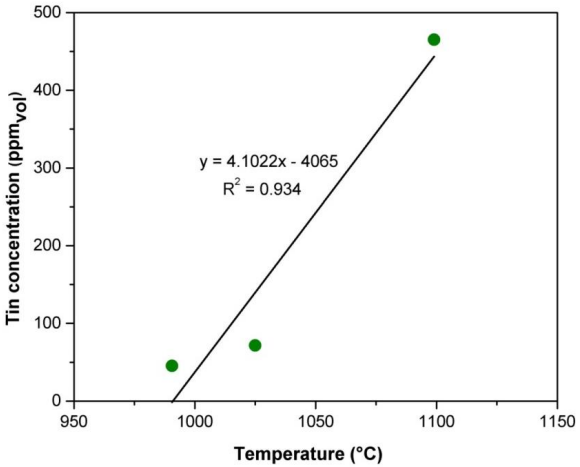

Figure 87. Correlation of tin concentration (ppm) and temperature (°C).

The experimental results of the condensation behaviour of tin under the presence of H_2O, HCl and H_2S in the atmosphere are shown below.

Influence of H_2O

The condensation distribution of tin species in the filters and in the outer tube when the atmosphere contained H_2O(g) is depicted in Figure 88. In this graph the results with 3 % vol H_2O and with 17 % vol H_2O in the atmosphere are shown. The percentage of arsenic condensed as metallic SnO_2, SnO, $SnCl_2$ and SnS are depicted in orange, red, blue and green colour, respectively.

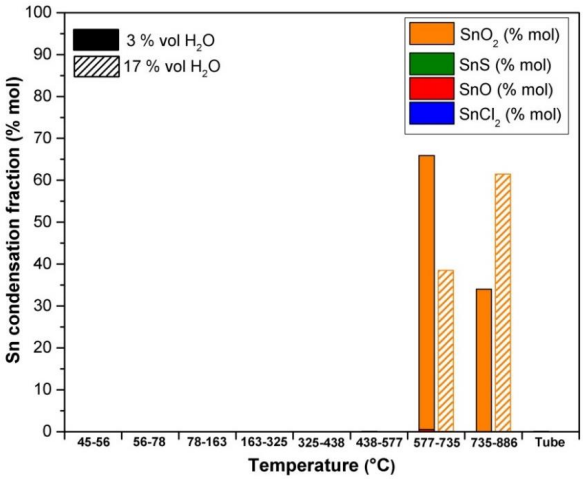

Figure 88. Condensation distribution of tin in the outer tube and in the filters placed along the cooling zone in an atmosphere containing 3 and 17 % vol of water vapour.

Tin condensed mostly as SnO_2 in atmospheres containing water vapour. A very tiny amount of SnO deposited as well. SnO_2 condensed in both experiments in the first and second filters, i.e. at temperatures between 886 and 577 °C. However, when the atmosphere contained 17 % vol water, more amount of SnO_2 condensed in the first filter than in the second. In the experiments with 3 % vol water the opposite trend was observed. SnO condensed in the second and third filter although the amount was so low that is almost inappreciable in the graph. The total percentage of tin that condensed as SnO was 0.6 and 0.1 % in the experiments with 3 % vol and 17 % vol of water.

In summary, an increase in the amount of $H_2O(g)$ introduced into the experiment caused the condensation of SnO_2 at higher temperatures.

Influence of HCl

Figure 89 shows the condensation behaviour of tin when HCl was introduced into the outer tube. The results of the experiments with 0, 50 and 500 ppm of HCl are shown. The bars on the left show the results obtained when the atmosphere contained 0 ppm HCl. The bars in the middle and on the right are the results with 50 and 500 ppm HCl.

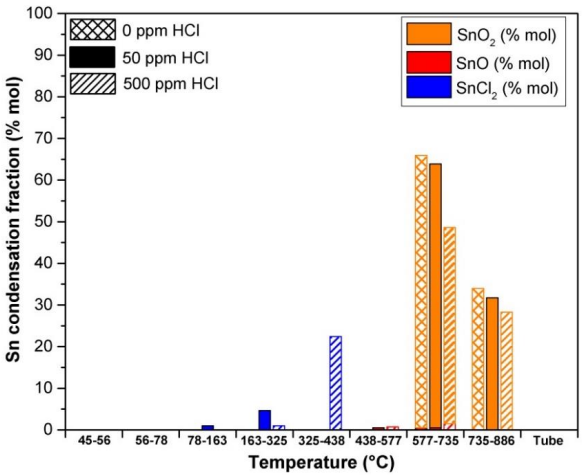

Figure 89. Condensation distribution of tin in the outer tube and in the filters placed along the cooling zone in an atmosphere containing 0 ppm HCl, 50 ppm HCl and 500 ppm of HCl.

As it can be observed in the graph, tin condensed mostly as SnO_2 at 886 – 577 °C in an atmosphere that only contained water vapour. A very tiny amount of SnO deposited as well.

When HCl was introduced into the experiment tin condensed as SnO_2, $SnCl_2$ and SnO. However, the great majority condensed as SnO_2 and $SnCl_2$. SnO_2 condensed like in the experiments containing only water, in the first and second filters at 886 – 577 °C. No difference was found in the condensation behaviour of SnO_2 with 50 ppm and 500 ppm HCl. The percentage condensed as SnO_2 was 95 % and 75.4 % in the experiments with 50 and 500 ppm of HCl, respectively. $SnCl_2$ condensed in the fifth and sixth filters (325 – 78 °C) in the experiment with 50 ppm of HCl. However, with 500 ppm of HCl it condensed at 438 – 163 °C, in the fourth and fifth filters. The percentage condensed as $SnCl_2$ was 4.7 % in the experiment with 50 ppm of HCl and 22.4 % in the experiment with 500 ppm of HCl. Moreover, SnO condensed in both experiments in the second and third filters. The percentage condensed as SnO was 0.3 % and 2.2 % in the experiments with 50 and 500 ppm of HCl.

In conclusion, the introduction of higher amounts of HCl caused the condensation of $SnCl_2$ at higher temperatures. The amount condensed as $SnCl_2$ was also greater with 500 ppm of HCl than with 50 ppm of HCl. The condensation behaviours of SnO_2 and SnO were not affected by the HCl amount. SnO condensed in both experiments in the second and third filter and the amount was very tiny. The percentage condensed as SnO_2 decreased when 500 ppm of HCl was introduced. However, this was only a consequence of the higher amount of $SnCl_2$ condensed.

Influence of H_2S

Figure 90 shows the condensation behaviour of tin when H_2S was introduced into the outer tube. The results of the experiments with 0, 50 and 500 ppm of H_2S are shown. The bars on the left show the results obtained when the atmosphere contained 0 ppm H_2S. The bars in the middle and on the right are the results with 50 and 500 ppm H_2S.

The experiments showed that tin condensed as SnS and SnO_2 when H_2S was introduced into the atmosphere. The deposits of SnS were found generally at higher temperatures than the deposits of SnO_2. As it can be seen in the graph, SnS condensed in both experiments in the first and second filters at 886 – 577 °C. The percentage of tin condensed as SnS in both experiments was very similar, 49.4 % and 50.5 % respectively. On the other hand, SnO_2 condensed in the second and third filters, at 735 – 438 °C, in both experiments.

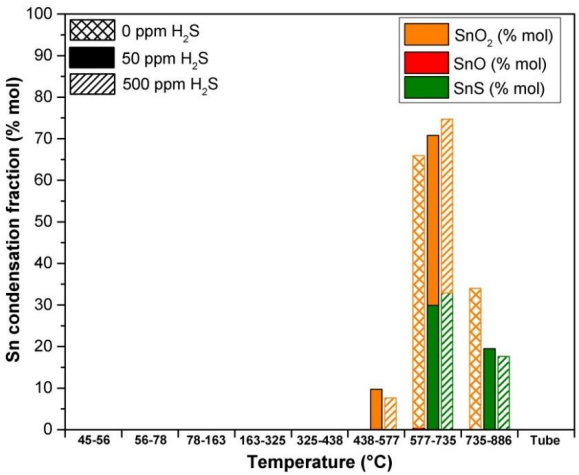

Figure 90. Condensation distribution of tin in the outer tube and in the filters placed along the cooling zone in an atmosphere containing 0 ppm H_2S, 50 ppm H_2S and 500 ppm of H_2S.

In summary, an increase in the amount of H_2S introduced into the atmosphere did not seem to affect the condensation behaviour of SnS. Under both experimental conditions SnS condensed at the same temperature range. Also the percentage of tin condensed as SnS was similar in both experiments. However, an increase in the amount of H_2S caused SnO_2 to condense at lower temperatures. Thus, with 0 ppm H_2S, SnO_2 condensed at 886 – 577 °C. However, with 50 and 500 ppm H_2S, SnO_2 condensed in the second and third filters, at 735 – 438 °C.

As it could be seen in the results of the experiments with H_2O and HCl, a small amount of tin condensed as SnO in the second and third filter. The total amount that condensed as SnO was

less than 2 % of the total deposition. However, in the experiments with H_2S, no SnO was found in the depositions. In order to check the origin of this species, the oxygen partial pressure in the experiments was calculated and integrated to the phase diagram for the system Sn-O_2 created with FactSage.

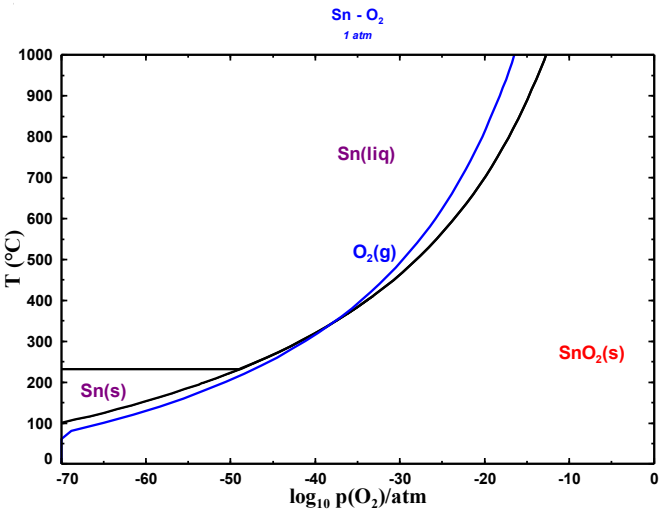

Figure 91. Phase diagram for the Sn-O_2 system including the equilibrium partial pressure of oxygen.

The graph shows the phase diagram for the Sn-O_2 system calculated by FactSage. The oxygen partial pressure in equilibrium versus the temperature for the experimental conditions is represented by a blue line. According to the graph, with the oxygen partial pressure present in the experiments, the condensation of SnO_2 was possible at low temperatures (350 – 50 °C). Besides, the phase diagram did not show the existence of SnO(s). Considering that in the experiments SnO_2 condensed at high temperatures, it is safe to say that the FactSage data base of tin is not appropriate for the prediction of the condensation of tin. Thus, the relative error associated to the analytical method for analysing the filters could be the reason for the detection of SnO in the filters. Another possibility could be the presence of a certain amount of oxygen during the cooling phase of the experiments due to the opening of the experimental setup after the experimental runs to take out the metal sample. However, it is important to consider that the amount condensed as SnO was less than 2 % and therefore, insignificant.

4.5.2. Thermodynamic pseudo-equilibrium model

Figure 92 shows the comparison between the model calculations and the experimental results of the condensation of tin in an atmosphere containing H_2O (3 – 17 % vol), HCl (50 – 500 ppm) and H_2S (50 – 500 ppm).

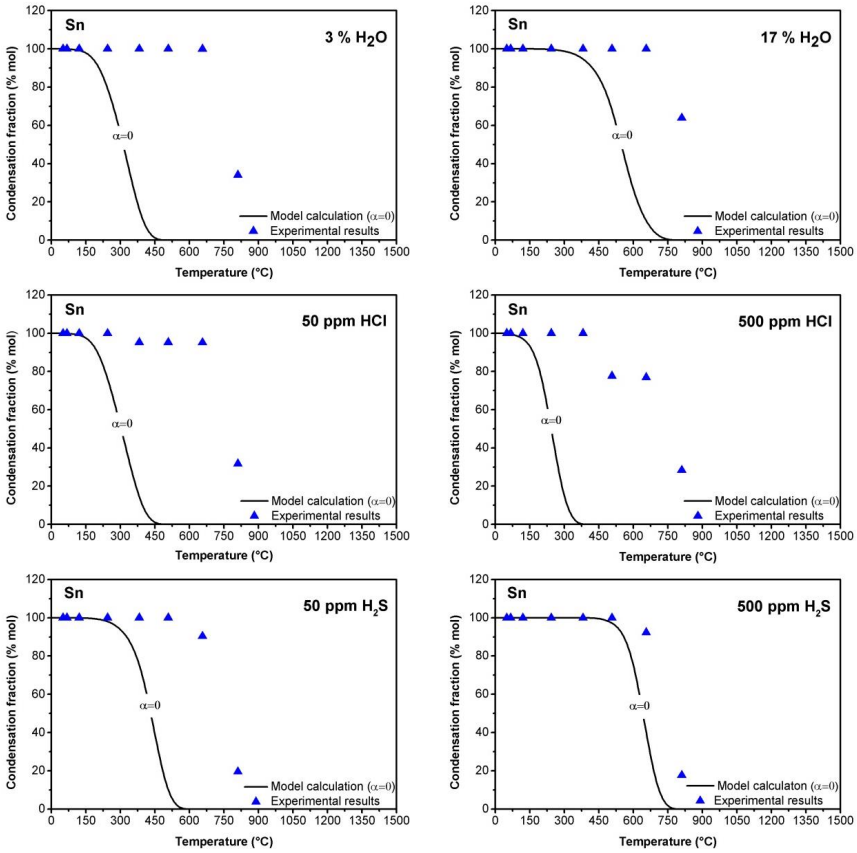

Figure 92. Comparison between the calculated and the experimental results of the condensation of tin vapours in the presence of H_2O (3 – 17 % vol), HCl (50 – 500 ppm) and H_2S (50 – 500 ppm).

As it can be seen in Figure 92, the condensation of tin vapours regardless of the atmospheric conditions took place at much higher temperatures than the temperatures that the thermodynamic model predicted.

In conclusion, the condensation behaviour of tin predicted by the pseudo-equilibrium model was considerably different to the tendency of the experimental results and therefore, any firm conclusions could not be drawn about the influence of the chemical reactions and super-cooling in the condensation behaviour of tin. Furthermore, according to the results, the condensation of the tin species took place at higher temperatures than the equilibrium calculations predicted (alpha ≈ 0). This was a strong proof to affirm that the database of tin available in FactSage was not appropriate for the prediction of the condensation of tin.

4.5.3. Scheil-Gulliver cooling calculations for the solid phase

The condensation calculations performed carried out with the Scheil-Gulliver cooling model in order to predict the condensation behaviour of tin are presented in this section. The calculations were performed at decreasing temperature steps of 25 °C starting from 1500 °C to room temperature. The results of the influence of H_2O, HCl and H_2S in the condensation behaviour of tin are depicted in Figure 93, Figure 94 and Figure 95.

Influence of H_2O

Figure 93 shows the speciation of the condensed phase predicted by the Scheil-Gulliver cooling calculations in an atmosphere containing water vapour and tin. The graph shows a comparison between the results obtained with 3 and 17 % vol of water vapour in the atmosphere. The results obtained with 3 % vol of water are depicted with a solid line and the results containing 17 % vol of water vapour are depicted with a dashed line.

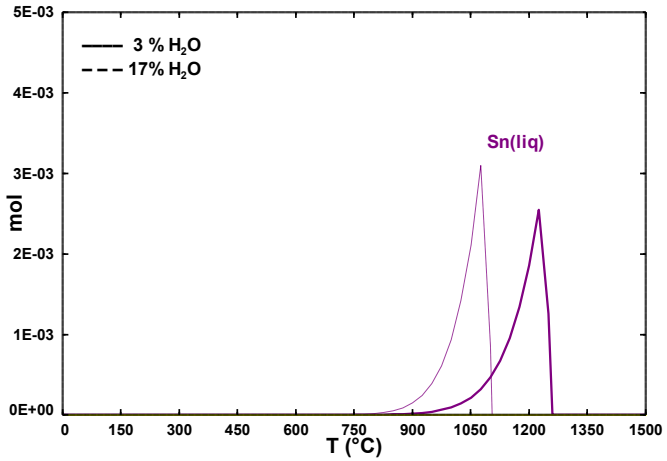

Figure 93. Speciation of the condensed phase during cooling from 1500 to 0 °C predicted by the Scheil-Gulliver cooling model in an atmosphere containing water vapour and tin.

The cooling calculations predicted the condensation of tin as Sn(liq) at 1250 – 900 °C when 3 % vol water vapor was present in the atmosphere. When the atmosphere had 17 % vol water, Sn(liq) condensed at slower temperatures (1100 – 800 °C). In summary, an increase of the water amount induced the condensation of Sn(liq) at lower temperatures. Furthermore, the model predicted the condensation of tin as SnO_2 at temperatures between 560 – 200 °C. However, its concentration was so low that it is not appreciated in the graph.

Influence of HCl

Figure 94 shows the results obtained from the Scheil-Gulliver cooling model when 50 and 500 ppm of HCl were present in an atmosphere containing tin. The results obtained when 50 ppm of HCl was in the atmosphere are depicted with a solid line and the results obtained when the atmosphere contained 500 ppm of HCl are depicted with a dashed line. The amount of tin condensed as SnO_2 and $SnCl_2$ are depicted in red and blue, respectively.

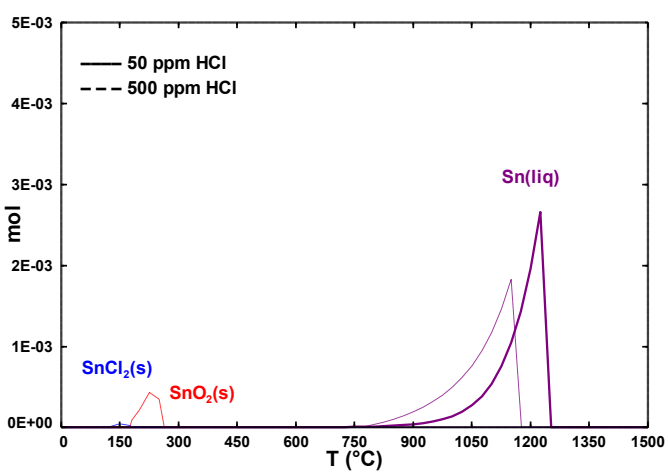

Figure 94. Speciation of the condensed phase during cooling from 1500 to 0 °C predicted by the Scheil-Gulliver cooling model in an atmosphere containing water HCl and tin.

When 50 ppm of HCl was considered, the program predicted the condensation of tin as Sn(liq) at 1250 – 900 °C. The calculations also predicted the existence of very low concentrations of $SnCl_2$ and SnO_2 at low temperatures. However, their amount was so low that is not appreciable in the graph. When the atmosphere had 500 ppm HCl, Sn(liq) condensed at lower temperatures (1170 – 750 °C). Besides, small amounts of SnO_2 and $SnCl_2$ condensed at 300 – 150 °C and 170 – 75 °C, respectively. In summary, an increase of the amount of HCl induced the condensation of

Sn(liq) at lower temperatures. Nevertheless, the concentrations of $SnCl_2$ and SnO_2 were so small that no firm conclusions could be drawn about their behaviour.

Influence of H_2S

The cooling calculations carried out with FactSage when H_2S was introduced in an atmosphere containing tin are shown in Figure 95. A comparison between the results with 50 ppm H_2S and 500 ppm H_2S is shown.

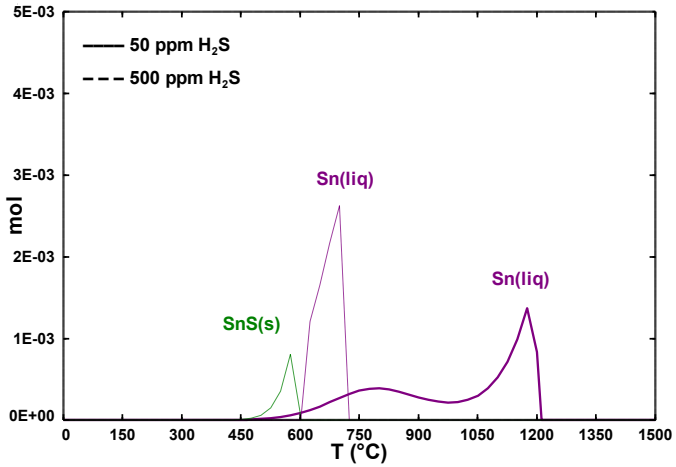

Figure 95. Speciation of the condensed phase during cooling from 1500 to 0 °C predicted by the Scheil-Gulliver cooling model in an atmosphere containing H_2S and tin.

The cooling calculations predicted the condensation of tin as Sn(liq) at 1200 – 500 °C when the atmosphere contained 50 ppm H_2S. However, when 500 ppm H_2S was considered, tin condensed as a mixture of Sn(liq) and SnS. SnS condensed at 600 – 450 °C and Sn(liq) at 730 – 600 °C. Therefore, the amount of H_2S considered caused the condensation of Sn(liq) at lower temperatures. Besides, some tin condensed as SnS.

4.5.4. Release experiments

The influence of water vapour, HCl and H_2S on the gas phase concentration and speciation of tin was investigated by MBMS. The gas flow was 4.3 l/min and the experiments were conducted at 1100 and 900 °C. As the mass spectrometer only determines the gaseous ionized species based on their mass-to charge ratios (m/z), it was necessary to carry out a calibration before starting the experiments. With this calibration it was possible to correlate the intensities of the isotopes present in the experiments with the heavy metal vapour concentration (ppm) obtained. In the experiments with tin the monitored species were $^{120}Sn^+$, $^{136}SnO^+$, $^{190}SnCl_2^+$,

$^{152}SnO_2^+$ and $^{158}SnS^+$. The correlation between the ion signal intensities of the monitored species and the obtained concentration (ppm) in the gas phase is shown in Figure 96.

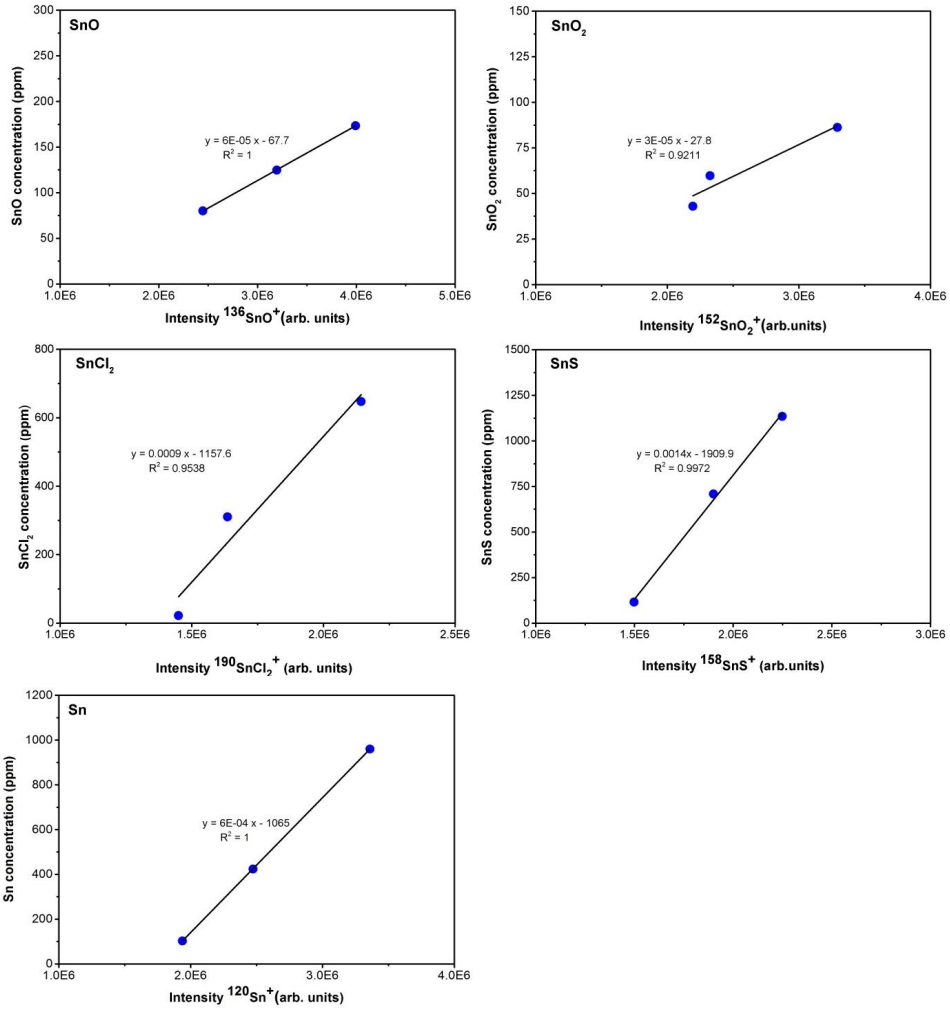

Figure 96. Calibration curves for the release experiments with tin.

Figure 97, Figure 98 and Figure 99 show the release behaviour of tin under the influence of H_2O, HCl and H_2S at different temperatures. The graphs show the speciation and behaviour of the tin-containing species that were in the gas phase at 1100 and 900 °C. Sn(g) was the major species in all experiments. Its concentration in the gas phase during the experiments was much

higher than the amounts of the other Sn-species present. However, in the graphs only the minor tin species present in the gas phase at 1100 and 900 °C are depicted. Due to the difficulty of vaporizing the same amount of tin in every experiment and therefore, obtaining a similar concentration each time, only a qualitative analysis could be achieved. An overview of the concentrations (in %) of all species detected in the gas phase is given in the tables on the right of the experimental results.

Influence of H_2O

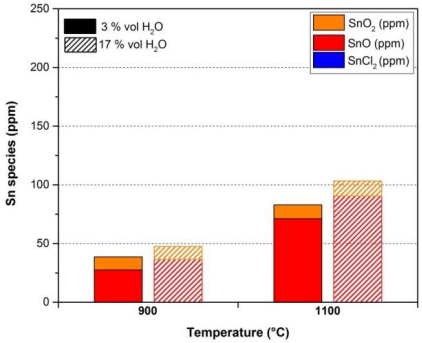

Concentration of gaseous Sn-species (%)						
	3 % vol H_2O			17 % vol H_2O		
	Sn	SnO	SnO_2	Sn	SnO	SnO_2
1100 °C	97.4	2.2	0.4	90.3	8.5	1.2
900 °C	99.0	0.7	0.3	98.0	1.6	0.5

Figure 97. Concentration of minor gaseous tin species at 1100 and 900 °C when the atmosphere contained water vapour (3 – 17 % vol). Note that Sn(g), the major species in the gas phase, is not represented.

Sn, SnO and SnO_2 were the species found in the gas phase during the experiments with H_2O. Sn was the major species. The concentration of SnO and SnO_2 increased with the temperature and with the amount of water. In other words, with 17 % vol of water a larger amount of both species was released than with 3 % vol. In general, the concentrations of SnO were larger than the concentrations of SnO_2.

Influence of HCl

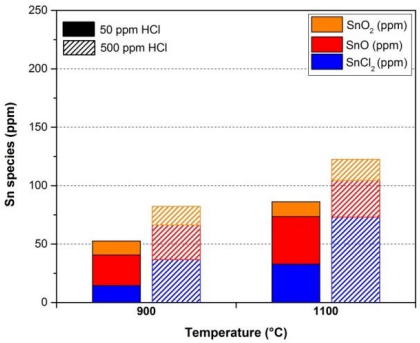

Concentration of gaseous Sn-species (%)								
	50 ppm HCl				500 ppm HCl			
	Sn	SnO	SnO_2	$SnCl_2$	Sn	SnO	SnO_2	$SnCl_2$
1100 °C	98.3	0.8	0.3	0.7	77.6	5.7	3.3	13.4
900 °C	96.2	1.9	0.9	1.1	55.6	16.0	8.5	19.8

Figure 98. Concentration of minor gaseous tin species at 1100 and 900 °C when the atmosphere contained HCl (50 – 500 ppm). Note that Sn(g), the major species in the gas phase, is not represented.

In the release experiments with HCl, Sn, $SnCl_2$, SnO_2 and SnO were the species found in the gas phase. Sn(g) was the major species in all the experiments. The concentrations of SnO and SnO_2 were low in comparison with the concentrations of $SnCl_2$. In general, the concentrations of SnO were higher than the concentrations of SnO_2. The concentrations of $SnCl_2$ decreased with the temperature. Furthermore, for both temperatures considered, the concentration of $SnCl_2$ was higher in the experiments with 500 ppm of HCl than in the experiments with only 50 ppm. Also the concentrations of SnO and SnO_2 were higher with 500 ppm HCl than with only 50 ppm. On this basis, it could be assumed that HCl influenced the release behaviour of all species.

Influence of H_2S

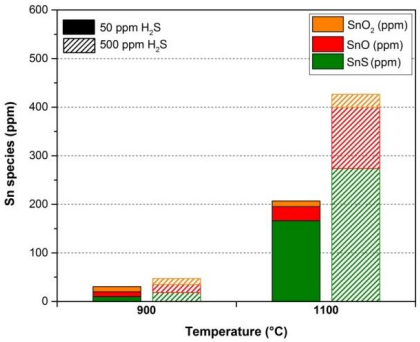

Concentration of gaseous Sn-species (%)								
	50 ppm H_2S				500 ppm H_2S			
	Sn	SnO	SnO_2	SnS	Sn	SnO	SnO_2	SnS
1100 °C	81.2	10.7	4.4	3.7	75.3	7.3	1.5	15.9
900 °C	95.8	0.2	0.2	3.7	97.6	0.8	0.6	0.9

Figure 99. Concentration of minor gaseous tin species at 1100 and 900 °C when the atmosphere contained H_2S (50 – 500 ppm). Note that Sn(g), the major species in the gas phase, is not represented.

In the release experiments with H_2S a mixture of Sn, SnS, SnO_2 and SnO was found in the gas phase. Sn(g) was the major species in all experiments, followed by SnS and SnO. The concentration of all these species increased with the temperature, especially SnS. In the experiments with 500 ppm of H_2S the concentration of SnS was much higher than in the experiments with 50 ppm H_2S, especially at 1100 °C. However, the concentration of SnO and SnO_2 did not seem to be affected by the amount of H_2S.

4.5.5. Scheil-Gulliver cooling calculations for the gas phase

The release behaviour of tin under the influence of H_2O, HCl and H_2S was predicted by the Scheil-Gulliver cooling model and is shown in this section. The calculations show the speciation of the main inorganic gaseous species at temperatures between 1200 °C and room temperature.

Influence of H_2O

The speciation of the gas phase predicted by the Scheil-Gulliver cooling calculations in an atmosphere containing water vapour and tin is shown in Figure 100. The graph shows the comparison of the results obtained with 3 and 17 % vol of water vapour in the atmosphere. The results obtained with 3 % vol are depicted with a solid line, whereas the results containing 17 % vol of water vapour are depicted with a dashed line.

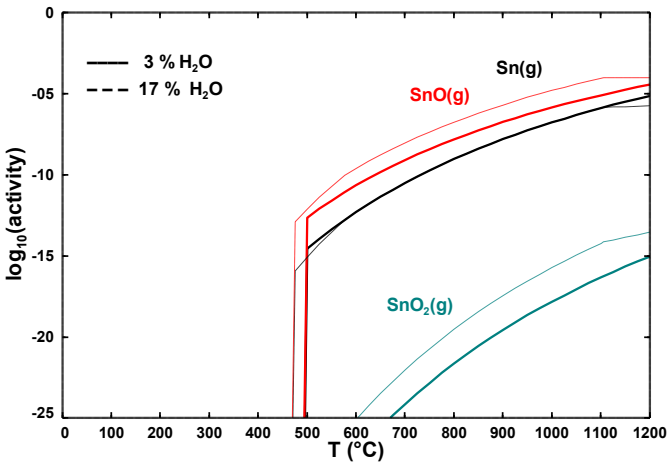

Figure 100. Gaseous tin-containing species versus temperature in an atmosphere containing 3 – 17 % vol of H_2O calculated by the Scheil-Gulliver cooling model.

The calculations predicted the existence of Sn, SnO and SnO_2 in the gas phase at temperatures between 1000 – 470 °C. Their concentration increased with rising temperatures. The concentration of SnO_2 was smaller than 1 ppb and was not considered. The behaviour of SnO was influenced by the considered amount of water. Thus, the concentration of SnO was higher with 17 % vol of water than with 3 % vol of water. The amount of H_2O did not influence the behaviour of Sn(g).

Influence of HCl

The predicted release behaviour of tin when 50 and 500 ppm of HCl were present in the atmospheric conditions is depicted in Figure 101. The simulations were carried out with the Scheil-Gulliver cooling model. In this case, the results for 50 ppm of HCl in the atmosphere are depicted with a solid line and the results for 500 ppm of HCl are depicted with a dashed line.

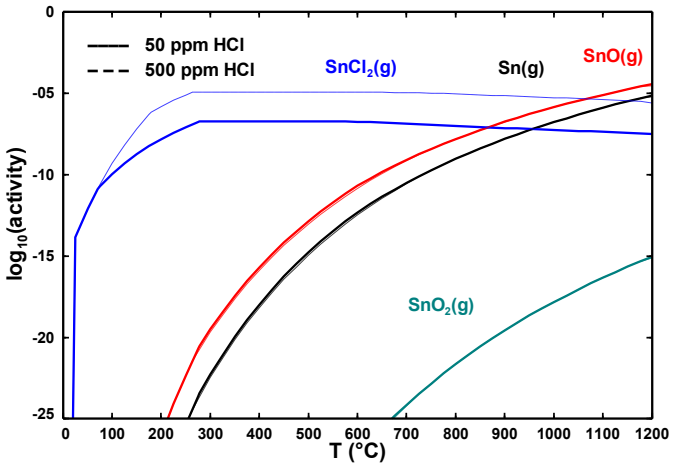

Figure 101. Gaseous tin-containing species versus temperature in an atmosphere containing 50 – 500 ppm of HCl calculated by the Scheil-Gulliver cooling model.

As it can be observed from the calculations, Sn, $SnCl_2$, SnO and SnO_2 were the species that appeared in the gas phase. The amount of SnO_2 was out of the concentration range considered in this study. The concentration of Sn and SnO increased with the temperature and they were present at approximately 1200 – 200 °C. The concentration of $SnCl_2$ was constant with the temperature. However, at 250 °C its concentration decreased abruptly. In general, the amount of HCl did not have a great influence on the release behaviour of SnO and Sn. However, when 500 ppm of HCl was in the atmosphere, the concentration of $SnCl_2$ was higher than when only 50 ppm of HCl was considered. Therefore, it could be concluded that the HCl amount influenced the behaviour of $SnCl_2$.

Influence of H_2S

Figure 102 shows the release behaviour of tin predicted by FactSage when H_2S was introduced into the atmosphere. A comparison between the results obtained with 50 ppm H_2S and 500 ppm H_2S is shown. The results for 50 ppm of H_2S in the atmosphere are depicted with a solid line and the results for 500 ppm H_2S are depicted with a dashed line.

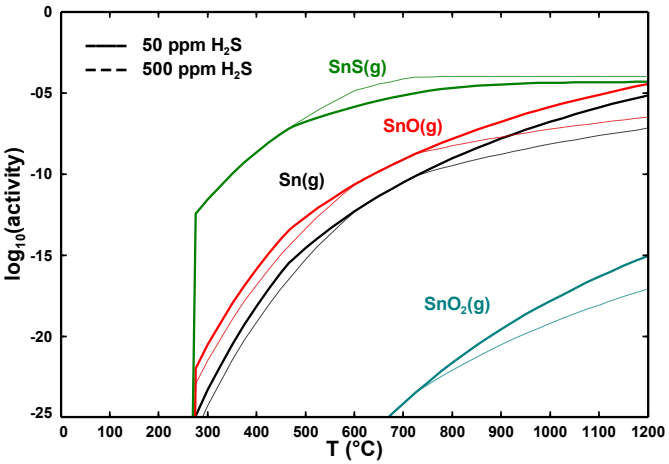

Figure 102. Gaseous tin-containing species versus temperature in an atmosphere containing 50 – 500 ppm of H_2S calculated by the Scheil-Gulliver cooling model.

In this case, the simulations predicted the existence of SnS, SnO, Sn and SnO_2 in the gas phase. Like in the other cases, the concentration of SnO_2 was too low for being considered. The concentrations of all species increased with rising temperatures. As shown in the graph, a higher amount of H_2S caused a higher concentration of SnS in the gas phase. In the same way, the calculations predicted that the concentrations of Sn and SnO were smaller with 500 ppm H_2S than with 50 ppm H_2S. Therefore, it seemed that the amount of H_2S influenced the behaviour of all tin-species.

4.5.6. Discussion

According to the comparison of the experimental results with the results of the cooling calculations and the thermodynamic pseudo-equilibrium model, the following conclusions of the condensation and release behaviour of tin could be drawn:

Condensation behaviour of tin

FactSage 6.3 predicted a temperature of 1370 °C for the evaporation of 100 ppm of tin under the atmospheric conditions considered in the experiments. However, the experiments showed that positioning the tin sample at 1025 °C a concentration of approximately 72 ppm in the gas phase was obtained. At 1100 °C 465 ppm of tin were evaporated. The correlation equation predicted a temperature of 1015 °C for the evaporation of 100 ppm of tin under the experimental conditions. Therefore, in all experiments the metal source was placed at 1015 °C.

Figure 88 shows that tin condensed mostly as SnO_2 (886 – 577 °C) in atmospheres containing water vapour. A small amount of SnO deposited at 735 – 438 °C. In general, an increase of the amount of H_2O caused the condensation of SnO_2 at higher temperatures. The cooling calculations (see Figure 93) predicted the condensation of tin as Sn(liq) at 1250 – 900 °C when 3 % vol water vapour was present in the atmosphere. However, with 17 % vol of water, Sn(liq) condensed at slower temperatures (1100 – 800 °C). In summary, an increase of the water amount induced the condensation of Sn(liq) at lower temperatures. The model also predicted the condensation of tin as SnO_2 at temperatures between 560 – 200 °C (see Figure 93). However, its concentration was very low. In the calculations the species deposited as well as the condensation temperature of SnO_2 were different to the experimental results. For this reason, the Scheil-Gulliver model was not capable of predicting accurately the condensation behaviour of tin when water was introduced into the atmosphere.

When HCl was introduced into the experiment tin condensed as SnO_2 (886 – 577 °C), $SnCl_2$ (438 – 78 °C) and SnO (735 – 438 °C). In general, the introduction of higher amounts of HCl caused the condensation of larger amounts of $SnCl_2$ at higher temperatures (see Figure 89). The condensation behaviour of SnO_2 and SnO was not affected by the HCl amount. The Scheil-Gulliver calculations, predicted the condensation of tin as Sn(liq) at 1250 – 900 °C (see Figure 94). The calculations also predicted the existence of very low concentrations of $SnCl_2$ and SnO_2 at low temperatures. With 500 ppm HCl, Sn(liq) condensed at lower temperatures (1170 – 750 °C). Besides, small amounts of SnO_2 and $SnCl_2$ condensed at 300 – 150 °C and 170 – 75 °C, respectively. In summary, an increase of the amount of HCl induced the condensation of Sn(liq) at lower temperatures. Nevertheless, the concentrations of $SnCl_2$ and SnO_2 were too small for drawing conclusions about their behaviour. The condensation temperatures and the concentrations of SnO_2 and $SnCl_2$ were much higher in the experiments than in the calculations. Furthermore, no Sn(liq) was found in the deposits of the experiments. Thus, the model did not predict appropriately the condensation of tin when HCl was introduced into the atmosphere.

Tin condensed as SnS (886 – 577 °C) and SnO_2 (735 – 438 °C) when H_2S was introduced into the atmosphere, as shown in Figure 90. The condensation of SnS and SnO was unaffected by H_2S. Under both experimental conditions they condensed at the same temperature range. The cooling calculations, however, predicted the condensation of tin as Sn(liq) at 1200 – 500 °C when the atmosphere contained 50 ppm H_2S (see Figure 95). With 500 ppm H_2S, tin condensed as Sn(liq) and SnS. SnS condensed at 600 – 450 °C and Sn(liq) at 730 – 600 °C. Therefore, the amount of H_2S caused the condensation of Sn(liq) at lower temperatures. As the speciation predicted from the model as well as the condensation temperatures did not match with the experimental results, the Scheil-Gulliver model was not a suitable tool to predict the condensation of tin when H_2S was in the atmosphere.

In the experiments with H_2O and HCl, a small amount condensed as SnO. According to the Sn-O_2 phase diagram and the oxygen partial pressure in the experiments, the only oxygen-containing species that could condense was SnO_2(s). The deposition of SnO_2 was possible at low temperatures (350 – 50 °C). Considering that in the experiments SnO_2 condensed at high temperatures, it could be assumed that the FactSage database of tin was not appropriate for the prediction of the condensation of tin. The detection of SnO in the filters could be an error of the analytical method utilized for analyzing the filters from the cooling zone. Another possibility could be the presence of a high amount of oxygen during the cooling phase of the experiments due to the opening of the experimental setup after the experimental runs to take out the metal sample. Nevertheless, it is important to consider that the amount condensed as SnO was less than 2 % of the total deposition of tin and therefore, insignificant.

As it can be seen in Figure 92, the condensation of tin vapours took place at much higher temperatures than the temperatures that the thermodynamic model predicted regardless of the atmospheric conditions. This was a strong proof to affirm that the database of tin available in FactSage was not appropriate for the prediction of the condensation of tin. The pseudo-equilibrium model could not be used for the prediction of the condensation of tin.

Release behaviour of tin

The influence of water vapour, HCl and H_2S on the speciation and concentration of tin in the gas phase was investigated by MBMS at 1100 and 900 °C. Due to the difficulty of vaporizing the same amount of tin in every experiment and therefore, obtaining a similar concentration each time, only a qualitative analysis could be achieved. However, Sn(g) was the major species in all experiments. Its concentration in the gas phase was much higher than the amounts of the other Sn-species present.

Sn, SnO and SnO_2 were the species found in the gas phase during the experiments with H_2O (see Figure 97). Sn was the major species. The concentration of SnO and SnO_2 increased with the temperature and with the amount of water. In general, the concentration of SnO was higher than the concentration of SnO_2. The same species were found in the Scheil-Gulliver calculations (see Figure 100). The concentrations of Sn, SnO and SnO_2 increased with rising temperatures. Besides, higher concentrations of SnO and SnO_2 were in the gas phase with higher amounts of water vapour. The only difference appreciated between the model and the experiments was the concentration of SnO_2. The model predicted the presence of this species at very low concentrations (lower than ppb). However, in the experiments, SnO_2 was found at ppm level. In conclusion, the model results did not match the experimental results appropriately.

The release experiments (Figure 98) as well as the calculations with HCl (Figure 101) showed that tin was present in the gas phase as a mixture of $SnCl_2$, SnO_2 and SnO. Sn was the major species in all experiments. The concentrations of SnO and SnO_2 were low in comparison with the concentrations of $SnCl_2$. In general, the concentrations of SnO were higher than the concentrations of SnO_2. The concentration of $SnCl_2$ seemed to be constant with the temperature. Like in the experiments with water, the calculations predicted very low concentrations of SnO_2. However, SnO_2 was detected at ppm level in the experiments. Furthermore, the concentration of all species was higher in the experiments with high amounts of HCl. Nevertheless, according to the calculations only $SnCl_2$ was influenced by the amount of HCl. Thus, the model did not predict accurately the behaviour of tin when HCl was introduced into the atmosphere.

In the release experiments with H_2S a mixture of Sn, SnS, SnO_2 and SnO was found in the gas phase (see Figure 99). Sn was the major species in all experiments, followed by SnS and SnO. The concentration of all those species increased with the temperature, especially SnS. The concentration of SnS was higher in the experiments with more amounts of H_2S. However, the concentration of SnO and SnO_2 did not seem to be affected by the amount of H_2S. The cooling calculations (see Figure 102) predicted the same speciation in the gas phases as well as a similar behaviour of the species. However, some differences were found. In the experiments Sn was the major species, followed by SnS. Nevertheless, in the calculations SnS was the major species, followed by SnO. Also the concentration of SnO_2 was supposed to be present in very low concentrations. However, SnO_2 was detected in the gas phase at ppm level. For all these differences, the Scheil-Gulliver model could not be considered as a good tool for the prediction of the behaviour of tin in the gas phase.

In general, the Scheil-Gulliver calculations did not match well the experimental results obtained in the condensation and release experiments. The data base for the tin species in the solid and gas phase should be extended in order to be able to obtain closer results to the experiments. Therefore, the pseudo-equilibrium model would also predict better the experimental results.

4.6. Vanadium

4.6.1. Condensation experiments

The temperature at which the metal boat containing vanadium had to be placed for obtaining 100 ppm of the metal in the gas was estimated with FactSage and is shown in Figure 103. The temperature predicted by FactSage 6.3 was 2000 °C. Placing the metal source at this temperature would give rise to a concentration of vanadium of 100 ppm in the experiment.

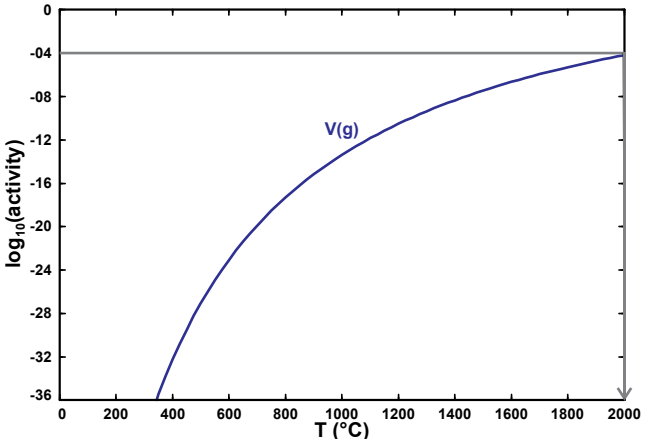

Figure 103. FactSage´s estimation of the necessary temperature for the vaporization of 100 ppm vanadium.

As the temperature profile present in the condensation experiments shows (Figure 12), the highest temperature in the reaction zone was 925 °C. Although this temperature was far below the temperature required to obtain a concentration of 100 ppm of vanadium, some experiments were carried out to determine the vanadium concentration reached at temperatures between 700 and 925 °C. In the calibration experiments vanadium powder was evaporated at 700, 900 and 925 °C during 24 h. As vanadium source it was used metallic vanadium.

The results obtained from the experimental runs carried out showed that vanadium did not evaporate under any of the considered temperatures. At 700, 900 and 925 °C the vanadium concentration in the experiments was 0 ppm. In other words, vanadium required a much higher temperature in order to evaporate than the temperatures available in the setup for the condensation experiments. According to this, the condensation experiments with vanadium could not be performed. Thus, the influence of H_2O, HCl and H_2S on the condensation behaviour of vanadium was only determined by the cooling calculations with the Scheil-Gulliver tool available in FactSage 6.3. Consequently, the results from the model calculations could not be compared with the experimental results.

4.6.2. Thermodynamic pseudo-equilibrium model

Figure 104 shows the condensation of vanadium calculated by the pseudo-equilibrium model in an atmosphere containing H_2O (3 – 17 % vol), HCl (50 – 500 ppm) and H_2S (50 – 500 ppm).

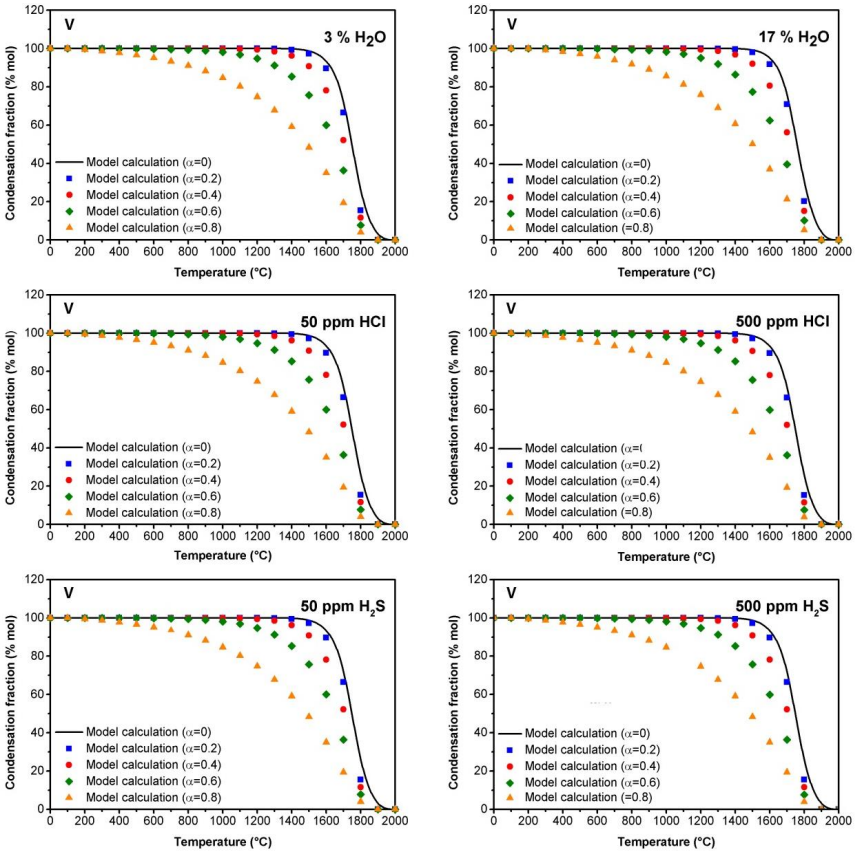

Figure 104. Calculated results of the condensation of vanadium vapours in the presence of H_2O (3 – 17 % vol), HCl (50 – 500 ppm) and H_2S (50 – 500 ppm).

As explained before, the condensation experiments with vanadium could not be carried out due to the high temperature necessary for the metal to evaporate under the experimental conditions. That is why for this case the results from the model calculations could not be compared with the experimental results. However, the pseudo-equilibrium model was implemented for the six experimental conditions in order to acquire a better understanding of the condensation of vanadium. The condensation fraction of vanadium was calculated under the values of alpha equal to 0, 0.2, 0.4, 0.6 and 0.8.

As it can be seen in Figure 104, vanadium showed the same condensation behaviour in each of the experimental conditions. That means that the results obtained for example with α = 0.2 had the same tendency under all atmospheric conditions considered. The only noticeable difference

was that in the experiment with 17 % vol H_2O, the vanadium condensed at slightly higher temperatures than in the experiment with only 3 % vol H_2O. However, the difference was very little and it is difficult to be appreciated. In every case the model predicted the condensation of vanadium as V_2O_3. Furthermore, the model predicted that all V_2O_3 condensed at temperatures higher than 400 °C regardless of the alpha value.

4.6.3. Scheil-Gulliver cooling calculations for the solid phase

The condensation calculations carried out with the Scheil-Gulliver cooling model in order to predict the condensation behaviour of vanadium are presented in this section. The calculations were performed at a decreasing temperature in steps of 25 °C, starting at 2600 °C and going down to room temperature. The results showing the influence of H_2O, HCl and H_2S on the condensation behaviour of vanadium are presented below.

Influence of H_2O

The speciation of the condensed phase predicted by the Scheil-Gulliver cooling calculations in an atmosphere containing water vapour and vanadium is shown in the Figure 105. The graph depicts a comparison of the results obtained with 3 and 17 % vol of water vapour in the atmosphere. The results obtained with 3 % vol of water vapour are illustrated with a solid line, the ones obtained with 17 % vol of water vapour are depicted with a dashed line.

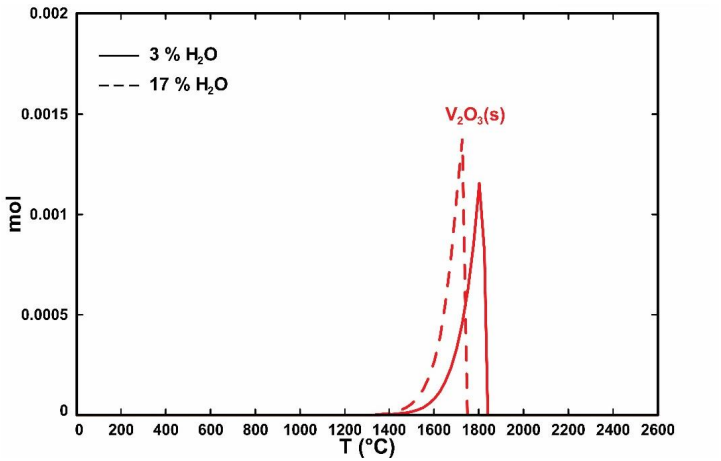

Figure 105. Speciation of the condensed phase during cooling from 2600 to 0 °C predicted by the Scheil-Gulliver cooling model in an atmosphere containing water vapour and vanadium.

The cooling calculations predicted the entire condensation of vanadium as V_2O_3 in both cases. The main difference was that with 3 % vol of water, V_2O_3 condensed at 1850 – 1400 °C, where-

as with 17 % vol H_2O, V_2O_3 condensed at lower temperatures (1750 – 1400 °C). This leads to the conclusion that a higher amount of water shifted the condensation of V_2O_3 to lower temperatures.

Influence of HCl

Figure 106 shows the results obtained from the Scheil-Gulliver cooling model when 50 and 500 ppm of HCl were present in an atmosphere containing vanadium. Once again, the results obtained with 50 ppm HCl are depicted with a solid line and the results obtained with 500 ppm of HCl are depicted with a dashed line.

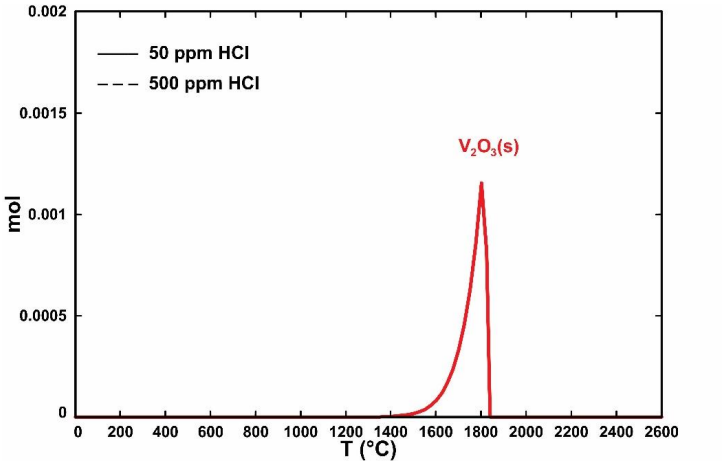

Figure 106. Speciation of the condensed phase during cooling from 2600 to 0 °C predicted by the Scheil-Gulliver cooling model in an atmosphere containing HCl and vanadium.

In this case, the results from the cooling calculations predicted the condensation of vanadium as V_2O_3 at 1850 – 1400 °C for both atmospheric conditions. The prediction of both simulations overlapped, as can be observed in Figure 106. The calculations predicted the same results as in the previous section when 3 % vol of water vapour was in the atmosphere. This means that HCl did not influence the condensation behaviour of vanadium. Furthermore, vanadium always condensed as V_2O_3 regardless of the amount of HCl considered.

Influence of H_2S

The condensation behaviour of vanadium predicted by FactSage when H_2S was introduced into the atmosphere is depicted in Figure 107. It shows the comparison of the results with 50 and 500 ppm of H_2S.

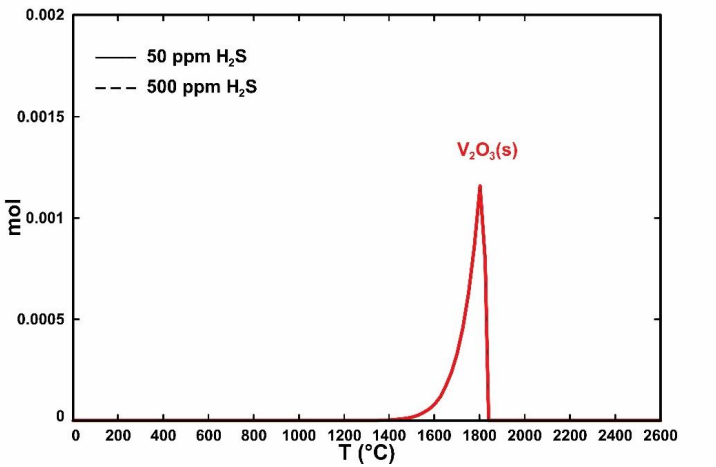

Figure 107. Speciation of the condensed phase during cooling from 2600 to 0 °C predicted by the Scheil-Gulliver cooling model in an atmosphere containing H_2S and vanadium.

As it can be observed, the results obtained from the cooling calculations when H_2S was added are equal to the results obtained when the atmosphere had HCl. Thus, vanadium condensed as V_2O_3 (1850 – 1400 °C) for both atmospheric conditions. Accordingly, neither HCl nor H_2S influenced the condensation behaviour of vanadium.

4.6.4. Release experiments

As it has been explained in section 4.6.1, the condensation experiments with vanadium could not been carried out due to the high temperature required to evaporate the metal. Vanadium was evaporated at 700, 900 and 925 °C. Therefore, a similar scenario was expected in the release experiments.

However, as the furnace for the release experiments did not have a cooling zone, the maximum achievable temperature was a little higher than in the condensation furnace. A temperature of 1100 °C was considered.

Vanadium was vaporised at 1100 °C under the same atmospheric conditions as in the experiments during 15 hours. Neither HCl nor H_2S were introduced. During the experimental run, the intensity of the isotopes $^{51}V^+$, $^{67}VO^+$, $^{83}VO_2^+$, $^{150}V_2O_3^+$ and $^{182}V_2O_5^+$ were monitored. After the experiment the metal source was removed and weighed. Intensity-time profiles for the release of vanadium compounds are shown in Figure 108.

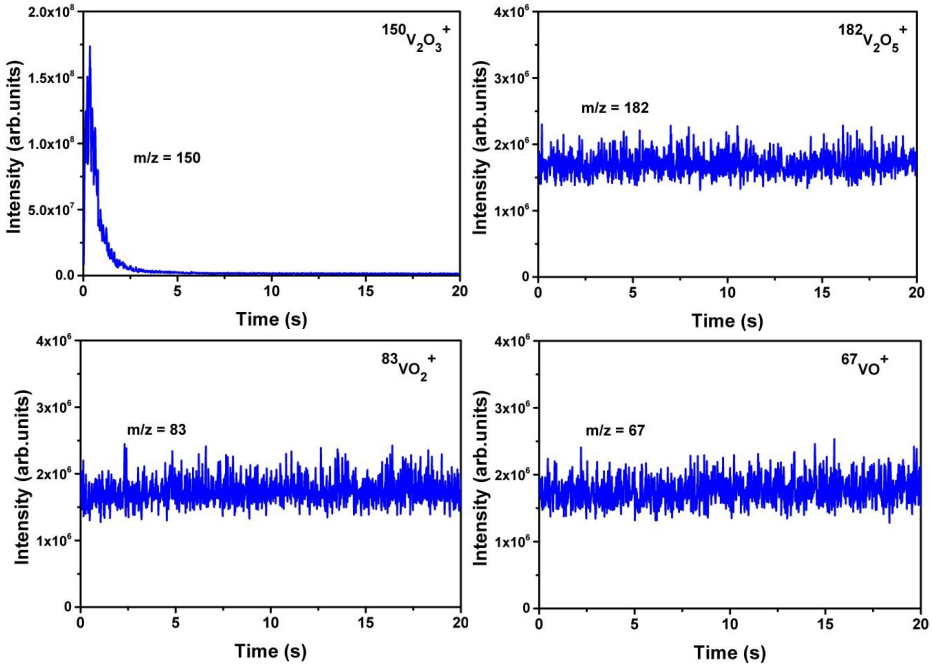

Figure 108. Intensity-time profiles of $^{150}V_2O_3^+$, $^{182}V_2O_5^+$, $^{83}VO_2^+$ and $^{67}VO^+$ during the release of vanadium at 1100 °C.

According to the spectrums only $^{150}V_2O_3^+$ was released with high intensity. Although over the time low intensity signals were observed for $^{67}VO^+$, $^{83}VO_2^+$ and $^{182}V_2O_5^+$, they were slightly higher than the background noise. However, they were too low for further interpretation.

The concentration of vanadium (ppm) in the gas phase could not be calculated due to the formation of an oxide layer on the top of the metal source. In consequence, the sample boat with the vanadium source became heavier than it was at the beginning of the experiment. A correlation between the intensities of the isotopes and their concentration in the experiment was not feasible. Since the vanadium source turned its colour from grey to blue, it could be assumed that vanadium oxidised to VO_2 during the experiment.

It may be expected that the following reactions took place in the furnace. This would explain the oxidation of vanadium during the experiment:

$$2VO_2 + {}^1/_2\, O_2 \rightarrow V_2O_5$$

$$V_2O_5 + 2H_2 \rightarrow 2H_2O + V_2O_3$$

According to these reactions, VO_2 reacted with oxygen to form V_2O_5. This compound, in turn, reacted with the introduced hydrogen from the gasification conditions and gave rise to V_2O_3. This may explain the existence of V_2O_3, V_2O_5 and VO_2 in the gas phase.

The difficulty of measuring the concentration of vanadium in the experiment and the low amount released to the gas phase at 1100 °C was a determining factor in the decision of not going on with the calibrations and the vanadium experiments, respectively. In order to evaporate vanadium in concentrations of 100 ppm higher temperatures were required

However, some interpretations of the release of vanadium could be done. The high-intensity signal of $^{150}V_2O_3^+$ during the experiment showed that $^{150}V_2O_3^+$ was the main compound released when H_2O was present in the atmosphere. Furthermore, the presence of $^{182}V_2O_5^+$, $^{83}VO_2^+$ and $^{67}VO^+$ during the experiments assumed the existence of low concentrations of these compounds during the release of vanadium. However, in terms of the amount of these compounds in the gas phase, definite conclusions cannot be drawn.

4.6.5. Scheil-Gulliver cooling calculations for the gas phase

The release behaviour of vanadium under the influence of H_2O, HCl and H_2S was predicted by the Scheil-Gulliver cooling model and it is shown in this section. The calculations show the speciation of the main inorganic gaseous species at temperatures between 2000 °C and room temperature.

Influence of H_2O

The speciation of the gas phase predicted by the Scheil-Gulliver cooling calculations in an atmosphere containing water vapour and vanadium is shown in Figure 109. The graph shows a comparison between the calculations obtained with 3 and 17 % vol of water vapour in the atmosphere. The results obtained with 3 % vol of water are depicted with a solid line and the results with 17 % vol of water vapour are depicted with a dashed line.

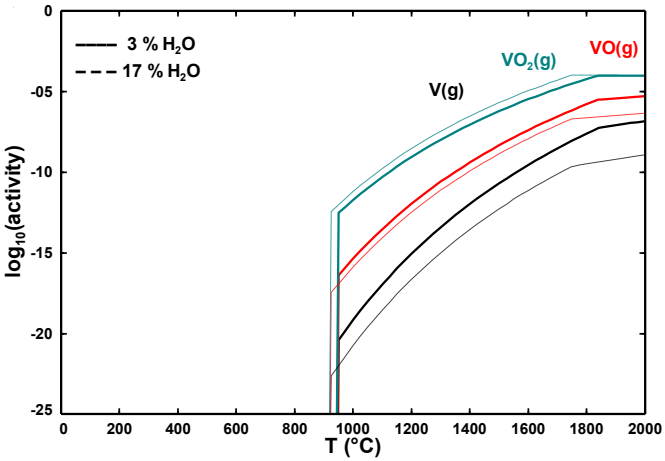

Figure 109. Gaseous vanadium-containing species versus temperature in an atmosphere containing 3 – 17 % vol of H_2O calculated by the Scheil-Gulliver cooling model.

The calculations predicted the existence of V, VO and VO_2 in the gas phase. They were present in the gas phase at temperatures between 2000 – 950 °C and their concentration increased with the temperature. The amount of water vapour did not have a great influence in the behaviour of the three species, as can be observed in the graph.

Influence of HCl

The predicted behaviour of vanadium when 50 and 500 ppm of HCl were present in the atmospheric conditions is depicted in Figure 110. The simulations were carried out with the Scheil-Gulliver cooling model. In this case, the results for 50 ppm of HCl in the atmosphere are depicted with a solid line and the results for 500 ppm of HCl are depicted with a dashed line.

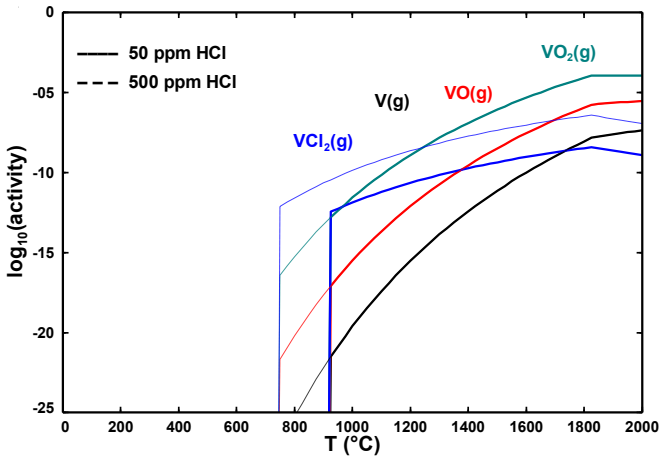

Figure 110. Gaseous vanadium-containing species versus temperature in an atmosphere containing 50 – 500 ppm of HCl calculated by the Scheil-Gulliver cooling model.

The main inorganic species present in the gas phase when the atmosphere contained HCl were VO_2, VCl_2, VO and V. The only appreciable difference between the results with different amounts of HCl was the concentration of VCl_2. VCl_2 was present in the gas phase at higher concentrations when the atmosphere contained 500 ppm of HCl. Thus, it could be concluded that an increase in the HCl amount caused the presence of a higher concentration of VCl_2 in the gas phase. However, the amount of HCl did not have any influence in the behaviour of VO_2, VO and V.

Influence of H_2S

Figure 111 shows the behaviour of vanadium predicted by FactSage when H_2S was introduced into the atmosphere. It shows a comparison of the results obtained with 50 and 500 ppm of H_2S. The results for 50 ppm of H_2S in the atmosphere are depicted with a solid line and the results obtained with 500 ppm of H_2S are depicted with a dashed line.

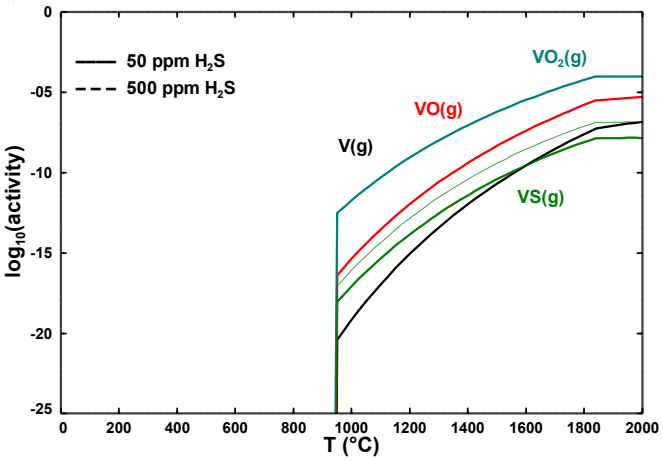

Figure 111. Gaseous vanadium-containing species versus temperature in an atmosphere containing 50 – 500 ppm of H_2S calculated by the Scheil-Gulliver cooling model.

The simulations predicted the presence of V, VO_2, VO and VS in the gas phase at temperatures between 2000 and 950 °C. Their concentrations increased with the temperature. VS was the only species that was affected by H_2S. With 500 ppm of H_2S in the atmosphere the amount of VS was higher than with only 50 ppm of H_2S.

4.6.6. Discussion

As it has been explained above the condensation and release experiments with vanadium could not be carried out due to the high temperature needed to evaporate the metal under the experimental conditions. Therefore, the results of the model calculations could not be compared with the experimental results. However, considering the results obtained with the Scheil-Gulliver model some conclusions could be drawn about the condensation and release of vanadium. The pseudo-equilibrium model was also implemented for the six experimental conditions in order to acquire a better understanding of the condensation of vanadium.

Condensation behaviour of vanadium

The cooling calculations predicted the entire condensation of vanadium as V_2O_3 when water was present in the atmosphere (see Figure 105). V_2O_3 condensed at 1850 – 1400 °C when the atmosphere had 3 % vol water. However, with 17 % vol H_2O, V_2O_3 condensed at lower temperatures (1750 – 1400 °C).

According to the calculations, HCl and H_2S did not have any influence on the condensation behaviour of vanadium. Like in the case with 3 % vol water, vanadium condensed as V_2O_3 at 1850 – 1400 °C regardless of the amount of HCl or H_2S.

The results of the pseudo-equilibrium model (Figure 104) showed that vanadium condensed as V_2O_3. It showed the same behaviour under all experimental conditions considered. Only with 17 % vol water vanadium started to condense at slightly higher temperatures.

Release behaviour of vanadium

Although the release experiments were not carried out due to the high temperature necessary for the evaporation of vanadium, some interpretations of the behaviour of vanadium could be done considering the experimental run that was carried out at 1100 °C.

$^{150}V_2O_3^+$ was the main compound in the gas phase when H_2O was present in the atmosphere. Furthermore, the presence of $^{182}V_2O_5^+$, $^{83}VO_2^+$ and $^{67}VO^+$ in the gas phase, assumed the existence of low concentrations of these compounds during the experiments with vanadium.

In the presence of water, the Scheil-Gulliver calculations predicted the existence of V, VO and VO_2 in the gas phase. The amount of water vapour did not have a great influence on the behaviour of these species (see Figure 109). The presence of VO and VO_2 was confirmed during the experimental run with vanadium.

According to the calculations, the main inorganic species present in the gas phase when the atmosphere contained HCl were VO_2, VCl_2, VO and V (see Figure 110). The behaviour of the oxides was exactly like in the calculations where only water was introduced. An increase of the HCl amount induced the presence of a higher concentration of VCl_2. However, HCl did not have any influence in the behaviour of VO_2, VO and V.

In the simulations with H_2S, the model predicted the release of V, VO_2, VO and VS. VS was the only species that was affected by the amount of H_2S. With 500 ppm H_2S in the atmosphere the amount of VS was higher than with only 50 ppm of H_2S. This was shown in Figure 111.

The thermodynamic-pseudo equilibrium model predicted that V_2O_3 condensed at temperatures higher than 400 °C regardless of the gas atmosphere and the kinetics of the reaction.

Due to the lack of experimental data, no definitive conclusions could be done. Release and condensation experiments with vanadium under different experimental conditions should be done in order to check the reliability of the data base for vanadium. Only in this way the accuracy of the models to predict the behaviour of vanadium could be established and conclusions could be made.

5. Summary and recommendations

The purpose of this work was to assess the influence of H_2O, HCl and H_2S on the condensation and release of some heavy metals. The metals considered were Zn, Cd, Pb, As, Sn and V. The condensation behaviour (temperature and speciation) of the heavy metal vapours was investigated in a heated flow channel reactor housed in a furnace with a gas cooling zone. Glass filters were placed on different stages along the cooling zone for the deposition of the metal compounds. The metal species deposited in the filters were firstly dissolved and afterwards determined by means of ion chromatography (IC) and inductively coupled plasma optical emission spectrometry (ICP-OES). Experiments on the release of the inorganic vapours were carried out in a heated flow channel reactor coupled to a molecular beam mass spectrometer (MBMS) in order to analyse the gas in-situ. The experiments were carried out under two typical gasification conditions with different concentrations of HCl and H_2S. Concentrations of 50 and 500 ppm of the trace gases in the experiments were considered.

The results of the experimental investigation were compared with “Scheil-Gulliver Cooling” calculations performed by FactSage 6.3. Furthermore, a thermodynamic pseudo-equilibrium model was utilized to help understanding the condensation mechanisms of the trace metals. This model provided information about the global kinetics of the experiments. The simulation results were compared with the experimental results in order to ascertain the capacity of the models for predicting the behaviour of the heavy metals under different atmospheric conditions. An enhanced knowledge about the behaviour of Zn, Cd, Pb, As, Sn and V was obtained and a better understanding of the release and condensation mechanisms was achieved.

Based on the experimental results and simulations on the condensation and release of the trace metals the following conclusions could be drawn:

Zinc

In an atmosphere containing H_2O zinc condensed as ZnO (735 – 438 °C). An increase of the water vapour induced ZnO to condense at higher temperatures. In the release experiments, Zn and ZnO were the only species present in the gas phase. Zn was the dominant species. Besides, the concentration of ZnO increased with the temperature and amount of water. This confirmed the results observed in the condensation experiments.

In the presence of HCl zinc condensed as ZnO (735 – 163 °C) and $ZnCl_2$ (577 – 163 °C). Approximately 25 % of the zinc condensed as $ZnCl_2$. A large concentration of HCl caused ZnO to condense at lower temperatures. Thus, in the release experiments more ZnO was present in the

gas phase at 800 – 500 °C in the experiment with 500 ppm HCl than in the one with 50 ppm. However, the dominant species in the gas phase was Zn.

Zinc condensed as a mixture of ZnO and ZnS at 735 – 438 °C in an atmosphere containing H_2S. The amount of zinc condensed as ZnS was 10 %. In general, a high amount of H_2S caused ZnS to condense at slightly higher temperatures. For this reason, the amount of ZnS in the gas phase with 500 ppm H_2S at 800 – 500 °C was lower than in the experiments with 50 ppm. The concentration of Zn in the gas phase was higher than the concentration of ZnS.

The thermodynamic pseudo-equilibrium model predicted the global kinetics of the experiments with zinc. The curve-fitting of the results indicated an alpha value of zero for all the experimental conditions except for the experiment with 500 ppm H_2S. That means that the equilibrium was reached in the experiments. Only the experiment with a high amount of H_2S was affected by super-cooling. Therefore, in the experiment with 500 ppm H_2S the zinc compounds condensed at lower temperatures than the ones predicted by the model.

Cadmium

When the atmosphere contained water vapour, cadmium condensed as metallic Cd at 325 – 78 °C. The release experiments showed that cadmium was released as Cd and CdO at 1000 – 900 °C. Cd was the major species in every experiment.

Cadmium condensed as a mixture of $CdCl_2$ (438 – 163 °C) and metallic Cd (325 – 78 °C) in the presence of HCl. In general, larger amounts of HCl lead Cd to condense at slightly higher temperatures. Cd, CdO and $CdCl_2$ were the species detected in the gas phase. In all the experiments the major species was Cd, followed by $CdCl_2$ and CdO.

Cadmium condensed as CdS (438 – 163 °C) and Cd (325 – 78 °C) regardless of the amount of H_2S. In the gas phase experiments, cadmium was present as a mixture of Cd, CdS and CdO. The concentration of CdS was in both experiments much higher with 500 ppm H_2S than with 50 ppm H_2S.

The thermodynamic pseudo-equilibrium model predicted the global kinetics of the experiments with cadmium. The curve-fitting of the results indicated an alpha value of zero for the experiments with water vapour and HCl. The model predicted the experimental results very well. According to the model, the equilibrium was reached in these experiments. Nevertheless, the experiments with H_2S were affected by super-cooling. Therefore, the cadmium compounds condensed at lower temperatures than the temperatures predicted by the model. Alpha values of 0.8 and 0.7 fit nicely the experimental results obtained with 50 and 500 ppm H_2S, respectively. Thus, alpha decreased with larger concentrations of H_2S, which confirmed that a larger for-

mation of CdS compensated the super-cooling effect and the condensation was slightly shifted to higher temperatures.

Lead

Lead condensed as a mixture of PbO_2 and PbO at 886 – 577 °C regardless of the volume of water vapour in the atmosphere. This was confirmed in the gas phase experiments, where only high concentrations of PbO and PbO_2 were found at 1100 °C. In the gas phase also high concentrations of Pb were detected.

Lead condensed as a mixture of PbO-PbO_2 (886 – 577 °C) and $PbCl_2$ (577 – 325 °C) when HCl was introduced into the experiment. An increase in the HCl amount increased the amount of lead condensing as $PbCl_2$ as well as the temperature at which it was deposited. As the lead oxides condensed at high temperatures, only high amounts of them were detected at 1100 °C in the gas phase experiments. $PbCl_2$ and Pb were also found in the gas. Pb was the major species. Due to the low condensation temperature of $PbCl_2$, high concentrations of this species were present in the gas phase experiments.

The experiments with H_2S showed that Pb condensed as PbS and PbO-PbO_2 at 886 – 577 °C. An increase in the amount of H_2S increased the amount of lead condensed as PbS as well as its condensation temperature. Nevertheless, the amount of H_2S did not affect the condensation behaviour of PbO-PbO_2. The same tendency was found in the gas phase experiments. Only high concentrations of PbS were released at 900 and 1100 °C. The species found in the gas phase in the experiments were Pb, PbO, PbO_2 and PbS.

The thermodynamic pseudo-equilibrium model provided information about the global kinetics of the experiments. The curve-fitting of the results indicated an alpha value of zero for the experiments with water vapour and HCl. The model predicted for these cases the experimental results very well. According to the model, the experiments were in equilibrium. However, the experiments with H_2S were affected by super-cooling. Therefore, the condensation of lead took place at lower temperatures than predicted by the model. Alpha values of 0.25 and 0.2 fit the experimental results obtained with 50 and 500 ppm H_2S, respectively. Thus, alpha decreased with larger concentrations of H_2S. That means that the condensation was shifted to higher temperatures due to the formation of PbS. The super-cooling effect was offset.

Arsenic

Arsenic condensed in atmospheres containing water vapour as metallic As (325 – 56 °C) regardless of the volume of water. In the gas phase experiments with H_2O, As, As_2O_3 and As_2O_5 were detected. As was the major species. No conclusions could be drawn due to the low condensation temperature of As.

When HCl was introduced into the experiment arsenic condensed as As (325 – 56 °C) and $AsCl_3$ (78 – 45 °C). Besides, the introduction of a higher concentration of HCl in the experiments did not have an appreciable influence on the condensation behaviour of arsenic. In the gas phase experiments, arsenic was found as a mixture of As, $AsCl_3$, As_2O_3 and As_2O_5, being As(g) the dominant species.

Arsenic condensed as metallic As (325 – 56 °C) and As_2S_2 (438 – 325 °C) when H_2S was introduced into the atmosphere. The percentage of arsenic condensed as As_2S_2 was generally less than 6 %. An increase in the amount of H_2S did not have a great influence on the condensation behaviour of As and As_2S_2. In the gas phase experiments arsenic was detected as a mixture of As, As_2S_2, As_2O_3 and As_2O_5.

In all the condensation experiments, a small concentration of As_2O_5 was found in the deposits. However, the presence of this species in the filters was due to an external source of oxygen during the cooling phases of the experiments. Thereby, the condensation of this species was not taken into account.

The thermodynamic pseudo-equilibrium model was able to predict acceptably the condensation behaviour of arsenic when the atmosphere contained H_2O and H_2S. With HCl the calculated results were very different to the experimental results and no alpha value could match the experimental results. According to the model, the experiments with HCl were very far away from reaching an equilibrium stage.

Tin

Tin condensed mostly as SnO_2 (886 – 577 °C) in atmospheres containing water vapour. Besides, a small amount of SnO deposited at 735 – 438 °C. In general, an increase in the amount of H_2O caused the condensation of SnO_2 at higher temperatures. Sn, SnO and SnO_2 were the species detected in the gas phase. Sn and SnO were the dominant species.

When HCl was introduced tin condensed as SnO_2 (886 – 577 °C), $SnCl_2$ (438 – 78 °C) and SnO (735 – 438 °C). In general, the introduction of higher amounts of HCl caused the condensation of larger amounts of $SnCl_2$ at higher temperatures. In the gas phase, Sn, SnO_2, SnO and $SnCl_2$ were detected. Sn was the major species. Due to the high condensation temperature of SnO_2, only small concentrations of this species were released at 900 and 1100 °C. However, SnO and $SnCl_2$ were released at higher concentrations.

Tin condensed as SnS (886 – 577 °C) and SnO_2 (735 – 438 °C) when H_2S was introduced into the atmosphere. The condensation of SnS and SnO was unaffected by H_2S. In the release experiments Sn, SnO, SnO_2 and SnS were detected. The concentration of every species especially SnS was higher in the experiments with 500 ppm H_2S. The condensation temperature of SnS was

confirmed in the release experiments. As SnS condensed at very high temperatures (886-577 °C), this species was only found in the gas phase experiments at low concentrations at 900 °C.

In the condensation experiments with H_2O and HCl, a small concentration of SnO was found in the deposits. Most likely, this was due to an error in the method utilized for analysing the filters. However, as the database for Sn was not found to be proper for the prediction of tin condensation, it could not be verified if the presence of SnO was possible under the atmospheric conditions considered.

According to the pseudo-equilibrium model, the condensation of tin compounds took place at higher temperatures than the equilibrium calculations predicted. As this is theoretically impossible, it could be concluded that the database of tin available in FactSage was not appropriate for the prediction of the condensation of tin.

Vanadium

The condensation and release experiments with vanadium could not be carried out due to the high temperature that the metal needed to evaporate under the experimental conditions considered. However, considering the results obtained with the Scheil-Gulliver model some conclusions could be drawn about the condensation and release of vanadium. The pseudo-equilibrium model was also implemented for the six experimental conditions in order to acquire a better understanding of the condensation of vanadium.

The cooling calculations predicted the condensation of vanadium as V_2O_3 when H_2O, HCl and H_2S were present in the atmosphere. V_2O_3 condensed generally at 1850 – 1400 °C. However, with 17 % vol of H_2O, V_2O_3 condensed at lower temperatures (1750 – 1400 °C). The results of the pseudo-equilibrium model also showed that vanadium condensed as V_2O_3.

In the presence of water, the Scheil-Gulliver calculations predicted the existence of V, VO and VO_2 in the gas phase. When the atmosphere had HCl or H_2S, VCl_2 and VS appeared as well.

The thermodynamic pseudo-equilibrium model predicted that V_2O_3 condensed at temperatures higher than 400 °C regardless of the gas atmosphere considered and the kinetics of the reaction.

In order to determine the accuracy of the models to predict the behaviour of vanadium, release and condensation experiments with this heavy metal under different experimental conditions should be done.

To sum up, the Scheil-Gulliver cooling calculations were found to be a good tool for the prediction of the condensation and release behaviour of zinc and cadmium. In general, a good agreement between the cooling calculations and the experimental results was found. The speciation as well as the temperatures at which the species were released or condensed under the influence of H_2O, HCl and H_2S had the same trend in the calculations as in the experimental results. However, in some cases small differences were found. These differences could be explained by the difficulty of keeping the same metal concentration in every experiment. Another reason could be the error associated to the analytic methods used for the determination of the condensed species in the cooling zone. However, accurate predictions of the release and condensation of zinc and cadmium under other atmospheric conditions not considered in this work could be done by the model. Good and reliable predictions would be obtained.

The data bases for lead, tin and arsenic should be modified or extended in order to improve the capacity of the Scheil-Gulliver model for predicting the condensation and release of the heavy metals under different atmospheric conditions. Closer results to the experimental results would be achieved with an optimisation of the data bases. The condensation and release behaviour of vanadium should be experimentally investigated in order to validate the Scheil-Gulliver model as well as the data base for vanadium of FactSage.

With this work a better understanding of the release and condensation mechanisms of Zn, Cd, Pb, As, Sn and V was achieved. The speciation as well as the behaviour of the trace metals under the influence of different concentrations of H_2O, HCl and H_2S were determined. The global kinetics in the experiments were clarified through the thermodynamic pseudo-equilibrium model. Furthermore, the Scheil-Gulliver Cooling was proved to be an excellent tool for the prediction of the release and condensation of Zn and Cd. Although in this study the model was only applied for some atmospheric conditions and the calculations were only compared with laboratory results, the model could be applied for wider conditions and bigger systems typical in gasification processes. In conclusion, a new insight into the gasification process was gained by this study. A better comprehension of the release and condensation of the trace metals was obtained. This is of vital importance for the development of hot gas cleaning systems to reduce the trace metal emissions in the next generation coal power plants.

Considering the results of this study, some recommendations can be made for the development of new hot fuel gas cleaning techniques. In gasification processes with 3 – 17 % vol H_2O, 50 – 500 ppm HCl or 50 – 500 ppm H_2S, the following species might be present in high concentrations in the gas and condensed phase (see Table 7, Table 8 and Table 9). Some discrepancies can be found in the temperatures due to the broad temperature ranges of the filters. The results are based on the experimental investigations. Only the speciation and temperature of vanadium is based on the Scheil-Gulliver cooling calculations.

Table 7. Trace element species in an atmosphere with water vapour

With H_2O (3 – 17 % vol)		
	Gas phase	**Condensed phase**
Zinc species	ZnO(g) : 900 – 500 °C	ZnO(s) : 886 – 438 °C
	Zn(g) : 900 – 500 °C	
Cadmium species	CdO(g) : 1000 – 900 °C	Cd(s) : 325 – 78 °C
	Cd(g) : 1000 – 900 °C	
Lead species	PbO_2-PbO(g) : 1100 – 600 °C	PbO_2-PbO(s) : 886 – 577 °C
	Pb(g) : 1100 – 600 °C	
Arsenic species	As_2O_3(g) : 1000 – 700 °C	As(s) : 325 – 56 °C
	As_2O_5(g) : 1000 – 700 °C	
	As(g) : 1000 – 700 °C	
Tin species	SnO_2(g) : 1100 – 900 °C	SnO_2(s) : 886 – 577 °C
	SnO(g) : 1100 – 900 °C	
	Sn(g) : 1100 – 900 °C	
Vanadium species	VO(g) : 2000 – 950 °C	V_2O_3(s) : 1850 – 1400 °C
	VO_2(g) : 2000 – 950°C	
	V(g) : 2000 – 950 °C	

Table 8. Trace element species in an atmosphere with HCl

With HCl (50 – 500 ppm)		
	Gas phase	**Condensed phase**
Zinc species	ZnO(g) : 900 – 500 °C	ZnO(s) : 735 – 438 °C
	$ZnCl_2$(g) : 900 – 500 °C	$ZnCl_2$(s) : 577 – 163 °C
	Zn(g) : 900 – 500 °C	
Cadmium species	$CdCl_2$(g) : 1000 – 700°C	$CdCl_2$(s) : 438 – 163 °C
	CdO(g) : 1000 – 700 °C	Cd(s) : 325 – 78 °C
	Cd(g) : 1000 – 700 °C	
Lead species	PbO_2-PbO (g) : 1100 – 600 °C	PbO_2-PbO(s) : 886 – 577 °C
	$PbCl_2$(g) : 1100 – 600 °C	$PbCl_2$(s) : 577 – 325 °C
	Pb(g) : 1100 – 600 °C	
Arsenic species	As_2O_3(g) : 1000 – 700 °C	As(s) : 325 – 56 °C
	As_2O_5(g) : 1000 – 700 °C	
	$AsCl_3$(g) : 1000 – 700 °C	$AsCl_3$(s) : 78 – 45 °C
	As(g) : 1000 – 700 °C	
Tin species	SnO_2(g) : 1100 – 900 °C	SnO_2(s) : 886 – 577 °C
	SnO(g) : 1100 – 900 °C	SnO(s) : 735 – 438 °C
	$SnCl_2$(g) : 1100 – 900 °C	$SnCl_2$(s) : 438 – 78 °C
	Sn(g) : 1100 – 900 °C	
Vanadium species	VO(g) : 2000 – 750 °C	V_2O_3(s) : 1850 – 1400 °C
	VO_2(g) : 2000 – 750 °C	
	VCl_2(g) : 2000 – 750 °C	
	V(g) : 2000 – 800 °C	

Table 9. Trace element species in an atmosphere with H_2S

With H_2S (50 – 500 ppm)		
	Gas phase	**Condensed phase**
Zinc species	ZnO(g) : 900 – 500 °C	ZnO(s) : 735 – 438 °C
	ZnS(g) : 900 – 500 °C	ZnS(s) : 735 – 438 °C
	Zn(g) : 900 – 500 °C	
Cadmium species	CdS(g) : 1000 – 700 °C	CdS(s) : 438 – 163 °C
	CdO(g) : 1000 – 700 °C	Cd(s) : 325 – 78 °C
	Cd(g) : 1000 – 700 °C	
Lead species	PbO_2-PbO(g) : 1100 – 600 °C	PbO_2-PbO(s) : 886 – 577 °C
	PbS(g) : 1100 – 600 °C	PbS(s) : 886 – 577 °C
	Pb(g) : 1100 – 600 °C	
Arsenic species	As_2O_3(g) : 1000 – 700 °C	As(s) : 325 – 56 °C
	As_2O_5(g) : 1000 – 700 °C	
	As_2S_2(g) : 1000 – 700 °C	As_2S_2(s) : 438 – 325 °C
	As(g) : 1000 – 700 °C	
Tin species	SnO_2(g) : 1100 – 900 °C	SnO_2(s) : 886 – 577 °C
	SnO(g) : 1100 – 900 °C	
	SnS(g) : 1100 – 900 °C	SnS(s) : 886 – 577 °C
	Sn(g) : 1100 – 900 °C	
Vanadium species	VO(g) : 2000 – 950 °C	V_2O_3(s) : 1850 – 1400 °C
	VO_2(g) : 2000 – 950 °C	
	VS(g) : 2000 – 950 °C	
	V(g) : 2000 – 950 °C	

6. Bibliography

[1] World Energy Outlook International Energy Agency. Paris: IEA, 2009.

[2] World Energy Outlook International Energy Agency. Paris: IEA/OECD, 2010.

[3] A. J. Minchener and J. T. McMullan, "Strategy for sustainable power generation from fossil fuels", Journal of the Energy Institute, vol. 81, 38-44, 2008.

[4] EIA, Annual Energy Review 2007, U.S. Department of Energy, 2008.

[5] B. G. Miller, *Clean coal engineering technology*, Butterworth-Heinemann, 2011.

[6] R. H. Wolk and J. McDaniel, "High efficiency coal fueled power generation", Energy Conversion and Management, vol. 33, 705-712, 1992.

[7] A. Inaba and K. Okada, "Coal utilization technology for reducing carbon dioxide emission", Coal Science and Technology, vol 24, 1919-1922, 1995.

[8] M. Bläsing, *Release of inorganic trace elements from high-temperature gasification of coal*, PhD-thesis, RWTH Aachen, 2011.

[9] I. G. C. Dryden, *The efficient use of energy*, IPC Science and Technology Press in collaboration with the Institute of Fuel acting on behalf of the UK Dept. of Energy, 602, 1975.

[10] T. Le Bris, S. Caillat, B. Baudoin, F. Cadavid, S. Pietrzyk, and J. Blondin, "Coal combustion modelling of large power plant for NOx abatement", Fuel, vol. 86, 2213-2220, 2007.

[11] J. E. Notestein, "Commercial gasifier for IGCC applications study report", 1990.

[12] J. D. Mondol, D. McIlveen-Wright, S. Rezvani, Y. Huang, and N. Hewitt, "Techno-economic evaluation of advanced IGCC lignite coal fuelled power plants with CO_2 capture", Fuel, vol. 88, 2495-2506, 2009.

[13] A. Newcomer and J. Apt, "Storing syngas lowers the carbon price for profitable coal gasification", Environmental Science and Technology, vol. 41, 7974-7979, 2007.

[14] J. Beer, "High efficiency electric power generation: The environmental role", Progress in energy and combustion science, vol. 33, 107-134, 2007.

[15] A. Neville, "IGCC Update: Are We There Yet?", Power, vol. 153, 52-57, 2009.

[16] B. Wate, "High temperature corrosion in gasifiers", Materials Research, vol. 7, 53-59, 2004.

[17] L. B. Clarke and L. L. Sloss, *Trace elements: emissions from coal combustion and gasification*, International Energy Agency Coal Research, 1992.

[18] D. A. Bell, B. F. Towler, and M. Fan, *Coal gasification and its applications,* Elsevier, 2011.

[19] I. M. Smith, "Trace Elements from Coal Combustion : Emissions", IEA Coal Research, 1987.

[20] J. G. Speight, *Handbook of coal analysis,* 2005.

[21] J. G. Speight, *The chemistry and technology of coal,* CRC Press, 2013.

[22] N. J. Hodges and D. G. Richards, "The fate of chlorine, sulphur, sodium, potassium, calcium and magnesium during the fluidized bed combustion of coal", Fuel, vol. 68, 440-445, 1989.

[23] A. Attar, "Chemistry, thermodynamics and kinetics of reactions of sulphur in coal-gas reactions: A review", vol. 57, 201-212, 1978.

[24] C. Karr, *Analytical methods for coal and coal products*, NY: Academic Pr., 1978.

[25] M. A. Elliott, *Chemistry of coal utilization*, NY: Wiley, 1981.

[26] D. J. Swaine, *Trace Elements in Coal*, Butterworth-Heinemann, 1-278, 1990

[27] D. C. Adriano, *Trace elements in the terrestrial environment,* Springer, 1986.

[28] L. L. Sloss, *NOx Emissions from Coal Combustion*, IEA Coal Research, 1991.

[29] E. Sabbioni, L. Goetz, A. Springer, and R. Pietra, "Trace metals from coal-fired power plants: Derivation of an average data base for assessment studies of the situation in the European communities", Science of The Total Environment, vol. 29, 213-227, 1983.

[30] R. D. Smith, "The trace element chemistry of coal during combustion and the emissions from coal-fired plants", Progress in Energy and Combustion Science, vol. 6, 53-119, 1980.
[31] M. J. Chadwick, N. H. Highton, and N. Lindman, *Environmental impacts of coal mining and utilization*, Pergamon press, 1987.
[32] V. Valkovic, *Trace elements in coal,* vol. 1, Boca-Raton: CRC Press, 1983.
[33] CIAB Report, *International Coal policy Developments*, 2011.
[34] D. Osborne, *The coal handbook: towards cleaner production,* Woodhead Publishing Series, 2013.
[35] S. A. Qader, *Natural gas substitutes from coal and oil,* Elsevier, 1985.
[36] C. Higman and M. Van der Burgt, *Gasification,* Elsevier, 2003.
[37] D. Merrick, *Coal combustion and conversion technology*, MacMillan, 1984.
[38] R. A. Newby and R. L. Bannister, "Advanced hot gas cleaning system for coal gasification processes", Journal of Engineering for Gas Turbines and Power, vol. 116, Start Page: 338, 1994.
[39] M. M. Joshi and S. Lee, "Integrated gasification combined cycle. A review of IGCC technology", Energy Sources, vol. 18, 537-568, 1996.
[40] S. R. A. Kather, C. Hermsdorf, M. Kostermann, A. Maschmann, K.Mieske, et al., "Research and development needs for clean coal deployment", IEA Clean Coal Centre, 2008.
[41] O. Shinada, A. Yamada, and Y. Koyama, "The development of advanced energy technologies in Japan: IGCC: a key technology for the 21st Century", 1221-1233, 2002.
[42] M. Müller, "Integration of hot gas cleaning at temperatures above the ash melting point in IGCC", Fuel, vol. 108, 37-41, 2013.
[43] C. Descamps, C. Bouallou, and M. Kanniche, "Efficiency of an Integrated Gasification Combined Cycle (IGCC) power plant including CO_2 removal", Energy, vol. 33, 874-881, 2008.
[44] T. D. Brown, "Coal gasification—combined cycles for electricity production", Progress in Energy and Combustion Science, vol. 8, 277-301, 1982.
[45] C. Christou, I. Hadjipaschalis, and A. Poullikkas, "Assessment of integrated gasification combined cycle technology competitiveness", Renewable and Sustainable Energy Reviews, vol. 12, 2459-2471, 2008.
[46] M. S. Germani and W. H. Zoller, "Vapor-phase concentrations of arsenic, selenium, bromine, iodine, and mercury in the stack of a coal-fired power plant", Environmental Science and Technology, vol. 22, 1079-1085, 1988.
[47] R. Meij, "Tracking trace elements at a coal-fired power plant equipped with a wet flue-gas desulphurisation facility", Kema Scientific & Technical Reports, vol. 7, 267-292, 1989.
[48] L. B. Clarke, *Management of by-products from IGCC power generation*, 1991.
[49] W. Mojtahedi and U.-M. Mroueh, *Trace elements removal from hot flue gases*, Valtion Teknillinen Tutkimuskeskus, 1989.
[50] L. B. Clarke and I. M. Smith, "Management of residues from coal utilisation: An overview of FBC and IGCC by-products", Studies in Environmental Science, vol. 48, 81-89, 1991.
[51] Y. Li, J. Zhang, Y. Zhao, and C. Zheng, "Volatility and Speciation of Mercury during Pyrolysis and Gasification of Five Chinese Coals", Energy & Fuels, vol. 25, 3988-3996, 2011.
[52] M. Šyc, M. Pohořelý, M. Jeremiáš, M. Vosecký, P. Kameníková, S. Skoblia, K. Svoboda, and M. Punčochář, "Behavior of Heavy Metals in Steam Fluidized Bed Gasification of Contaminated Biomass", Energy & Fuels, vol. 25, 2284-2291, 2011.
[53] A. J. Bushell and J. Williamson, "The fate of trace elements in coal during gasification", Coal Science and Technology, vol. 24, Elsevier, 1967-1970, 1995.
[54] Y. Sekine, K. Sakajiri, E. Kikuchi, and M. Matsukata, "Release behavior of trace elements from coal during high-temperature processing", Powder Technology, vol. 180, 210-215, 2008.
[55] W. Mojtahedi, "Trace Metals Volatilisation in Fluidised-Bed Combustion and Gasification of Coal", Combustion Science and Technology, vol. 63, 209-227, 1989.

[56] J. J. Helble, W. Mojtahedi, J. Lyyränen, J. Jokiniemi, and E. Kauppinen, "Trace element partitioning during coal gasification", Fuel, vol. 75, 931-939, 1996.

[57] O. Font, X. Querol, F. Plana, P. Coca, S. Burgos, and F. García Peña, "Condensing species from flue gas in Puertollano gasification power plant, Spain", Fuel, vol. 85, 2229-2242, 2006.

[58] J. R. Bunt and F. B. Waanders, "Trace element behaviour in the Sasol–Lurgi MK IV FBDB gasifier. Part 1 – The volatile elements: Hg, As, Se, Cd and Pb", Fuel, vol. 87, 2374-2387, 2008.

[59] J. R. Bunt and F. B. Waanders, "Trace element behaviour in the Sasol–Lurgi MK IV FBDB gasifier. Part 2 – The semi-volatile elements: Cu, Mo, Ni and Zn",Fuel, vol. 88, 961-969, 2009.

[60] J. R. Bunt and F. B. Waanders, "Trace element behaviour in the Sasol-Lurgi fixed-bed dry-bottom gasifier. Part 3 – The non-volatile elements: Ba, Co, Cr, Mn, and V", Fuel, vol. 89, 537-548, 2010.

[61] G. P. Reed, D. R. Dugwell, and R. Kandiyoti, "Control of Trace Elements in a Gasifier Hot Gas Filter: A Comparison with Predictions from a Thermodynamic Equilibrium Model", Energy & Fuels, vol. 15, 1480-1487, 2001.

[62] M. Díaz-Somoano and M. R. Martínez-Tarazona, "Trace element evaporation during coal gasification based on a thermodynamic equilibrium calculation approach", Fuel, vol. 82, 137-145, 2003.

[63] F. Frandsen, K. Dam-Johansen, and P. Rasmussen, "Trace elements from combustion and gasification of coal—An equilibrium approach", Progress in Energy and Combustion Science, vol. 20, 115-138, 1994.

[64] B. Miller, D. R. Dugwell, and R. Kandiyoti, "The Influence of Injected HCl and SO_2 on the Behavior of Trace Elements during Wood-Bark Combustion", Energy & Fuels, vol. 17, 1382-1391, 2003.

[65] O. Font, X. Querol, M. Izquierdo, E. Alvarez, N. Moreno, S. Diez, R. Álvarez-Rodríguez, C. Clemente-Jul, P. Coca, and F. Garcia-Peña, "Partitioning of elements in a entrained flow IGCC plant: Influence of selected operational conditions", Fuel, vol. 89, 3250-3261, 2010.

[66] F. Jiao, Y. Cheng, L. Zhang, N. Yamada, A. Sato, and Y. Ninomiya, "Effects of HCl, SO_2 and H_2O in flue gas on the condensation behavior of Pb and Cd vapors in the cooling section of municipal solid waste incineration", Proceedings of the Combustion Institute, vol. 33, 2787-2793, 2011.

[67] L. B. Clarke, "The fate of trace elements during coal combustion and gasification: an overview", Fuel, vol. 72, 731-736, 1993.

[68] M. Díaz-Somoano and M. R. Martínez-Tarazona, "Retention of trace elements using fly ash in a coal gasification flue gas", Journal of Chemical Technology & Biotechnology, vol. 77, 396-402, 2002.

[69] L. Gmelin, *Gmelin-Handbuch der anorganischen Chemie, Wolfram: System-Nr.54, Metal chemical reactions with metals zinc to lawrencium*, Springer, 1988.

[70] F. Huber and W. Petz, *Pb: organolead compounds. System number 47/R2PbR'2, R2PbR'R'', RPBR'R''R''', and R4 - nPbHn (n = 1 to 3) compounds S*, Springer, 1996.

[71] H. Schumann, I. Schumann, and U. Krüerke, *Sn: organotin compounds. Compounds with bonds between tin and transition metals of groups VIII, I and II*, Springer, 1995.

[72] H. Schumann, I. Schumann, and U. Krüerke, *Sn: organotin compounds. Tin centered radicals, Tin(II) compounds, compounds with tin element double bonds, Tin(II) complexes with aromatic systems, stannacarboranes, and other organotin compounds*, Springer, 1995.

[73] L. Gmelin, *Gmelin handbook of inorganic and organometallic chemistry,* Springer, 1997.

[74] H.J. Fachmann and L. Gmelin, *Gmelin handbook of inorganic and organometallic chemistry. Sulfur : System number 9 : Sulfur nitrogen compounds*, Springer, 1996.

[75] J. H. Gross and P. Roepstorff, *Mass Spectrometry: A Textbook,* Springer, 2011.

[76] E. de Hoffmann and V. Stroobant, *Mass Spectrometry: Principles and Applications*, Wiley, 2007.

[77] D. Porbatzki, *Freisetzung anorganischer Spezies bei der thermochemischen Umwandlung biogener Festbrennstoffe,* PhD-thesis, RWTH Aachen, 2008.

[78] K. J. Wolf, *Untersuchungen zur Freisetzung und Einbindung von Alkalimetallen bei der reduzierenden Druckwirbelschichtverbrennung*, PhD-thesis, RWTH Aachen, 2003.

[79] H. Oleschko and M. Mueller, "Influence of coal composition and operating conditions on the release of alkali species during combustion of hard coal", Energy and Fuels, vol. 21, 2007.

[80] H. Oleschko, *Freisetzung anorganischer Spezies bei der thermochemischen Umwandlung biogener Festbrennstoffe,* PhD-thesis, RWTH Aachen, 2008.

[81] K. J. Wolf, M. Müller, K. Hilpert, and L. Singheiser, "Alkali sorption in second-generation pressurized fluidized-bed combustion", Energy and Fuels, vol. 18, 1841-1850, 2004.

[82] M. Rieß, *Freisetzung und Einbindung von Schwermetallen bei der Hochtemperaturvergasung,* PhD-thesis, RWTH Aachen, 2010.

[83] M. Stemmler, *Chemische Heißgasreinigung bei Biomassevergasungsprozessen*, PhD-thesis, RWTH Aachen, 2011.

[84] D. C. Dayton, R. J. French, and T. A. Milne, "Direct observation of alkali vapor release during biomass combustion and gasification. Application of molecular beam/mass spectrometry to switchgrass combustion", Energy and Fuels, vol. 9, 855-865, 1995.

[85] T. A. Miller, "Chemistry and Chemical Intermediates in Supersonic Free Jet Expansions", Science, vol. 223, 545-553, 1984.

[86] C. W. Bale, P. Chartrand, S. A. Degterov, G. Eriksson, K. Hack, R. Ben Mahfoud, J. Melançon, A. D. Pelton, and S. Petersen, "FactSage thermochemical software and databases", Calphad, vol. 26, 189-228, 2002.

[87] C. W. Bale, E. Bélisle, P. Chartrand, S. A. Decterov, G. Eriksson, K. Hack, I. H. Jung, Y. B. Kang, J. Melançon, A. D. Pelton, C. Robelin, and S. Petersen, "FactSage thermochemical software and databases — recent developments", Calphad, vol. 33, 295-311, 2009.

[88] K. Froment, F. Defoort, C. Bertrand, J. M. Seiler, J. Berjonneau, and J. Poirier, "Thermodynamic equilibrium calculations of the volatilization and condensation of inorganics during wood gasification", Fuel, vol. 107, 269-281, 2013.

[89] A. E. Gheribi, C. Audet, S. Le Digabel, E. Bélisle, C. W. Bale, and A. D. Pelton, "Calculating optimal conditions for alloy and process design using thermodynamic and property databases, the FactSage software and the Mesh Adaptive Direct Search algorithm", Calphad, vol. 36, 135-143, 2012.

[90] D. E. Laughlin and K. Hono, *Physical Metallurgy (Fifth Edition)*, Oxford: Elsevier, 2014.

[91] F. Jiao, L. Zhang, W. Song, Y. Meng, N. Yamada, A. Sato, and Y. Ninomiya, "Effect of inorganic particulates on the condensation behavior of lead and zinc vapors upon flue gas cooling", Proceedings of the Combustion Institute, vol. 34, 2821-2829, 2013.

[92] F. Jiao, L. Zhang, N. Yamada, A. Sato, and Y. Ninomiya, "Effect of HCl, SO_2 and H_2O on the condensation of heavy metal vapors in flue gas cooling section", Fuel Processing Technology, vol. 105, 181-187, 2013.

7. Appendix

7.1. Setup of the MBMS

Table A.1. Adjustments of the MBMS.

Ionisation:	Cathode	Emission voltage:	-70 V
		Emission current:	1.0 mA
Lens:	Optic	Ion region:	3.4 V
		Extractor:	-16 V
		Lens 1/3:	7 V
		Lens 2:	-351 V
		Quadrupole entrance:	-39 V
		Quadrupole exit:	-29 V
		Dynode voltage:	4000 V
		Dynode polarity:	negative
Recipient:		Front nozzle:	0.3 mm
		Skimmer:	1.0 mm
		Blende Kammer 2/3:	1.5 mm

7.2. Condensation experiments

Table A.2. Concentrations of heavy metals (ppm) in the condensation experiments.

Experimental run	Atmosphere	Zn (ppm)	Cd (ppm)	Pb (ppm)	As (ppm)	Sn (ppm)
Influence of H_2O	3 % vol H_2O	133.9	113.2	*	205.5	154.8
Influence of H_2O	17 % vol H_2O	134.3	21.2	102.9	159.4	384.3
Influence of HCl	50 ppm HCl	33.1	20.4	88.7	140.8	55.2
Influence of HCl	500 ppm HCl	193.5	30.2	106.2	179.6	23.6
Influence of H_2S	50 ppm H_2S	160.1	37.4	*	104.5	*
Influence of H_2S	500 ppm H_2S	183.3	153.3	*	143.5	*

*The total concentration could not be determined. The sample boat broke during the cooling stage after the experiment

Acknowledgments

There are many people without whom this work would have never seen the light of day. I would like to thank all those who have helped, supported and inspired me during this time and have contributed, in one way or another, in completing this thesis.

First of all I would like to thank my doctoral thesis supervisor, Prof. Dr.-Ing Lorenz Singheiser, for his support and for giving me the opportunity to carry out this thesis at the Institute of Energy and Climate Research (IEK-2) at Forschungszentrum Jülich.

I specially thank Priv.-Doz. Dr. Michael Müller for letting me be part of the "Thermochemistry Group" and for the competent supervision and continuous support during this work. I really appreciated that his door was always open for me to discuss about the progress of the thesis and to give helpful advices. He encouraged me from the beginning to take the initiative and to think independently, as well as, to speak German. Many things I have learnt in these years will be very useful in my life.

Very sincere thanks go to Prof. Dr. Yoshihiko Ninomiya for the collaboration in this thesis with his thermodynamic pseudo-equilibrium model and for offering me the opportunity to work with him and his group in Japan. I will never forget this experience and the hospitality and effort that he and his students made to make me feel like at home.

I am particularly grateful to Egon Seelbach for all the help and technical support with the mass spectrometer.

I would like to thank Andreas Schwaitzer and Giovanni D´Orsaneo and their team from ZEA-1 for their kindness and help during the design of the glass parts of the experimental setups. In the same way, I appreciate the hard and thorough work carried out by the colleagues from ZEA-3 to analyse each of my million samples.

I am also deeply grateful to my colleagues from Thermochemistry Group, especially to Dr. Emanuel Forster, Dr. Marc Bläsing as well as Dr. Elena Yazhenskikh, for their sincere help and for finding always time for priceless discussions regarding the experiments and the thermodynamic modelling. I am also thankful to Elora Borkowski for her interest in carrying out an internship under my supervision and for her contribution to my experimental results.

I thank all the colleagues of IEK-2, the current members and the ones who already left, for the good atmosphere at work and for all the nice time we have spent together. I have had the fortune to work with some people that not only helped me, but also became good friends.

De todo corazón me gustaría agradecer a todos mis amigos y a mi familia, en especial a mis padres y a mi hermana, por su apoyo incondicional. Papá, mamá, gracias por dármelo todo, por ser para mí un ejemplo y por creer siempre en mí. Me habéis dado la fuerza necesaria que he necesitado en los momentos difíciles. Sin vosotros a mi lado no hubiera llegado hasta aquí. Gracias Lara por traer tanta alegría y felicidad a nuestra familia. A vosotros os dedico esta tesis.

Last but not least, I would like to express my endless gratitude to Chris, my partner, for his full support and understanding during the difficult times of my PhD. Thanks for encouraging me and finding always a way to make me laugh. I wholeheartedly appreciate that you are always by my side. This thesis is also yours.

Band / Volume 297
The role of abiotic processes in the formation and degradation of gaseous nitrogen compounds in the soil
J. Heil (2015), XIV, 106 pp
ISBN: 978-3-95806-106-4

Band / Volume 298
12th Carolus Magnus Summer School on Plasma and Fusion Energy Physics
edited by Kristel Crombé (2015), 468 pp
ISBN: 978-3-95806-107-1

Band / Volume 299
Optical near-field investigations of photonic structures for application in silicon-based thin-film solar cells
A. M. Ermes (2015), vi, 157 pp
ISBN: 978-3-95806-108-8

Band / Volume 300
Strom- und Gasmarktdesign zur Versorgung des deutschen Straßenverkehrs mit Wasserstoff
M. Robinius (2015), VI, 255 pp
ISBN: 978-3-95806-110-1

Band / Volume 301
Alterung von Vakuum-plasmagespritzten MCrAlY-Schutzschichten und ihre Wechselwirkung mit Nickel- und Cobalt-basierten γ/γ'-Superlegierungen
P. J. Terberger (2015), IX, 149 pp
ISBN: 978-3-95806-113-2

Band / Volume 302
Verbundvorhaben ELFA Effiziente Luftfahrzeuge
Brennstoffzellensysteme zur Energieerzeugung BREZEN – Teilprojekt: Kerosinaufbereitung
R. Peters, J. Meißner, J. Pasel, R. C. Samsun, D. Stolten
(2016), viii, 84 pp
ISBN: 978-3-95806-114-9

Band / Volume 303
Cavity-Ringdown-Spektroskopie zur Untersuchung der Rolle höherer Stickoxide für den nächtlichen Schadstoffabbau in der unteren Atmosphäre
S. Schrade (2016), II, 118 pp
ISBN: 978-3-95806-116-3

Band / Volume 304
Thermo-mechanical Properties of Mixed Ionic-Electronic Conducting Membranes for Gas Separation
V. K. Stournari (2016), 167 pp
ISBN: 978-3-95806-117-0

Band / Volume 305
Untersuchungen zu suspensionsplasmagespritzten Wärmedämmschichtsystemen
N. Schlegel (2016), X, 136 pp
ISBN: 978-3-95806-118-7

Band / Volume 306
Laser processing for the integrated series connection of thin-film silicon solar cells
B. Turan (2016), XII, 190 pp
ISBN: 978-3-95806-119-4

Band / Volume 307
Development and Application of a Multiscale Model for the magnetic Fusion Edge Plasma Region
F. Hasenbeck (2016), 190 pp
ISBN: 978-3-95806-120-0

Band / Volume 308
Emissions of Biogenic Volatile Organic Compounds and Ozone Balance under Future Climate Conditions
C. Wu (2016), VI, 105 pp
ISBN: 978-3-95806-121-7

Band / Volume 309
Computerunterstützte Auslegung eines Brennstoffzellen-Batterie-Hybridsystems für die Bordstromversorgung
C. Krupp (2016), iii, 207 pp
ISBN: 978-3-95806-124-8

Band / Volume 310
Influence of H_2O, HCl and H_2S on the Release and Condensation of Trace Metals in Gasification
M. Benito Abascal (2016), XIX, 172 pp
ISBN: 978-3-95806-125-5

Energie & Umwelt /
Energy & Environment
Band / Volume 310
ISBN 978-3-95806-125-5